University of Porto

Lecture course notes of Curricular Unit

Tópicos Avançados em Galáxias e Cosmologia (UC AST603)

Module: *Cosmological Structure Formation and Evolution*

Doctoral Program in Astronomy

Elements of Cosmology and Structure Formation

António J. C. da Silva

2012 / 2013

Contents

1 The Standard Model of Cosmology **7**

1.1 The basis of the standard model of Cosmology 7

1.2 Fundamental equations 8

1.2.1 The dynamical equations 9

1.2.2 Epochs 10

1.2.3 The observed universe 11

1.3 Exact solutions 13

1.3.1 The age of the universe 13

1.3.2 Scale factor 14

1.3.3 Distances, horizons and volumes 15

1.4 Initial conditions and Inflation 17

1.4.1 Problems with the Big Bang 17

1.4.2 The theory of inflation 19

2 Cosmological Structure Formation **23**

2.1 Density contrast and the power spectrum 23

2.2 Linear perturbation theory 26

2.3 Sub-horizon perturbations in non-relativistic fluids 27

2.4 Relativistic fluids and super-horizon perturbations 30

2.4.1 Relativistic multi-fluid case 31

2.4.2 Density transfer function and the power spectrum 32

2.5 Non-linear evolution of perturbations 34

2.5.1 Spherical collapse model 34

2.5.2 Zel'dovich approximation 35

2.5.3 Press–Schechter theory 36

2.5.4 Numerical simulations of large–scale structure 37

3 Cosmic Microwave Background Radiation 47

3.1 The intensity spectrum 47

3.2 The angular power spectrum 49

3.3 Fontes geradores de anisotropias CMB: "A primer" 52

3.3.1 Anisotropias Primárias 53

3.3.2 Anisotropias Secundárias 55

3.3.3 Anisotropias Terciárias 61

A Cálculo das anisotropias do CMB a grandes escalas angulares 73

A.1 Integração da equação das geodésicas para fotões 73

A.2 O Efeito de Sachs-Wolfe 77

A.2.1 Cálculo de C_l para grandes ϑ. Patamar de Sachs-Wolfe 81

B Geodésicas e velocidades próprias 85

B.1 Geodésicas nulas e velocidades próprias em ds^2 e $d\bar{s}^2$ 85

B.2 Velocidades próprias de partículas materias em universos perturbados (1^a ordem de aprox.) 85

C Temperature fluctuations in a small patch of sky 87

List of Figures

2.1 Gas cooling functions for collisional ionization equilibrium in the optically-thin limit 44
2.2 Simulation Box at redshift zero 46

3.1 CMBR spectral distortion caused by energy release in the early universe. . . . 48
3.2 General features of the CMBR angular power spectrum 51
3.3 O efeito Sachs Wolfe integrado 55
3.4 Efeitos do lensing gravitacional, reionização global e efeito Vishniac sobre o espectro CMBR 58
3.5 Efeito da reonização na radiação de fundo 59
3.6 Distorções espectrais CMBR provovadas pelo efeito Sunyaev– Zel'dovich . . . 59
3.7 Funções de distorção espectral dos efeitos SZ térmico e cinético 60
3.8 Sensibilidade angular e espectral de várias experiências CMB 63
3.9 Foregrounds e ruídos do fundo de micro-ondas 64

A.1 Parametrisação das geodésicas luz no espaço não perturbado de $d\bar{s}^2$ 76
A.2 Última superfície de scattering. 82

List of Tables

3.1 Processos que geram anisotropias na CMBR 52

Chapter 1

The Standard Model of Cosmology

In the following sections we review the basic elements of standard cosmology needed for the remainder of the course. The majority of the results presented here can be found in many textbooks of cosmology, e.g. in Refs. [18, 61, 65, 75, 76, 79, 80].

1.1 The basis of the standard model of Cosmology

The standard model (**SM**) of cosmology is presently based on the Hot Big Bang paradigm. The universe is expanding and cooling from an initial ultra dense state, where matter and radiation were prisoners in a gaseous hot plasma of fundamental particles. The basic mathematical framework of the SM is set by the following assumptions:

- The universe is homogeneous and isotropic when observed on large scales.
- The dynamics of space-time is described by Einstein's theory of general relativity.

The first of these assumptions derives from the cosmological principle, which states that the universe on large scales should have no privileged positions or directions and therefore at a given time should look the same to all observers. The most general homogeneous and isotropic solution of the Einstein equations of GR is the FLRW line element,

$$ds^2 = c^2 dt^2 - a^2(t) \left[\frac{dr^2}{1 - kr^2} + r^2 \left(d\theta^2 + \sin^2 \theta d\phi^2 \right) \right], \tag{1.1}$$

where c is the speed of light, t is the universal time, r, θ, ϕ are the comoving spatial coordinates and $a(t)$ is the *scale factor*, which describes the overall expansion (or contraction) of the three-dimensional space. The constant k gives the spatial curvature of the universe. It can be negative, zero or positive depending on whether the universe is open, closed or flat. If $k \leq 0$ the universe has an infinite extension and the r coordinate ranges from zero to infinity. If k is positive the universe is finite in size and r ranges from 0 to $1/\sqrt{k}$. With an appropriate rescaling of coordinates it is always possible to make k to take the values: -1, 0, $+1$. Observers

with fixed coordinates in the comoving coordinate system experience no external forces and are said to be fundamental comoving observers as they move with the expansion (or contraction) of the cosmological fluid. The proper distance between two of these observers scales as:

$$\ell(t) = \frac{a(t)}{a_0}\ell_0, \tag{1.2}$$

where a_0 and ℓ_0 are the scale factor and the proper distance at some initial time t_0. Taking the derivative of this expression with respect to time we obtain the relative speed between fundamental observers:

$$v(t) = \frac{d\ell}{dt} = \frac{\dot{a}(t)}{a_0}\ell_0 = \frac{\dot{a}(t)}{a(t)}\ell(t) \equiv H(t)\ell(t). \tag{1.3}$$

This expression shows that in an expanding universe ($\dot{a}(t) > 0$) the further away any two observers are, the faster they recede from one another due to the cosmic expansion. This is known as the **Hubble law**, first derived from observations by Edwin Hubble in 1929. The proportionality factor between velocity of recession and distance,

$$H(t) = \frac{\dot{a}(t)}{a(t)}, \tag{1.4}$$

gives the expansion rate of the universe at a given time. Its present value is usually parametrized as $H_0 = 100\,h$ km s^{-1} Mpc where h is the so-called *Hubble parameter*. H_0 is also known as the **Hubble constant** and has units of an inverse of time.

The cosmological expansion produces a *redshift* in the spectrum of the light emitted from distant objects. This redshift is defined as the change of energy of a photon measured by fundamental observers between the epochs of emission of the radiation, at t, and the present time, t_0,

$$z = \frac{E - E_0}{E_0} = \frac{\nu}{\nu_0} - 1 = \frac{\lambda_0}{\lambda} - 1 = \frac{a\,(t_0)}{a\,(t)} - 1. \tag{1.5}$$

Here E, ν and λ are the photon's energy, frequency and wavelength at t and the subscript '$_0$' denotes the same quantities at the present. To obtain this expression we use the quantum mechanics' proportionality between the energy and frequency of a photon $E = h\nu = hc/\lambda$ (h is the Planck's constant) and the fact that the wavelength of a free photon stretches as the other lengths with $a(t)$.

1.2 Fundamental equations

In GR the dynamics of space-time is set by Einstein's field equations,

$$G_{ab} = R_{ab} - \frac{1}{2}Rg_{ab} = \frac{8\pi G}{c^4}T_{ab} + \Lambda g_{ab}, \tag{1.6}$$

where G and Λ are the gravitational and cosmological constants, g_{ab} is the metric of space-time, G_{ab} is the Einstein tensor, R_{ab} is the Ricci tensor and R is the Ricci scalar (this last

two quantities result from successive contractions of the Riemann tensor and are functions of the metric and its derivatives). The inclusion of the cosmological constant term in Eq. (1.6), originally introduced by Einstein in order to describe a static universe, is presently supported by observations of distant Type Ia supernovae [83, 84, 89]. Finally T_{ab} is the stress–energy tensor, which describes the gravitational contributions from all forms of energy in the universe. To satisfy the requirements of homogeneity and isotropy implied by the cosmological principal, the stress–energy tensor has to be that of a perfect fluid:

$$T_{ab} = (\rho + \frac{p}{c^2})U_a U_b - \frac{p}{c^2} g_{ab} \tag{1.7}$$

where $\rho = \rho(t)$ and $p = p(t)$ are the fluid's energy density and pressure and U_a is the four velocity field of a fundamental observer. In this case the solution of Einstein's field equations is the metric (1.1). The energy–momentum conservation law is expressed by the condition

$$T^{ab}{}_{;b} = 0 \tag{1.8}$$

where the symbol ';' denotes covariant derivative. This is a set of four equations giving the conservation of the energy density and the 3-momentum. The 'temporal component' equation gives,

$$\dot{\rho} = -3\frac{\dot{a}}{a}\left(\rho + \frac{p}{c^2}\right) \quad \Rightarrow \quad d\left(\rho c^2 a^3\right) = -p d\left(a^3\right). \tag{1.9}$$

This expression has a simple physical interpretation. It translates the first law of thermodynamics applied to a comoving volume element: in an adiabatical process the variation of energy is given by the work produced by the pressure forces. It is often assumed that during several periods of the history of the universe the energy density and pressure can be related by an *equation of state* with a simple form:

$$p = w\rho c^2 \quad -1 \leq w \leq 1, \tag{1.10}$$

where w is a constant. In this case the integration of (1.9) gives

$$\rho(t) = \rho_i \left(\frac{a(t)}{a_i}\right)^{-3(1+w)}, \tag{1.11}$$

where $\rho_i = \rho\left(t_i\right)$, $a_i = a\left(t_i\right)$ are the energy density and the scale factor at some initial time t_i. The cases $w = 0$, $w = 1/3$ and $w = -1$ are classical examples which are appropriate to describe the phases when the universe is dominated by a fluid of (non relativistic) matter, radiation (and relativistic matter) and vacuum energy associated with the Λ term in (1.6).

1.2.1 The dynamical equations

Using Eqs. (1.1) and (1.7) in (1.6) one can derive two equations which give the expansion and acceleration rates of the universe as a function of its matter contents and geometry:

$$\left(\frac{\dot{a}}{a}\right)^2 = \frac{8\pi G}{3}\rho + \frac{\Lambda c^2}{3} - \frac{kc^2}{a^2} \tag{1.12}$$

$$\frac{\ddot{a}}{a} = -\frac{4\pi G}{3}\left(\rho + 3\frac{p}{c^2}\right) + \frac{\Lambda c^2}{3}. \tag{1.13}$$

These are known as the Friedmann and Raychaudhuri (or acceleration) equations, respectively. If we set $\Lambda = 0$ we find that $\ddot{a}$ is negative whenever $p > -\rho c^2/3$ ($a(t)$ is always positive). In this case both radiation ($w = 1/3$) and matter ($\omega = 0$) dominated epochs are periods of decelerated expansion (if the universe has a flat or open geometry) or decelerated contraction (only possible with closed geometries).

If we take as an observational fact that the universe is expanding ($\dot{a} > 0$) and assume that in the past $\ddot{a}$ was always negative ($\ddot{a} < 0$) then going backwards in time there's a moment, t_i, where $a(t_i) = 0$. This is the Big Bang event. The instant t_i is usually redefined as the origin of time, $t_i = 0$. The FLRW models are Big Bang universes for many combinations of energy densities, cosmological constant and geometries. However one should note that there are FLRW models (with $\Lambda > 0$, $k = 1$), which do not "start" from a Big Bang. This is the case of the Eddington–Lemaitre and Einstein universes (see e.g. Ref. [22]). Because equations (1.12), (1.13) and (1.9) are related by the Bianchi identities (see e.g. Ref. [97]) we only need to consider two of these equations to describe the dynamics of FLRW models. These are usually taken to be the Friedmann and energy conservation equations (the later usually in the form Eq. (1.11)).

We can re-write the Friedmann equation as a "conservation law of densities",

$$\frac{8\pi G}{3H^2}\rho + \frac{\Lambda c^2}{3H^2} - \frac{kc^2}{a^2H^2} = 1 \quad \Leftrightarrow \quad \Omega + \Omega_\Lambda + \Omega_k = 1 \tag{1.14}$$

where,

$$\Omega = \frac{\rho}{\rho_c}, \qquad \Omega_\Lambda = \frac{\Lambda c^2}{3H^2}, \qquad \Omega_k = -\frac{kc^2}{a^2H^2}, \qquad \rho_c = \frac{3H^2}{8\pi G} \tag{1.15}$$

are the matter (Ω), vacuum (Ω_Λ) and curvature (Ω_k) density parameters and ρ_c is the critical energy density of the universe. All these quantities evolve in time satisfying Eq. (1.14). Therefore only two of the above density parameters are independent. For $\Lambda = 0$ ($\Omega_\Lambda = 0$) models, the universe is geometrically closed ($k = 1$), flat ($k = 0$) or open ($k = -1$), depending on whether its total energy density, ρ, is greater, equal or smaller than the critical density, ρ_c. The acceleration rate of the universe is often expressed in terms of the *deceleration parameter* which is defined as:

$$q \equiv -\frac{\ddot{a}a}{\dot{a}^2} = -\frac{\ddot{a}}{a}\frac{1}{H^2} = \frac{1+3w}{2}\Omega - \Omega_\Lambda \tag{1.16}$$

where the last equality results from combining Eq. (1.15) with Eqs. (1.13) and (1.11).

1.2.2 Epochs

In general the cosmological fluid can be regarded as a mixture of ideal fluids describing different matter components, each of these having a particular energy density, ρ_i, and pressure, p_i. Considering that we have only two components consisting of non-relativistic matter, ρ_m, and radiation, ρ_r, ($\rho = \rho_r + \rho_m$) we can write the Freedmann equation as:

$$H^2(t) \;=\; \frac{8\pi G}{3}\left(\rho_r + \rho_m\right) - \frac{kc^2}{a^2} + \frac{\Lambda c^2}{3}$$

$$= H_0^2 \left[\Omega_{r0} \left(\frac{a_0}{a} \right)^4 + \Omega_{m0} \left(\frac{a_0}{a} \right)^3 + \Omega_{k0} \left(\frac{a_0}{a} \right)^2 + \Omega_{\Lambda 0} \right]. \quad (1.17)$$

The second equality results from using Eq. (1.11) for matter ($w = 0$) and radiation ($w = 1/3$), with $t_i = t_0$ being the present time ($a(t_i) = a(t_0) = a_0$). The quantities H_0, Ω_{r0}, Ω_{m0}, Ω_{k0} and $\Omega_{\Lambda 0}$ are respectively the Hubble constant, $H_0 = H(t_0)$, the matter, radiation, vacuum and curvature density parameters evaluated at the present time ($\Omega_{r0} = 8\pi G\rho_r(t_0)/3{H_0}^2$, $\Omega_{m0} = 8\pi G\rho_m(t_0)/3{H_0}^2$).

Equation (1.17) shows the relative contribution from the different fluid components to the expansion rate of the universe. In a Big Bang scenario $a \to 0$ in the limit $t \to 0$. The expansion rate is therefore initially dominated by the radiation component, Ω_r. As the universe expands, the contribution from the other terms becomes progressively important and can dominate the expansion. When matter becomes the dominant component, $H(t)$ is driven by the Ω_m term in Eq. (1.17). If the universe keeps on expanding and has a non-zero cosmological constant the dynamics of the expansion becomes dominated by the vacuum term, Ω_Λ. By comparing the first with second term inside the square brackets of Eq. (1.17) we obtain the redshift at which matter and radiation contribute equally to the expansion rate. This is

$$1 + z_{\rm eq} = \Omega_{m0}/\Omega_{r0} \simeq 2.4 \times 10^4\, \Omega_0 h^{-2},$$

where the last equality derives from the observed energy density of radiation (see next section). The redshift $1 + z_{\rm eq}$ gives the time when the universe changes from being radiation dominated to became dominated by matter. It is usually referred to as the matter–radiation equality redshift.

Going back enough in time we find the universe in a stage where photons, electrons and baryons are tightly coupled in a collisional plasma. When the temperature dropped to about 3600 Kelvin ($z_{\rm rec} \simeq 1300$) [61], electrons and baryons recombined to form the first neutral Hydrogen atoms. Soon after this short period, known as *recombination*, the number of free electrons drops dramatically and the scattering between the remaining free electrons and photons is no longer sufficient to keep matter and radiation in contact. At this point ($z_{\rm dec} \simeq 1100$) the CMBR photons decoupled from the fluid. Present observations of Ω_0 and h indicate that the matter–radiation equality happens before recombination ($z_{\rm eq} \simeq 14300$, see next section).

1.2.3 The observed universe

Our understanding of the universe relies ultimately on our ability to make measurements and to compare those measurements with theoretical models. As (1.17) indicates, the key observational parameters in the FLRW Big Bang models are the Hubble parameter and the present-day densities of the mass–energy contents of the universe. Despite great progress in the past decades there is still a considerable amount of uncertainty regarding the majority of these parameters.

- **Hubble parameter**: The quest for the measurement of the Hubble parameter, h, is the oldest among the cosmological parameters. It started soon after the discovery of the

universal expansion and today it is still not known to high accuracy (see Refs. [47, 54] for reviews). There are two basic ways of measuring h. One involves the measurement of distances to nearby galaxies, typically by observing the periods and luminosities of Cepheid stars within them, and then use these determinations to calibrate other methods of measuring distances to more distant galaxies. This strategy is known as the *cosmic distance ladder* [92]. The second way consists of using *fundamental physics* methods, which permit the direct measurement of distances to faraway objects without using the cosmic distance ladder approach. This is the case of methods involving Type Ia or Type II supernovae, gravitational lensing, and the Sunyaev–Zel'dovich effect (see Section **??**). Although different approaches can still lead to different results, the range of h determinations has been shrinking with time. Presently different observational techniques seem to start to converge inside the range $h \in [0.5, 0.9]$ to a mid-value of $h \simeq 0.7$. This is the case of the methods based on the observation of distant Cepheids using the Hubble Space Telescope [36, 37] and the observation of Type Ia supernovae [56, 90].

- **Total matter/energy density**: The total matter or energy density of the universe, $\Omega_{tot,0} = \Omega_{r0}+\Omega_{m0}+\Omega_{\Lambda 0}+\Omega_{k0}$, is presently most accurately constrained from observations of the angular scale (or multipole) of the first acoustic peak in the angular power spectrum of the CMB anisotropies. The position of the peak is highly sensitive to $\Omega_{tot,0}$. According to recent determinations from different CMB experiments its position is located at a multipole value of $l_p \sim 210$. Assuming Gaussian adiabatic initial perturbations, the Boomerang, MAXIMA and DASI experiments provide the following constraints on the total matter/energy density: $\Omega_{tot,0} = 1.02^{+0.06}_{-0.03}$ [21, 74]; $\Omega_{tot,0} = 0.9^{+0.18}_{-0.16}$ [103]; and $\Omega_{tot,0} = 1.04 \pm 0.06$ [88], respectively. These estimates are remarkably consistent with an $\Omega_{tot,0} = 1$ (flat) universe.

- **Radiation density**: The energy density in all forms of electromagnetic radiation, $\Omega_{\gamma 0}$, is dominated by the contribution of the CMB, $\Omega_{CMB,0}$ (see e.g. Ref. [96]). This can be computed accurately from the observed CMB mean temperature, $T_{CMB} = 2.725 \pm 0.001$ K [33], by using the Stefan-Boltzmann law, $\Omega_{\gamma 0} \simeq \Omega_{CMB,0} = 2.48 \times 10^{-5}\, h^{-2}$. To estimate Ω_{r0} we need also to consider the contribution from the other relativistic species. Of particular importance is the *neutrino background*. If in addition to radiation we assume the existence of three families of massless neutrinos we obtain [18], $\Omega_{r0} \simeq 4.17 \times 10^{-5}\, h^{-2}$.

- **Matter density**: Many different techniques have been used to infer constraints on the present day value of the matter density parameter, Ω_{m0}. These include methods based on observations from CMB anisotropies, Type Ia supernovae, gravitational lensing, the evolution of the abundance of X-ray clusters with redshift, gas mass fraction in galaxy clusters, observational fits to the matter power spectrum of extra galactic objects, and measurements of large scale peculiar velocities of galaxies (for an overview on these and other methods see e.g. Ref. [91] and references therein). Results indicate that we are still far from having an accurate determination of Ω_{m0}. In some cases different techniques

can even show some degree of inconsistency.[1] However, combined data analysis using results from many of these methods give evidence in favor of a matter density parameter of about $\Omega_{m0} = 1/3$. For example, the authors in Ref. [44] have performed a likelihood analysis using results from six independent data sets and found $\Omega_{m0} = 0.31 \pm 0.04 \pm 0.04$, assuming a flat Universe. In this determination the first error is mainly statistical and the second is systematical. The observational data included constraints from recent CMB observations made with Boomerang and MAXIMA, Type Ia supernovae, double radio galaxies, lensing and large scale structure formation data.

- **Cosmological constant**: The strongest evidence for a positive cosmological constant derives from observations of high-redshift Type Ia supernovae, which indicate that the universe is currently evolving in accelerated phase of expansion. Independently, a positive Λ is also supported from a combination of observations indicating that $\Omega_{m0} < 1$ in conjunction with the CMB results which show that the universe is approximately flat. Under the assumption of a flat Universe, with matter density $\Omega_{m0} \sim 0.3$, the energy density associated with a cosmological constant term is $\Omega_{\Lambda 0} \sim 0.7$.

Although there's still a considerable amount of uncertainty in the determination of many of the above parameters, the combination of data from present observations seem to indicate that the Universe is consistent with being flat, and the ratio between the vacuum and matter densities, $\Omega_\Lambda/\Omega_{m0}$, is of the order of 2. For discussions on the current status of measurements of cosmological parameters see e.g. Refs. [35, 87].

1.3 Exact solutions

The time dependence of the scale factor and the age of the universe result from the integration of Eq. (1.17). The usual way to proceed is first to multiply Eq. (1.17) by $(a/a_0)^2$ and use $\Omega_{k0} = 1 - \Omega_0 - \Omega_{\Lambda 0}$,

$$\frac{d}{dt}\frac{a(t)}{a_0} = H_0 \sqrt{1 - \Omega_0 + \Omega_{m0}\left(\frac{a}{a_0}\right)^{-1} + \Omega_{r0}\left(\frac{a}{a_0}\right)^{-2} - \Omega_{\Lambda 0}\left[1 - \left(\frac{a}{a_0}\right)^2\right]}. \tag{1.18}$$

1.3.1 The age of the universe

The integration of this expression, with the condition $a(t = 0) = 0$, gives

$$t = H_0^{-1} \int_0^{\frac{a(t)}{a_0} = (1+z)^{-1}} \frac{1}{\sqrt{1 - \Omega_0 + \Omega_{m0} x^{-1} + \Omega_{r0} x^{-2} - \Omega_\Lambda (1 - x^2)}}\, dx, \tag{1.19}$$

[1] For example, preliminary constraints from the Cosmic Lens All-Sky Survey (CLASS) [46] appear to be in strong conflict with the results from the Type Ia supernovae data [83, 84, 89].

where we have put $x = a(t)/a_0 = 1/(1+z)$. This gives the age of the universe as a function of the scale factor and the present day density parameters, $t = f(a, \Omega_0, \Omega_{m0}, \Omega_{r0}, \Omega_{\Lambda 0})$. Observationally we know that $\Omega_{r0} \ll \Omega_{m0} \simeq \Omega_0$ but at early times the radiation term dominates Eq. (1.19). Using current estimations of the density parameters it is easy to see that the radiation-dominated period is very short when compared to the present age of the universe, t_0. This means that in practice t_0 can be calculated to a very good approximation by setting $\Omega_{r0} = 0$ in Eq. (1.19). Analytical expressions for the age of the universe can be found in many textbooks for a range of cosmologies. Three cosmological scenarios of historical interest are the flat universe with cosmological constant ($\Omega_0 + \Omega_{\Lambda 0} = 1$), the critical density universe ($\Omega_0 = 1$) and the open universe without Λ ($\Omega_0 < 1$; $\Omega_{\Lambda 0} = 0$). The integration of Eq. (1.19) for these models is also analytical and can be found for example in Ref. [61].

In some situations of interest is useful to define time in terms of the so-called conformal time, $d\eta = dt/a$. This gives,

$$\eta(t) = \int_0^t \frac{dt'}{a(t')} = \int_0^{a(t)} \frac{da}{a(t')\dot{a}(t')}. \tag{1.20}$$

1.3.2 Scale factor

The inversion of $t = f(a, \Omega_0, \Omega_{m0}, \Omega_{r0}, \Omega_{\Lambda 0})$ with respect to a gives the dependence of the scale factor with time. However since the expansion rate of the universe is dominated at different phases by different fluid components (see Eq. (1.17)) it's quite useful to examine the solutions of the Friedmann equation for each of these phases. Restricting ourselves to the case $\Lambda = 0$, the Friedmann equation for a single component fluid reads,

$$\dot{a}^2 = a_0^2 H_0^2 \left[1 - \Omega_{w0} + \Omega_{w0} \left(\frac{a}{a_0} \right)^{-(1+3w)} \right] , \tag{1.21}$$

where Ω_{w0} is the present-day density of the fluid and w is the equation of state parameter in Eq. (1.10). The solution of Eq. (1.21) is straightforward in the case of $\Omega_{w0} = 1$ (flat geometry)

$$\frac{a(t)}{a_0} = \left(\frac{3(1+w)}{2} H_0 t \right)^{2/(3(1+w))} \tag{1.22}$$

$$H(t) = \frac{\dot{a}}{a} = \frac{2}{3(w+1)t} \tag{1.23}$$

$$q(t) = -\frac{\ddot{a}a}{\dot{a}^2} = \frac{1+3w}{2} = \text{const}\,. \tag{1.24}$$

These expressions are particularly useful for fluids dominated by matter ($w = 0$) and radiation ($w = 1/3$). General solutions of Eq. (1.21) for this type of fluids are also not difficult to derive and can be found in many cosmology textbooks (see e.g. Ref. [61]).

1.3.3 Distances, horizons and volumes

Of particular importance to the study of physical processes acting on different cosmological scales is to determine the size of the largest causally connected regions at a given time. In a universe described by Eq. (1.1) the regions in causal contact with an observer of coordinates $O = (t, r_0, \theta_0, \phi_0)$ are those for which light rays emitted at the instant t_e reach O before or at the instant t. Light rays arriving at (r_0, θ_0, ϕ_0) later than t are beyond the *horizon* of O. Since light rays travel along null geodesics ($ds^2 = 0$), the **coordinate distance** travelled by light between $t_e = 0$ and t is easily obtained from Eq. (1.1)

$$\int_0^{r_e} \frac{dr}{\sqrt{1-kr^2}} = c\int_0^t \frac{dt'}{a\,(t')} = c\,\eta(t), \tag{1.25}$$

where r_e is the radial coordinate at emission. Without loss of generality we set $r_0 = 0$ and assumed radial $d\theta = d\phi = 0$ geodesics. The corresponding (physical) **proper distance** is

$$d_H(t) = \int_0^{r_e} \sqrt{|g_{rr}|}dr = a(t)\int_0^{r_e} \frac{dr}{\sqrt{1-kr^2}} = c\,a(t)\eta(t). \tag{1.26}$$

This forms a spherical surface centered at (r_0, θ_0, ϕ_0) known as the **particle horizon** of O. For any observer, $d_H(t)$ separates the regions which can establish causal contact with the observer at t (regions within the horizon) from those which cannot (regions beyond the horizon). Using Eqs. (1.20) and (1.21) in Eq. (1.26) one obtains the following expression, valid for $1 + z \gg (1/\Omega_{w0} - 1)^{1/(1+3w)}$ and $w > -1/3$ (see Ref. [18])

$$d_H(t) \simeq \frac{2}{3w+1}\frac{c}{H_0}\Omega_{w0}^{1/2}\left(\frac{a}{a_0}\right)^{3(1+w)/2} = 3\frac{1+w}{1+3w}ct\ . \tag{1.27}$$

For $\Omega_{w0} = 1$ this is in fact an exact solution of Eq. (1.26), whenever $w > -1/3$ (see e.g. Ref. [61]). For universes with $w < -1/3$, the distance to the particle horizon becomes infinite. This is the case of the vacuum-dominated de Sitter universe ($w = -1$), for which there's no particle horizon.

Another important length scale is the **Hubble length**, R_H (also referred to as *Hubble radius* or *speed of light sphere*). This is defined as the distance to the spherical surface (centered in O) made by all points that at the time t have cosmological recessional velocities equal to the speed of light. Setting $v = c$ in the Hubble expansion law (1.3) one finds,

$$R_H(t) = \frac{c}{H(t)} = \frac{3(w+1)}{2}ct, \tag{1.28}$$

where the last equality results from Eq. (1.23) and therefore it is only true for Einstein–de Sitter universes. The Hubble length can be thought as the proper distance travelled by light during the characteristic time scale of expansion, H^{-1}. Comparing Eq. (1.28) with Eq. (1.27) we see that R_H and d_H only differ by a factor of the order of the unity (in particular for $w = 1/3$, $R_H = d_H$). This explains why both of these quantities are often used interchangeably and referred to as the horizon. In practice the largest distance one can observe with electromagnetic

radiation is limited by what is called the **visual horizon**. This is defined as the distance to the surface where the Cosmic Microwave Background Radiation was last scattered. Beyond this *last scattering surface* (LSS) the universe becomes opaque due to the strong interaction (Compton scattering) between matter and radiation. The CMB photons we observe today suffered their last scattering at $z \sim 1000$ when they were at a distance of about $6h^{-1}$ Mpc. This corresponds to a present distance to the LSS of $\sim 6000\, h^{-1}$ Mpc.

Let us now briefly examine how angular sizes and distances to faraway objects are defined. Light emitted from the edges of an object (e.g. a galaxy cluster) located at a coordinate position r and time t, occupies an angular size in the sky given by

$$\theta = \frac{D}{d_A} = \frac{D}{a(t)r} = \frac{D(1+z)}{a_0 r}, \tag{1.29}$$

where D is the object's proper diameter and $d_A(t) = a(t)r$ is the proper distance to the object at the moment of light emission. The second equality results from the fact that the object is observed presently with redshift z. The quantity d_A is called the **angular diameter distance**. The present distance to the object is,

$$a_0 r = a_0 \int_{r_e}^{0} \frac{dr}{\sqrt{1-kr^2}} = a_0 c \int_{a(t)}^{a_0} \frac{da}{a\dot{a}} = \frac{c}{H_0} \int_{a(t)}^{a_0} \frac{da}{a\mathscr{H}(a)}. \tag{1.30}$$

where $\mathscr{H} = H/H_0 = (1-\Omega_0+\Omega_{m0}x^{-1}+\Omega_{r0}x^{-2}+\Omega_{\Lambda 0}(1-x^2))^{0.5}$ and $x = a/a_0 = 1/(1+z)$ (see Eq. (1.18)). The relation between the angular size of objects and their redshifts is therefore dependent on the underlying cosmological model and can in principle be used to constrain cosmological parameters, provided one can find "standard rulers" (see e.g. Ref. [96] for a review on "the standard tests of classical cosmology"). The evaluation of Eq. (1.30) is of particular interest for matter-dominated universes (the phase we believe structures like galaxies and clusters form). For $\Lambda = 0$ the expression Eq. (1.30) can be computed analytically (it was first derived by Mattig in 1958 [70]). One obtains,

$$a_0 r = \frac{2c}{H_0} \frac{\Omega_0 z + (\Omega_0 - 2)\left(\sqrt{1+\Omega_0 z} - 1\right)}{\Omega_0^2 (1+z)}. \tag{1.31}$$

In the case $\Lambda \neq 0$, the evaluation of Eq. (1.30) has to be done numerically. A widely used fitting formula for flat cosmologies with Λ was derived by Ref. [82]:

$$a_0 r = \frac{c}{H_0} \left[\eta(0, \Omega_0) - \eta(z, \Omega_0)\right], \tag{1.32}$$

where

$$\begin{aligned} \eta(z, \Omega_0) &= 2\sqrt{s^3+1}\left[(1+z)^4 - 0.1540 s(1+z)^3 + 0.4304 s^2 (1+z)^2 \right. \\ &\quad \left. + 0.19097 s^3 (1+z) + 0.066941 s^4\right]^{-1/8} \end{aligned} \tag{1.33}$$

and $s^3 = 1/\Omega_0 - \Omega_0$. This fitting formula shows an accuracy better then 0.4% for $0.2 < \Omega_0 < 1$ and any z.

Also useful is the definition of the volume element in the FLRW universes. This is,

$$dV = \sqrt{|g|}\, dr\, d\theta\, d\phi = (ar)^2 \frac{a\, dr}{\sqrt{1-kr^2}}\, d\Omega \tag{1.34}$$

where $|g|$ is the determinant of the metric (1.1) and $d\Omega = \sin\theta\, d\theta\, d\phi$ is the solid angle element. Using Eq. (1.1) and the definition of redshift, one obtains the (physical) volume element per unit of solid angle and unit of redshift,

$$\frac{dV}{d\Omega\, dz} = \frac{c}{H(z)} \frac{(a_0 r)^2}{(1+z)^3} = \frac{c}{H_0} \frac{d_A^2}{\mathscr{H}(z)(1+z)} \tag{1.35}$$

where $\mathscr{H}(z) = H(z)/H_0$ and $a_0 r$ is given by Eq. (1.30).

Combining Eqs. (1.27) and (1.31) we can write an expression for the angular size of the horizon scale at a given time in matter-dominated universes with $\Lambda = 0$. Setting $D = d_H$ we find,

$$\theta_H \simeq 2 \tan \frac{\theta_H}{2} = \frac{\Omega_0^{3/2}\sqrt{1+z}}{\Omega_0 z + (\Omega_0 - 2)\left(\sqrt{1+\Omega_0 z} - 1\right)}. \tag{1.36}$$

Although Eq. (1.27) is an approximate expression for non-flat universes, it's possible to show that Eq. (1.36) is in fact exact for all geometries (see e.g. Refs. [18, 106, 111] for general expressions of d_H and θ). At high redshifts Eq. (1.36) reduces to

$$\theta_H \simeq \frac{180}{\pi} \sqrt{\frac{\Omega_0}{z}}\, \text{deg}. \tag{1.37}$$

This expression tells us that the size of the horizon at the time of last scattering ($z \sim 1000$) occupies today an angular area in the sky no larger then ~ 2 degrees.

1.4 Initial conditions and Inflation

As a mathematical framework of the Big Bang theory, the FLRW models have the great virtue of describing well the dynamical properties of the observable universe (in particular its expansion rate and age). They also give the correct temperature dependence on redshift, which allows Big Bang nucleosynthesis to reproduce the observed light element abundances so well. However, as we will see next, these models alone show an extreme sensitivity to the "initial conditions" required to explain why the universe is the way we observe today. This extreme "fine tuning" of the initial conditions raises a number of important questions which led to the development of the theory of inflation.

1.4.1 Problems with the Big Bang

Some of the main problems regarding the initial conditions of the Big Bang theory are:

- **Horizon problem**: According to Eq. (1.37) there are about 14000 to 65000 causally disconnected regions in the CMB sky, assuming $\Omega_0 \in [0.2\,,\,1]$. If this is true why is the CMBR very isotropic (showing blackbody spectrums with so similar temperatures in all directions)? This is very difficult to understand if these regions were never in thermal contact. Without any other mechanism to explain why the whole sky presents such similar properties one is forced to impose this as an initial condition.

- **Flatness problem**: At early times the Friedmann equation can be written as:

$$|\Omega(t) - 1| = \frac{|k|}{a^2(t)H^2(t)} = \frac{|k|}{\dot{a}^2(t)} \quad , \tag{1.38}$$

  where the quantity $a^2H^2 = \dot{a}^2(t)$ is a decreasing function of time in all matter or radiation dominated Big Bang FLRW universes.[2] This means that as we go back in time the energy density of universe has to be very close to the critical density, $\Omega(t) \to 1$. Dividing Eq. (1.38) by itself written at the present we find that in order to get $\Omega_0 \sim 1$, the energy density needs to be extremely fine tuned in the past. For instance, when the universe was $t = 1$ second of age (nucleosynthesis period) $|\Omega - 1|$ as to be of the order of $\sim 10^{-18}$. This becomes even more drastic at earlier times. At the Planck epoch ($t \sim 10^{-43}$ – a time scale beyond which the classical GR equations should not be used) Ω can deviate from the unity only one part in 10^{60}! This shows $\Omega = 1$ as an unstable critical point, from which any initial deviation larger then what's allowed by Eq. (1.38) leads to a universe much different from that we observe today. So why has the universe to start with an energy density so close to one?

- **Monopoles and other relics problem**: According to particle physics, the standard Big Bang model meets the necessary conditions for variety of "exotic" particles (such as the magnetic monopole, a very stable and massive particle) to be produced during the early radiation dominated phase of the universe. Since these particles are diluted by the expansion as a^{-3} they can very easily become the dominant component of the universe. However no such particles have yet been observed. This either implies that the predictions from particle physics are wrong, or their densities are very small and therefore there's something missing from this evolutionary picture of the Big Bang.

- **Origin of structure problem**: Locally the universe is not homogeneous. It displays a complex hierarchical pattern of galaxies, clusters and super clusters. The general view is that structure forms via gravitational instability from very small "initial" density perturbations. But, what is the origin of these initial perturbations? Without a mechanism to explain their existence one has to assume that they "were born" with the universe already showing the correct amplitudes on all scales, so that gravitational instability can correctly reproduce the present-day structures.

- **Homogeneity and isotropy problem**: Why is the universe homogeneous on large scales? At early times this "homogeneity" had to be even more "perfect". The homogeneous and isotropic FLRW universes form a very special subset of all types of solutions

[2] This can be easily verified by noting that for both matter and radiation dominated universes the second member of Eq. (1.13) is always negative.

of the GR equations. So why would nature "prefer" homogeneity and isotropy from the beginning as opposed to, e.g., having evolved into that stage?

1.4.2 The theory of inflation

The theory of inflation (or simply inflation) was originally proposed by Guth [40] in an attempt to solve some of the above difficulties of the standard Big Bang model. This theory does not replace the Big Bang scenario. It's rather an additional mechanism attached to the early phases of the universe (prior to the radiation-dominated period), which liberates the Big Bang model from its extreme sensitivity to the initial conditions. The mechanism proposed by Guth solves the horizon, flatness and monopole problems. With time it would turn out that inflation is a powerful falsifiable theory for the origin of cosmic structure, which makes predictions that can be confirmed or ruled out against observations.

Inflation is simply defined as any period of the universe's history during which the scale factor $a(t)$ is accelerating,

$$\text{Inflation} \Leftrightarrow \ddot{a} > 0 \Leftrightarrow \frac{d}{dt}\left(cH^{-1}/a\right) < 0. \tag{1.39}$$

These are all equivalent ways of defining inflation. From the last equality we see that during an inflationary phase the comoving Hubble length always decreases. This is a necessary and sufficient condition for inflation to happen. As we noted before, in the early phases of the standard Big Bang scenario $aH = \dot{a}$ is bound to decrease continuously. This leads to the flatness problem. So if we reverse this situation ($aH = \dot{a} > 0$) i.e if the universe experiences a period of accelerated expansion, the energy density parameter in Eq. (1.38) is forced to move away from the critical value $\Omega = 1$ instead of approaching it. This would solve the flatness problem. But when and in what way can inflation occur within the Big Bang scenario?

In its simplest form, inflation is sourced by a homogeneous scalar field φ, known as the *inflaton*, with a stress energy tensor given by $T_{ab} = \varphi_{;a}\ \varphi_{;b} - g_{ab}\mathscr{L}(\varphi)$ and a Lagrangian $\mathscr{L}(\varphi) = \frac{1}{2}\varphi_{;a}\ \varphi_{;b}g^{ab} - V(\varphi)$. The shape of the potential $V(\varphi)$ depends on the details of the model of inflation under consideration. Scalar fields play a central role in describing spontaneous symmetry breaking phenomena in particle physics theories. They usually represent particles with spin zero, such as the Higgs field which is the particle responsible for electroweak symmetry breaking. At this point and for the reminder of the chapter we adopt a unit system where $c = \hbar = 1$.

When we include the contribution of the inflaton field into the second term of Eq. (1.6), the FLRW metric is still the solution of the Einstein equations of GR. The Friedmann and acceleration equations are now modified to:

$$\left(\frac{\dot{a}}{a}\right)^2 = \frac{8\pi G}{3}\left(\rho + \rho_\varphi\right) - \frac{k}{a^2} \tag{1.40}$$

$$\frac{\ddot{a}}{a} = -\frac{4\pi G}{3}\left(\rho + \rho_\varphi + 3(p + p_\varphi)\right). \tag{1.41}$$

where ρ_φ and p_φ are the density and pressure of the field, respectively given by $\rho_\varphi = \dot{\varphi}^2/2 + V(\varphi)$ and $p_\varphi = \dot{\varphi}^2/2 - V(\varphi)$. One should note that although we are not assuming the existence

of the Λ term in Eq. (1.6), the above equations possess the same form of Eqs. (1.12) and (1.13) if we have $\Lambda = -8\pi G p_\varphi = 8\pi G \rho_\varphi \Leftrightarrow p_\varphi = -\rho_\varphi$.

By either applying the conservation law (1.6) to $T_{ab}(\varphi)$ or using the Euler–Lagrange equations on $\mathscr{L}(\varphi)$, we can derive the following equation of motion for the inflaton field,

$$\ddot{\varphi} + 3\frac{\dot{a}}{a}\dot{\varphi} + \frac{dV}{d\varphi} = 0. \tag{1.42}$$

This tells us that whenever the first two terms are negligible ($\ddot{\varphi}\,,\ \dot{\varphi} \simeq 0$) the field experiences a *slow-roll* period, during which its pressure and density are related by $p_\varphi = -\rho_\varphi \simeq V = \text{const.}$ Moreover since ρ_φ is approximately constant and initially ρ decreases as $\rho \propto a^{-4}$, after some time t_i from the Big Bang the energy density of the inflaton field dominates the dynamics of the expansion. This is the beginning of the inflationary period, during which the solution of the Friedmann equation (1.40) is,

$$\frac{a(t)}{a_i} = \begin{cases} \cosh\left[H(t-t_i)\right] & \text{if} \quad \Omega > 1 \\ \exp\left[H(t-t_i)\right] & \text{if} \quad \Omega = 1 \\ \sinh\left[H(t-t_i)\right] & \text{if} \quad \Omega < 1 \end{cases} \tag{1.43}$$

where $a_i = a(t_i) = (3/8\pi GV)^{1/2}$ and the Hubble expansion rate $H = (8\pi GV/3)^{1/2} \simeq \text{const.}$ This is the same dynamical behaviour we find in the de Sitter universe. Regardless of the geometry, after a time interval $t - t_i \gg (3/8\pi GV)^{1/2}$ the scale factor begins to grow exponentially and the universe rapidly behaves as flat ($\Omega = 1$). This is sufficient to remove the unpleasant fine-tuning condition on Ω required by the standard Hot Big Bang theory. However inflation cannot continue indefinitely. At some point the universe needs to re-enter in a decelerating phase which allows primordial nucleosynthesis to reproduce the correct light elements abundances. With an exponential expansion we would now be inhabitants of an "empty" universe.

Inflation ends when the scalar field approaches the minimum of the potential, V. At this point φ ends its slow-roll motion and starts to oscillate around the minimum, V_{min}. As it oscillates the particles described by the field annihilate and the resulting energy is transferred to the cosmological fluid, which experiences a (very rapid) temperature increase. This process is known as *re-heating*. After the re-heating phase the universe becomes radiation dominated and returns to its standard evolution. In a typical inflationary scenario, inflation starts just before the GUT (Grand Unified Theory) phase transition, for $t_i \sim 10^{-34}$s, and finishes soon after this at $t_f \sim 10^{-32}$s. The "amount of inflation" generated during this very short period is usually expressed in terms of number of *e-foldings*,

$$N = \ln\frac{a(t_f)}{a(t_i)} \simeq \int_{t_i}^{t_f} H dt \simeq -8\pi G \int_{\varphi_i}^{\varphi_f} V/V' d\varphi, \tag{1.44}$$

where the last equality results from the use of Eqs. (1.40) and (1.42) under the slow-roll approximation and φ_i and φ_f are the values of the inflaton field at the beginning and the end of the inflationary phase. The amount of inflation produced during this period is therefore

dependent on the inflationary potential. The distance travelled by light during the same time interval is then

$$d(t_f, t_i) = a(t_f) \int_{t_i}^{t_f} \frac{dt}{a(t)} = H^{-1} \left(e^{H(t_f - t_i)} - 1 \right) \simeq H^{-1} e^N \quad , \tag{1.45}$$

which shows that a causally-connected region with size equal to the Hubble volume is exponentially expanded by e^N at the end of inflation, whereas the Hubble radius itself remains approximately constant during the same period, $R_H = H^{-1} \simeq$ const. After the end of inflation the Hubble radius starts to grow again and eventually may enclose at some point regions which were beyond the Hubble volume before inflation started. Another way of restating this is to think in terms of comoving coordinates. During inflation the comoving Hubble length decreases proportionally to $\sim e^{-N}$. Comoving scales of the size of the Hubble radius and smaller are therefore pushed outside the comoving Hubble sphere. After inflation these scales re-enter progressively the Hubble volume as the comoving Hubble radius starts to increase. If the number of e-foldings is sufficiently large, scales that didn't have time to establish causal contact before inflation are still today beyond our observable horizon. This would explain the high degree of isotropy and homogeneity we observe today.

This can also explain why magnetic monopoles and other Big Bang relics are unobservable today. If inflation happens before or during the phase when these particles are created, their density at the end of the inflationary period will decrease by a maximum factor of e^{3N}. Again, if N is big enough the density of these particles can still be very small today and therefore, in practice, unobservable. Of course, this only works if inflation has enough time to dilute these relics (see Ref. [65] for a discussion on the conditions required for this argument to hold for different kinds of relics). It can be shown that the minimum amount of inflation needed to solve these and other problems of the standard Big Bang model is about $N \sim 60$ (see e.g. Refs. [64, 65]).

Despite inflation's success to bring the primordial universe towards homogeneity and a flat geometry (as required by the standard Big Bang model), inflation's most remarkable feature is that it provides a theory for the origin of the primordial inhomogeneities. In the inflationary scenario these inhomogeneities arise from quantum fluctuations about the vacuum state of the inflaton field, which are always present due to the *Uncertainty Principle* (see Refs. [4, 41, 45, 65, 101]). The resulting irregularities can be of scalar (density perturbations) or tensorial (gravitational waves) nature. Their amplitudes on a given scale can be fully specified by the value of inflationary potential, and its derivative with respect to the inflaton field, at the time the scale crosses outside the Hubble radius during the inflationary phase (see e.g. Refs. [63, 64]).

Nowadays the title "standard model of cosmology" usually refers to the Hot Big Bang scenario plus the theory of inflation as the mechanism responsible for the origin of cosmic structure. Inflation generated perturbations are solely produced during the inflationary period and their subsequent evolution is governed by the effects of gravity and cosmic expansion alone. For this reason inflation-generated perturbations are said to be *passive*. Non-gravitational effects, such as gas cooling and heating, only become important at later times when highly non-linear structures (e.g. galaxy clusters) form. An alternative paradigm to inflation are the

theories which consider *topological defects* as the main source of cosmic structure (see e.g. Refs. [25, 49, 60, 110]. In this case, perturbations are said to be *active* as they can arise at any time and evolve also under the effect of non-gravitational forces. This significantly complicates their treatment. However topological defect theories have been recently excluded from being the main source of cosmic structure as they fail to predict the observed features (namely a pronounced first peak and the indication for the existence of secondary acoustic peaks) in the CMB anisotropy spectrum (see Ref. [25]).

Chapter 2

Cosmological Structure Formation

The formation of structure in the universe is one of the most outstanding problems of astronomy. The key point is to understand how small inhomogeneities present in a highly uniform primordial universe can give rise to the complex pattern of structures we observe today. In 1902 Jeans [55] was the first to demonstrate that small density perturbations can grow with time in a homogeneous and isotropic self-gravitating fluid. Slightly overdense regions provide extra gravitational attraction towards them, which causes the in fall of the surrounding material and the increase of their densities. Pressure gradients can resist the effect of gravity and stop the growth of perturbations below a critical minimum length. This process became known as the *gravitational Jeans instability*, and it was first studied in an attempt to describe the formation of planets and stars in a static universe. The theory of gravitational instability was applied to an expanding universe by Lifshitz in 1946 [66], which presented the first general analysis on the evolution of inhomogeneities in FLRW models using *linear perturbation theory*. Since then many authors have worked on achieving a theory that successfully describes the formation of structure in the universe (see e.g. Ref. [79]).

Presently, it is widely accepted that structures grew via gravitational instability from passive density perturbations produced in the primordial universe. As long as the perturbations are small they can be well described in linear perturbation theory. However the accuracy of this perturbative method starts to decrease as perturbations grow larger and higher-order terms would need to be considered at later times. Eventually the perturbative theory itself breaks down at the point when complex non-linear structures form. At this stage other methods need to be used to follow the evolution of structure.

2.1 Density contrast and the power spectrum

Density perturbations are conveniently described by the density contrast or excess function field,

$$\delta(\mathbf{x}, t) \equiv \frac{\rho(\mathbf{x}, t) - \rho_0(t)}{\rho_0(t)} \quad , \tag{2.1}$$

which is a dimensionless quantity that measures, at each point of the space–time, the deviation of the density field $\rho(\mathbf{x},t)$ from the mean density of the universe, $\rho_0(t) = \langle\rho(\mathbf{x},t)\rangle$. If nothing is said in contrary, from hereafter we will assume the spatial coordinates, $\mathbf{x}$, to be comoving. In perturbation theory $\rho_0(t)$ is the density of the unperturbed *background* universe and $\delta\rho_0(t)$ is the perturbation to that background. The time dependence of δ can be followed in linear perturbation theory, which applies whenever δ is small. Predictions for the spatial properties of the density contrast can only be inferred from a statistical approach. Specific predictions for each region of the universe would require the knowledge of its initial conditions. This is something we do not know *a priori* and even if we had information on the specific initial conditions of each point, it would be practically impossible to follow the evolution of large regions of space.

In cosmology, fields like the overdensity contrast, are assumed to be *random fields*, which are fully specified by an infinite set of joint probability distribution functions of the form, $\langle A(\mathbf{x})\rangle$, $\langle A(\mathbf{x})A(\mathbf{x}')\rangle$,... , $\left\langle A(\mathbf{x})A(\mathbf{x}')...A(\mathbf{x^{(n)}})\right\rangle$,... . These are respectively the one-point, two-point,..., n-point probability distribution or *correlation* functions of the field A. The angle brackets denote averages over an ensemble of possible universes. Since we are limited to our own universe, these distributions are inaccessible to us even in principle. In practice it is always assumed that cosmological random fields are **ergodic** and therefore the true probability distribution functions (pdf) can be estimated by replacing the ensemble averages by spatial averages over very large volumes of our universe. Another common assumption is that cosmological random fields are invariant under rotations and translations. This implies, for example, that the one-point pdf is independent of $\mathbf{x}$ and the two-point correlation function is only function of the distance $r = |\mathbf{x} - \mathbf{x}'|$.

A direct consequence of the ergodic hypothesis is that the one-point correlation function of the overdensity contrast is zero, $\langle\delta(\mathbf{x})\rangle = 0$. The two-point correlation function $\xi(r) \equiv \langle\delta(\mathbf{x})\delta(\mathbf{x}+\mathbf{r})\rangle$, can be computed by expanding the overdensity field in a Fourier series[1] over a large box of volume $V = L^3$

$$\delta(\mathbf{x},t) = \sum \delta_k(\mathbf{k},t)e^{-i\mathbf{k}\cdot\mathbf{x}} \tag{2.2}$$

$$\delta_k(\mathbf{k},t) = \frac{1}{V}\int \delta(\mathbf{x},t)e^{i\mathbf{k}\cdot\mathbf{x}}d^3x \tag{2.3}$$

with periodical boundary conditions, which restrict the allowed wave numbers to be $\mathbf{k} = 2\pi(n_1,n_2,n_3)/L$. The numbers n_1, n_2 and n_3 are integers. If the scales of interest are small compared to the box size the summation in Eq. (2.2) can be replaced by an integral multiplied by a prefactor of $V/(2\pi)^3$. The correlation function $\xi(r)$ then reads,

$$\xi(r,t) = \frac{V}{(2\pi)^3}\int \left\langle|\delta_k(\mathbf{k},t)|^2\right\rangle e^{-i\mathbf{k}\cdot\mathbf{r}}d^3k \tag{2.4}$$

$$P(k,t) = \left\langle|\delta_k(\mathbf{k},t)|^2\right\rangle = \frac{1}{V}\int \xi(r,t)\, e^{i\mathbf{k}\cdot\mathbf{r}}d^3r \tag{2.5}$$

[1]We should note that Fourier expansions are only appropriate for flat geometries. For volumes larger then the curvature radius in non-flat universes it's more appropriate to use the generalized solutions of the Helmholtz equation as a basis, see Ref. [51].

where $P(k,t)$, the Fourier transform of the correlation function $\xi(r,t)$, is the *power spectrum* of the density perturbations. The power spectrum is usually redefined in a dimensionless form, as variance per (natural) logarithm interval (e.g. as in Ref. [65, 76]),

$$\mathscr{P}(k,t) \equiv \frac{V}{(2\pi)^3}\, 4\pi k^3\, P(k,t) = \frac{2}{\pi} k^3 \int_0^\infty \xi(r,t)\, \frac{\sin kr}{kr}\, r^2\, dr. \tag{2.6}$$

With this definition the variance of the overdensity field (the zero-lag correlation function $\xi(0,t)$) is simply given by

$$\sigma^2(t) \equiv \left\langle \delta(\mathbf{x},t)^2 \right\rangle = \int_0^\infty \mathscr{P}(k,t)\, \frac{dk}{k}. \tag{2.7}$$

Most models of inflation favour density perturbations of adiabatic nature, with a Gaussian probability distribution of variance σ^2 and a primordial density power spectrum, $P_\delta(k)$, well described by a power law,

$$P_\delta(k) = A\, k^n\,. \tag{2.8}$$

Here n is called the spectral index of scalar perturbations and in most cases it's expected to be close to the unity. The value $n = 1$ is also known as the scale–invariant or Harrison–Zel'dovich power spectrum, [43, 119]. From Eq. (2.1) we see that values of $\delta < -1$ are unphysical. This means that, in reality, the density perturbations can only be considered Gaussian as long as $\sigma(t)$ is small ($\sigma(t) \ll 1$).

A very useful quantity in the study of the statistical properties of the density field is the smoothed density contrast, $\delta(R,\mathbf{x},t)$. This is defined as the convolution of the overdensity field with some normalized *window function*, $W(R, r = |\mathbf{x}-\mathbf{x}'|)$ (the smoothing kernel), which falls rapidly to zero beyond $r > R$,

$$\delta_k(R,\mathbf{x},t) = \frac{1}{V} \int W(R, |\mathbf{x}-\mathbf{x}'|)\, \delta(\mathbf{x},t)\, d^3x'\,. \tag{2.9}$$

The normalization factor is such that $V = \int W(R, |\mathbf{x}-\mathbf{x}'|)\, d^3x'$. The concept of smoothing is important not only because many observational procedures automatically introduce smoothing (due to resolution effects), but also because it produces a cut-off on the large k modes of δ that describe small-scale structure. In practice smoothing erases the contribution from modes with k larger then $\sim 1/R$. Smoothing is also useful as it reduces the variance of the overdensity field and therefore it allows to use linear perturbation theory to follow the evolution of the smoothed density field for longer times. Common smoothing kernels are the Gaussian and the Top-hat filters (see e.g. Ref. [76]),

$$\text{Gaussian} : W = \frac{V}{(2\pi)^{3/2} R^3}\, e^{-r^2/2R^2} \quad ; \quad W_k = e^{-k^2R^2/2} \tag{2.10}$$

$$\text{Top} - \text{hat} : W = \frac{3V}{4\pi R^3} \begin{cases} 1 & \text{if } r < R \\ 0 & \text{otherwise} \end{cases} \quad ; \quad W_k = 3\left[\frac{\sin(kR)}{(kR)^3} - \frac{\cos(kR)}{(kR)^2}\right], \tag{2.11}$$

where the right-hand side expressions are the Fourier transforms of each of the filters.

Of more importance than the smoothed overdensity field itself (which is zero for large integration volumes) is its variance and higher moments of the power spectrum. These can be defined as,

$$\sigma_N^2(R,t) \equiv \frac{V}{(2\pi)^3} \int W_k^2(R,k)\, P(k,t)\, k^{2N}\, d^3k\,, \tag{2.12}$$

from which is easy to obtain the variance of the smoothed overdensity on the scale R,

$$\sigma^2(R,t) \equiv \left\langle \delta^2(R,\mathbf{x},t) \right\rangle = \int_0^\infty W_k^2(R,k) \mathscr{P}(k,t)\, \frac{dk}{k}. \tag{2.13}$$

A similar expression is valid for the variance of the smoothed peculiar velocity field,

$$\sigma_V^2(R,t) \equiv \left\langle \delta V^2(R,\mathbf{x},t) \right\rangle = \int_0^\infty W_k^2(R,k) \mathscr{P}_V(k,t)\, \frac{dk}{k}. \tag{2.14}$$

where $\mathscr{P}_V$ is the power spectrum of the peculiar velocity field. At the present we have $\mathscr{P}_V(k,t_0) \simeq H_0\, \Omega_0^{0.6}\, \mathscr{P}(k,t_0)/k^2$, [65]. The smoothing scale R is often specified by the mass within the volume defined by the window function at the present time. In the case of the Top-hat filter this is $M = \rho_0(t_0) 4\pi R^3/3 = 1.16 \times 10^{12}\, h^{-1}\, (R/(h^{-1}\mathrm{Mpc}))^3\, \mathrm{M}_\odot$ and the variance of the smoothed overdensity field coincides with the mass fluctuation on the mass scale M [18].

2.2 Linear perturbation theory

The evolution of the density perturbations in an expanding FLRW universe is in general a difficult problem to tackle as it implies the study of the behaviour of perturbations on a large range of scales for different matter components of the cosmic fluid. At a given time, the total energy density depends on the nature and relative abundance of the individual fluid components, which can exist in the form of collisional or collisionless material and be of relativistic or non-relativistic nature. Free-streaming effects and the relative size of the perturbations with respect to both the Hubble and the *curvature radius*, defined as $R_K = a|k|^{-1/2}$, are other factors which affect the growth of perturbations and influence the shape of the observable density power spectrum $\mathscr{P}(k,t)$.

An important simplification to the structure formation problem is that perturbations are expected to be small during the first stages of the structure formation process and therefore the equations governing their evolution can be written in a perturbative form where all non-linear terms can be neglected. In general this *linear regime* proves to be a good approximation whenever $\delta \ll 1$. Although the detailed analysis of the growth of perturbations in a multi-component cosmological fluid requires a general relativistic treatment (see Ref. [65]), many fundamental aspects of the evolution of perturbations on scales smaller then the Hubble radius can be followed by using Newtonian mechanics.[2] This is ultimately justified by Birkhoff's theorem [9] of GR which states that the space inside a spherical volume (smaller then the

[2]Note that for "reasonable" values of $\Omega + \Omega_\Lambda$ the Hubble radius is always smaller then curvature radius, R_K. From Eq. (1.14) we have $R_K = a|k|^{-1/2} = |\Omega + \Omega_\Lambda - 1|^{-1/2} cH^{-1} > R_H$ in the range $0 < \Omega + \Omega_\Lambda < 2$.

curvature radius) embedded in a FLRW universe must be flat and unaffected by the matter distribution outside the sphere. Perturbations on scales larger then the Hubble radius need to be treated within the framework of GR. However one should note that as the universe expands the Hubble radius gradually encompasses perturbations of larger wavelengths. This is true for both matter and radiation-dominated eras where the Hubble radius, $R_H \propto t$, grows faster then physical wavelength of any given scale, $\lambda_{\rm phy} = a(t)\lambda_{\rm com} \propto t^{\alpha}$ with $\alpha < 1$ in both cases. In the reminder of this section we will use the terms horizon and Hubble length interchangeably.

2.3 Sub-horizon perturbations in non-relativistic fluids

Here we introduce the basic equations which govern the linear growth of perturbations on scales smaller then the horizon, in non-relativistic fluids, for both collisional and collisionless systems. In a collisional system particles interact and experience short-lived accelerations due to "shocks" with other particles. Collisionless particles practically don't interact and their motions are usually a lot less susceptible to strong accelerations as they generally move under the influence of a mean force field. Examples of collisional and collisionless systems are respectively the baryon-photon fluid at matter–radiation equality and the cold dark matter component of the universe.

Collisional matter: the classical equations describing the dynamical evolution of an ideal fluid of collisional gas particles, evolving adiabatically, in an expanding universe are respectively the *continuity*, *Euler* and *Poisson* equations:

$$\frac{\partial \rho}{\partial t} + \nabla \cdot (\rho \mathbf{v}) = 0 \tag{2.15}$$

$$\frac{\partial \mathbf{v}}{\partial t} + (\mathbf{v} \cdot \nabla)\mathbf{v} = -\nabla \left(\phi + \frac{p}{\rho} \right) \tag{2.16}$$

$$\nabla^2 \phi = 4\pi G \rho \tag{2.17}$$

where $\rho(\mathbf{r}, t)$, $p(\mathbf{r}, t)$ and $\phi(\mathbf{r}, t)$ are the density, pressure and gravitational potential at the physical position $\mathbf{r} = a(t)\mathbf{x}$ and time t. The velocity field $\mathbf{v}$ is simply $\mathbf{v} = \dot{a}\mathbf{x} + a\mathbf{u}$ where $\mathbf{u} = \dot{\mathbf{x}}$ is the peculiar velocity in a comoving reference frame, which measures the deviations of the velocity field $\mathbf{v}$ to the Hubble flow $\mathbf{v}_0 = \dot{a}\mathbf{x} = H\mathbf{r}$. In these $a(t)$ is the scale factor obeying the Friedmann equation. Since we are assuming the existence of small inhomogeneities, the peculiar velocity field $\mathbf{u}$ is generally non-zero and constitutes a perturbation to $\mathbf{v}_0$. The usual way to proceed to describe the perturbations is to expand the other fields ρ, ϕ and p in terms of their unperturbed values, respectively, $\rho_0(t)$, $\phi_0(t)$ and $p_0(t)$, plus perturbations and substitute them in Eqs. (2.15–2.17). Rewriting the resulting system of equations in comoving coordinates, dropping all non-linear terms and Fourier transforming all quantities with respect to $\mathbf{x}$, one obtains (after some algebra) the following second-order differential equation, describing the evolution of each Fourier mode of the density contrast:

$$\ddot{\delta} + 2\frac{\dot{a}}{a}\dot{\delta} + \left(\frac{c_S^2 k^2}{a^2} - 4\pi G \rho_0 \right) \delta = 0 \,. \tag{2.18}$$

Note that $k = |\mathbf{k}|$ is a comoving wavenumber and $c_S^2 \equiv (\partial p/\partial\rho)_S$ is the adiabatic sound speed. This well-known result introduces an important length scale (and corresponding wavenumber), known as *Jeans length* (and *Jeans wavenumber*),

$$\lambda_{\rm J} = \frac{2\pi}{k_{\rm J}} \quad ; \qquad k_{\rm J} = \frac{2a}{c_S}\sqrt{\pi G\rho_0}, \tag{2.19}$$

which separates two different regimes for the evolution of δ:

1. **For $\mathbf{k} < \mathbf{k}_{\rm J}$ ($\lambda > \lambda_{\rm J}$)**: perturbations on these scales are gravitationally unstable. In this case Eq. (2.18) admits two independent solutions, one with increasing and another with decreasing amplitude. The decaying solution erases itself with time. The growing solution is physically more interesting. Its growth depends on the evolution of the scale factor.

2. **For $\mathbf{k} > \mathbf{k}_{\rm J}$ ($\lambda < \lambda_{\rm J}$)**: perturbations on these scales do not grow. In fact their amplitudes oscillate like an acoustic wave and even may decrease depending on the evolution of the sound speed, c_S.

An important example of a collisional system is the baryon–photon fluid prior to recombination. Perturbations of size smaller then the horizon can be followed with Eq. (2.18) during the period between matter radiation equality and recombination, $z_{\rm eq} > z > z_{\rm rec}$. The adiabatic sound speed is that of a plasma with matter and radiation, $c_S = c/\sqrt{3}(1+3\rho_m/4\rho_r)^{-1/2}$, and varies with redshift. Using this result in Eq. (2.19) we find that $\lambda_{\rm J}$ is always larger then the Hubble radius, for $z > z_{\rm rec}$ (see e.g. Ref. [18]). This implies that all perturbations re-entering the horizon during this period are unable to grow as they start to oscillate soon after the horizon re-entry. For wavemodes larger then the Hubble radius, Eq. (2.18) is no longer applicable. At this point one has to resort to GR linear perturbation theory. Equation (2.18) is also not accurate for redshifts earlier then $z_{\rm eq}$, as the energy density of the fluid is dominated by relativistic particles.

Collisionless matter: An important characteristic of collisionless systems is that they can develop multi-stream flows for which there may not exist a unique matter velocity at a given position. In this case the continuity and Euler equations, (2.15), (2.16), are not applicable and need to be replaced by the *Liouville-Vlasov* or *collisionless Boltzmann* equation. The dynamical evolution of a collisionless system is then described by

$$\frac{\partial f}{\partial t} + \mathbf{v}\cdot\frac{\partial f}{\partial \mathbf{r}} - \nabla\phi\cdot\frac{\partial f}{\partial \mathbf{v}} = 0 \tag{2.20}$$

$$\nabla^2\phi = 4\pi G\rho\,, \tag{2.21}$$

where $f(\mathbf{r},\mathbf{v},t)$ is the *phase space density* or *distribution function* of the system. It gives the number density of particles in the volume element d^3r centered at $\mathbf{r}$, with velocities in the range d^3v around $\mathbf{v}$. The density field is then $\rho = m\int f(\mathbf{r},\mathbf{v},t)d^3v$, where m is the mean mass of the particles. To describe the linear evolution of density perturbations one proceeds in a similar way to what was done in collisional case. The starting point is to write f, ϕ and ρ in terms

of their unperturbed values, $f_0(\mathbf{v},t)$, $\rho_0(t) = m\int f_0(\mathbf{v},t)d^3v$ and $\phi_0(t)$ plus perturbations and then substitute these in the above equations rewritten in terms of a comoving coordinate system. After dropping all non-linear terms and Fourier transforming all quantities, one finds again two distinct regimes of evolution separated by the wavenumber,

$$k_{\rm FS} = \frac{2a}{v_*}\sqrt{\pi G\rho_0} \quad ; \qquad v_*^{-2} = \frac{\int \frac{\mathbf{k}\cdot\partial f_0/\partial \mathbf{v}}{\mathbf{k}\cdot\mathbf{v}}\, d^3v}{\int f_0\, d^3v}\,, \tag{2.22}$$

where v_* is generally of the order the mean velocity dispersion of the particles. When $f_0(\mathbf{v})$ is assumed to be Maxwellian distributed, v_* coincides with the value of σ of the distribution. We have:

1. **For $\mathbf{k} < \mathbf{k}_{\rm FS}$**: perturbations on these scales are gravitationally unstable. The equation describing the evolution of the density contrast for each of these modes is [79]:

$$\ddot{\delta} + 2\frac{\dot{a}}{a}\dot{\delta} - 4\pi G\rho_0\delta = 0\,. \tag{2.23}$$

   As in the collisional case, the growing solution of this equation depends on the expansion rate of the universe.

2. **For $\mathbf{k} > \mathbf{k}_{\rm FS}$**: perturbations on these scales are damped due to the free-streaming of particles from overdense regions into regions of low density. This dissipation process is known as *phase mixing* or *Landau damping*. The typical time-scale for the dissipation of a perturbation of size λ is $\tau \simeq \lambda/v_*$. In the case of CDM particles the "dissipation speed", v_*, is very small and therefore perturbations on cosmological scales are practically unaffected. However in a HDM scenario this effect can be very strong. Assuming HDM is made of massive (light) neutrinos, perturbations on scales smaller then the free-streaming scale $\lambda_{FS} \simeq 20\ (m_\nu/30\,{\rm eV})^{-1}$ Mpc, are strongly suppressed (see e.g. Ref. [61]). In fact more accurate calculations indicate even larger λ_{FS}'s for neutrino masses of the order of $m_\nu \simeq 30$ eV, [12].

Due to the similarity with Eq. (2.19), the wavenumber $k_{\rm FS}$ is sometimes referred to as Jeans wavenumber and denoted by $k_{\rm J}$.

It's particularly interesting to investigate the solutions of Eq. (2.23) for matter and curvature (if it exists) dominated universes. Since pressure is negligible the results derived also apply to collisional systems (Eqs. (2.18) and (2.23) coincide for $c_S \simeq 0$). The main conclusions are that perturbations grow as $\delta_k \propto t^{2/3}$ during matter domination and remain practically constant as soon as curvature begins to be the driving term of the expansion (if ever). Detailed solutions following through a matter–curvature transition can be found in Ref. [79]. Another important scenario for the late evolutionary stages of the universe is when the Friedman equation becomes dominated by a cosmological constant term. In this case the growth of perturbations is also strongly suppressed as soon as $\Omega_\Lambda \gg \Omega_m$ [79].

Equation (2.23) can also be used to study the evolution of perturbations in the CDM component during the radiation-dominated phase of the universe ($z > z_{\rm eq}$). During this period the

"effect" of radiation on any collisionless non-relativistic material is simply that of controlling the overall rate of expansion. In this case the solution of Eq. (2.23) is $\delta_k \propto 1 + 3y/2$ with $y = \Omega_m/\Omega_r = a(t)/a(t_{\rm eq})$ [79]. Therefore perturbations on the collisionless non-relativistic component remain 'frozen' practically until $1 + z_{\rm eq} = a_0/a(t_{\rm eq})$. The transition from radiation to matter domination is smooth and matches the law $\delta_k \propto t^{2/3}$ found above, soon after $z_{\rm eq}$. This "stagnation" period is known as the Mészáros effect.

2.4 Relativistic fluids and super-horizon perturbations

As mentioned earlier, during the radiation-dominated period, $z > z_{\rm eq}$, photons and baryonic matter constitute a collisional system, with sound speed rapidly approaching $c_S = c/\sqrt{3}$. During this period the classical equations which lead to Eq. (2.18) are no longer applicable. On scales smaller then the horizon, perturbations can be well described by special relativistic fluid mechanics. The resulting equation for the evolution of δ_k has the same form of Eq. (2.18) with the factor '4' in the last term inside the parenthesis replaced by '32/3' (see e.g. Ref. [18]). This 'relativistic correction' decreases the Jeans length definition by $\sqrt{8/3}$. Accounting also for $c_S = c/\sqrt{3}$, the baryonic Jeans length is $\lambda_{\rm J} \simeq 3\,c\,t$, which is larger then the Hubble radius. This extends what we said earlier regarding baryon-photon perturbations to redshifts higher then $z > z_{\rm eq}$. Density perturbations in the baryon-photon fluid are forced to oscillate (without growth) as soon as they re-enter the horizon.

There's another important effect in which perturbations in the baryon-photon fluid can be suppressed. Before recombination photons and baryons are tightly coupled due to Thomson scattering. The mean free path of the photons is $\lambda_\gamma \equiv 1/(n_{\rm e}\sigma_{\rm T}) \propto x_{\rm e}^{-1}(1+z)^{-3}(\Omega_B h^2)^{-1}$, where $\sigma_{\rm T}$ is the Thomson cross section and $x_{\rm e}$ and $n_{\rm e}$ are respectively the fraction and number density of free electrons. The ideal fluid approximation holds as long λ_γ is small. As the universe recombines and the fraction of free electrons decreases, the mean free path of the radiation becomes larger and the perfect fluid approximation starts to break down. Photons can then diffuse out of perturbations of size comparable to the mean free path, dragging with them the electron-baryon plasma. This effect is known as *Silk damping* and can erase perturbations on scales smaller than $\lambda_{\rm S} = 3.5(\Omega_0/\Omega_B)^{1/2}(\Omega_0 h^2)^{-3/4}$ Mpc [61].

Density perturbations on scales larger than the Hubble radius (super-horizon modes) need to be treated within the general relativistic theory of cosmological perturbations. The main difficulty with these modes is that the density perturbation, $\delta\rho$, is a *gauge* dependent quantity and therefore different gauge choices can lead to distinct predictions for the behaviour of $\delta\rho$ outside the horizon. A natural approach to the problem is to formulate the evolution of the perturbations in terms of gauge-invariant quantities (see e.g. Refs. [2, 73]). Of particular importance to $\delta\rho$ is the gauge-invariant variable ξ, which is related to the density perturbation by $\xi = \delta\rho/(p_0 + \rho_0)$ at horizon crossing [4]. A very nice feature of ξ is that it is constant outside the horizon. So the problem of finding the amplitude of a given mode of the density perturbations at the horizon re-entry reduces to the problem of computing ξ at the moment that modes crossed outside the Hubble radius during inflation. Evaluating ξ at both horizon

crossings we have:

$$\frac{1}{(1+w)}\left(\frac{\delta\rho}{\rho_0}\right)_{\text{hor. in}} = \left(\frac{\delta\rho_\varphi}{\rho_{\varphi 0}+p_{\varphi 0}}\right)_{\text{hor. out}} = \left(\frac{V'(\varphi)\delta\varphi}{\dot{\varphi}^2}\right)_{\text{hor. out}}, \tag{2.24}$$

where V is the inflationary potential, φ the inflaton field and, during inflation, $\rho_\varphi + p_\varphi = \dot{\varphi}^2$ (see Section 1.4.2). The value of w depends on the instant a given scale re-enters the horizon ($w = 1/3$ during radiation domination and $w = 0$ during the matter-dominated period). This result directly connects the amplitude of the density perturbations at the horizon re-entry with the primordial quantum mechanical fluctuations of the inflaton field, which can be computed for a given model of inflation. The evolution of the perturbations after horizon re-entry can then be followed by using the above equations of fluid mechanics, valid inside the horizon.

2.4.1 Relativistic multi-fluid case

Unlike the systems we have considered so far, the real universe does not behave like a simple fluid. We know for a fact that the universe is made of different species of relativistic and non-relativistic particles co-existing in a multi-component system. Detailed predictions for evolution of the density perturbations therefore require a careful analysis of the evolution of the perturbations in each of these components. In general each component can be considered as a single fluid subjected to its own pressure (described by an individual equation of state) and the gravity produced by all existing particles. In some cases collisions between particles of different species give rise to energy exchanges between fluids, which then evolve as coupled systems. The evolution of such a multi-component fluid is therefore described by a system of coupled second-order equations (each representing a different component), which usually can only be solved numerically.

Observations indicate that we need to consider at least four types of particles: Collisionless dark matter, baryons (which in an abuse of language account also for the electron population), collisional photons and collisionless (relativistic) neutrinos. We are mainly interested in the evolution of the total density perturbations of this system and in particular we want to determine how the amplitude of a perturbation mode at the horizon re-entry evolves to the present. The most general treatment involves solving the appropriate Boltzmann transport equations for both matter and radiation in a evolving universe. This is a non-trivial task as diffusion and free-streaming effects on both collisional and collisionless particles need to be considered and relativistic particles can become non-relativistic as the temperature decreases. Particular difficulties arise due to the fact that photons change from being a tightly-coupled fluid with the baryons to become a "collisionless" component after decoupling.[3] The result of solving the transport equations is usually expressed in terms of a *transfer function*, $T(k,t)$, which encodes all of the above effects and gives the amplitude of the total density perturbation of the mode k at the time t.

[3]Photons are believed to interact again with free electrons when the universe becomes re-ionized at later times.

2.4.2 Density transfer function and the power spectrum

The transfer function is commonly defined as the ratio between the amplitude of a given mode and the amplitude of a mode with an arbitrary large wavelength, so that in the limit $k \to 0$ we have $T(k,t) \to 1$. In practice $\delta_k(k,t) = T(k,t)\,\delta_k(k_{\rm hor},t)$ where $k_{\rm hor}$ is the largest mode inside the horizon at t. Many codes have been developed to compute numerically the detailed shape of the transfer function given a particular model of the universe (e.g. the recently popular code CMBFAST [1,98]). Results depend on the type of mechanism responsible for the perturbations and on the relative abundance and nature of the matter and radiation components assumed for that model. Once these are specified the shape of $T(k,t)$ reflects the effects of growth under self-gravity, pressure and damping due to diffusion and free-streaming, discussed earlier. In general, the overall effect is to reduce the amplitude of the short-wavelength modes relative to the amplitude of the long-wavelength modes. In a typical CDM scenario, the transition point is around the wavenumber corresponding to the size of the horizon at the redshift of matter–radiation equality, $k_{\rm eq} \simeq 14\Omega_0^{-1}h^{-2}\,{\rm Mpc}^{-1}$. This is because the dark matter component dominates the fluid and perturbations entering the horizon after $z_{\rm eq}$ ($k < k_{\rm eq}$) can start to grow more efficiently, whereas modes with $k > k_{\rm eq}$ are unable to grow essentially due to the Mészáros effect and Silk damping.

The transfer function for cold dark matter models can be approximated by the following analytical fitting formula derived in Ref. [3]:

$$T(q) = \frac{\ln(1+2.34q)}{2.34q}[1+3.89q+(16.1q)^2+(5.46q)^3+(6.71q)^4]^{-1/4}\,, \qquad (2.25)$$

where $q \equiv (k\theta/h\ {\rm Mpc}^{-1})/\Gamma$, $\theta = T_{CMB}/2.73$, and T_{CMB} is the CMBR mean temperature. The *shape parameter*, Γ, is given by [104]

$$\Gamma = \Omega_0 h\,\exp[-\Omega_{B0}(1+\sqrt{2h}/\Omega_0)]\,. \qquad (2.26)$$

The fitting formula (2.25) is known as the BBKS transfer function for CDM models and it was first derived assuming a pure cold dark matter scenario ($\Omega_{B0} = 0$). The inclusion of a baryonic component preserves the same functional shape of Eq. (2.25) but has the effect of lowering the "apparent" dark matter density parameter by the exponential factor in Eq. (2.26), [77, 104]. These expressions also assume a number of families of massless neutrinos equal to $N_\nu = 3$. For different values of N_ν a multiplicative factor of $(g_*/3.36)^{-1/2}$ is sometimes considered in Eq. (2.26), where $g_* = 2 + 2(7/8)(4/11)^{4/3}\,N_\nu$ is the number of effective degrees of freedom of the neutrinos [24]. Fitting formulae for other popular structure formation transfer functions can be found in Refs. [3, 29].

According to Eq. (2.5), the density power spectrum $P(k,t)$ differs from its primordial value $P_\delta(k)$ simply by the square of the transfer function, $P(k,t) \propto T(k,t)^2\,P_\delta(k)$. Since most of the modulating processes shaping $T(k,t)$ finish by the recombination epoch, $t_{\rm rec}$, only times after $t > t_{\rm rec}$ are of interest. After recombination the power spectrum $\mathscr{P}(k,t)$ can be written as [64, 65, 76]

$$\mathscr{P}(k,t) = \frac{g^2(\Omega,\Omega_\Lambda)}{g^2(\Omega_0,\Omega_{\Lambda 0})}\left(\frac{k}{aH}\right)^4 T^2(k,t)\,\delta_H^2(k)\,, \qquad (2.27)$$

where $g(\Omega, \Omega_\Lambda)$ is the linear growth suppression factor, $\delta_H^2(k) \equiv \langle(\delta\rho/\rho)^2\rangle_{aH=k}$ specifies the amplitude of the density power spectrum at the horizon re-entry and the quantities Ω, Ω_Λ and aH are to be computed at the time t. The suppression factor $g(\Omega, \Omega_\Lambda)$ gives the rate of growth of the density perturbations relative to the growth in the Einstein–de Sitter Universe, $\delta_k \propto (aH)^{-2} \propto t^{2/3}$. Note that with this definition all cosmological models give the same density power spectrum at the present. Since perturbations grow less rapidly in low-density models (with or without cosmological constant), structures need to form earlier so that the same density power spectrum is obtained with these models at the present. The suppression growth factor can be calculated analytically for open models without cosmological constant (see Ref. [79]). For flat models with Λ the calculation involves an integral which cannot be done analytically. In practice it's common to use the following accurate approximation, valid during the matter domination era, for both cases [16],

$$g[\Omega(z), \Omega_\Lambda(z)] = \frac{5}{2}\Omega(z)\left[\Omega(z)^{4/7} - \Omega_\Lambda(z) + \left(1 + \frac{1}{2}\Omega(z)\right)\left(1 + \frac{1}{70}\Omega_\Lambda(z)\right)\right]^{-1}, \qquad (2.28)$$

where the redshift dependence of the matter and cosmological constant density parameters ($\Omega \equiv \Omega_m$) are respectively,

$$\Omega(z) = \begin{cases} \frac{\Omega_0(1+z)}{\Omega_0(1+z)+(1-\Omega_0)}\,, & \text{if} \quad \Omega < 1;\ \Lambda = 0 \\ \\ \frac{\Omega_0(1+z)^3}{\Omega_0(1+z)^3+1-\Omega_0}\,, & \text{if} \quad \Omega = 1 - \Omega_\Lambda \end{cases} \qquad (2.29)$$

and

$$\Omega_\Lambda(z) = \frac{1 - \Omega_0}{\Omega_0(1+z)^3 + 1 - \Omega_0}\,, \qquad (2.30)$$

which is only valid for flat cosmologies. If the primordial power spectrum is well described by the power-law in Eq. (2.8) we have,

$$\delta_H^2(k) = \delta_H^2(k_0)\left(\frac{k}{k_0}\right)^{n-1}, \qquad (2.31)$$

where $\delta_H(k_0)$ is a normalization factor at some arbitrary comoving scale k_0. The value of $\delta_H(k_0)$ can be set so that (2.27) reproduces the correct amplitude of the CMBR anisotropies on the scales observed by COBE. Another way of specifying the normalization of the density power spectrum is by quoting the *rms* dispersion of the overdensity field smoothed on some scale probed by large-scale structure observations. Traditionally, the smoothing chosen is the Top-Hat filter on a scale of size $8h^{-1}\,\mathrm{Mpc}^{-1}$. The corresponding smoothed *rms* dispersion is denoted by $\sigma_8 \equiv \sigma(R = 8h^{-1}\,\mathrm{Mpc}^{-1}, t_0)$. The normalization is then $\sigma_8^2 = \mathscr{P}(k_{\rm eff})$, where $k_{\rm eff}$ is an effective wavenumber well approximated by $k_{\rm eff} = 0.172 + 0.011\,[\ln(\Gamma/0.34)]^2$ for a CDM-like power spectrum [76]. One of the best methods to constrain the value of σ_8 is by confronting the observed number density of local galaxy clusters (selected in various ways) with the predictions given by the Press–Schechter theory [86] or other mass-function models. This method, originally proposed in Refs. [32, 48] and later popularized by the work in Ref. [116], has been developed by many authors (see e.g. Refs. [81, 85, 109] and references therein) to alow the normalization of the density power spectrum for a range of cosmologies. For example, according to the work in Ref. [109]: $\sigma_8 = 0.56\,\Omega_0^{-\alpha}$, with $\alpha = 0.47$ and $\alpha = 0.34$ respectively for flat ($\Omega_{k0} = 0$) and open ($\Omega_0 < 1$, $\Omega_{\Lambda 0} = 0$) cosmologies.

2.5 Non-linear evolution of perturbations

As mentioned earlier, linear perturbation theory applies when perturbations are small, $\delta \ll 1$. This is guaranteed almost everywhere in space as long as the *rms* fluctuations of the density contrast are much smaller then the unity, $\sigma(t) \ll 1$. Regions of space with $\delta(\mathrm{x}, t) \gtrsim 1$ are initially very rare, but as perturbations evolve under the effects of gravitational instability more and more of such regions appear and the linear perturbation theory become inappropriate to describe a progressively larger number of regions. A way of extending the use of linear theory is to consider the linear evolution equations applied to the smoothed density contrast $\delta(R, \mathrm{x}, t)$ instead of $\delta(\mathrm{x}, t)$. As before the linear regime applies as long as $\sigma(R, t) \ll 1$, in which case perturbation modes smaller then $k \lesssim R^{-1}$ evolve linearly. Of course, this is only useful if the scales of interest are larger then the smoothing scale R.

A natural way to proceed to describe perturbations during their first stages of non-linear evolution (*quasi-linear* regime) is to consider second order terms in the evolution equations of δ [79]. This method has however a limited range of applicability because higher-order terms become also important very rapidly. In general is considered that the transition from the linear regime to the stage of quasi-linear or non-linear evolution occurs around $\sigma(R, t) \sim 1$.

The best way to follow the full evolution of perturbations is, undoubtly, by using numerical N–body simulation techniques. Some of these will be described in detail in Chapter **??**. However there are some very useful analytical approximations which can give a good insight on the general problem of describing perturbations during the first stages of their non-linear evolution. Some of these will be reviewed next. The major advantage of such analytical or semi-analytical methods is that they are generally more flexible and a lot less time consuming then numerical simulations.

2.5.1 Spherical collapse model

The spherical collapse model (see e.g. Refs. [75, 79]) can be used to give an estimate of how dense and when a spherically symmetric overdense distribution of matter abandons the general expansion of the universe and starts to gravitationally collapse towards its centre.

When the density of the overdense region becomes slightly larger then the critical density it starts to behave as a small closed universe, which evolves independently of the outside space. Initially the sphere will keep on expanding with the universe until it reaches a maximum radius, known as the *turnaround* point, and subsequently collapses after a time interval, t_{coll}, equal to double the time it takes to get to maximum expansion, t_{max}. Assuming matter domination and that the universe is globally Einstein–de Sitter, it's possible to show that the linear evolution of the density perturbation inside the sphere is given by $\delta_{\mathrm{lin}} = 3/20(6\pi t/t_{\mathrm{max}})^{2/3}$. This indicates that the linear overdensity at turnaround and collapse are respectively:

$$\delta_{\mathrm{lin}}^{\mathrm{turn}} = 3/20(6\pi)^{2/3} \simeq 1.06 \quad ; \qquad \delta_{\mathrm{lin}}^{\mathrm{coll}} = 3/20(12\pi)^{2/3} \simeq 1.686\,. \tag{2.32}$$

The spherical collapse model also allows one to compute the non-linear density contrast at

both of these instants. In the first case we have

$$1 + \delta_{\rm nonlin}^{\rm turn} = (3\pi/4)^2 \simeq 5.55 \tag{2.33}$$

and at collapse the spherical model predicts an infinite density. This happens because pressure forces resisting the gravitational infall are ignored. More realistically we expect that part of the kinetic energy of collapse is converted into random motion of particles and the object will eventually reach a state of *virial equilibrium* characterized by a temperature, $T_{\rm v}$, and radius, $R_{\rm v}$. Using the virial theorem to equate the virial energies at the instants of maximum expansion and compression one finds that $R_{\rm v} = R_{\rm max}/2$, where $R_{\rm max}$ is the radius of the spherical region at maximum expansion. Numerical simulations confirm that $R_{\rm v}$ is in fact a good estimate of the radius of the collapsed sphere and that $\delta_{\rm lin}^{\rm coll}$ is a good indicator of when the object becomes virialized. If we assume that at the time of collapse, $t_{\rm coll} = 2t_{\rm max}$, the object virializes with radius $R_{\rm v}$, the non-linear overdensity is then

$$1 + \delta_{\rm nonlin}^{\rm vir} = 18\pi^2 \simeq 178 \tag{2.34}$$

which is in very good agreement with results from simulations, see Ref. [17].

For non Einstein–de Sitter universes the predictions from the spherical collapse model are slightly changed. In general both linear and non-linear overdensities at collapse are functions of the matter density, Ω_0. However in low-density models, it's possible to show that the variations in $\delta_{\rm lin}^{\rm coll}$ are less than $\sim 5\%$ in the range $\Omega_0 \sim 0.1$–1 and that the overdensity at collapse needs to be corrected by $\Omega_0^{-0.7}$ for $\Omega_\Lambda = 0$ universes and by $\Omega_0^{-0.45}$ for flat universes with Λ [30, 31, 116]. Sometimes the non-linear overdensity is expressed in terms of the critical density instead of the background density, $\Delta \equiv \rho(t)/\rho_{\rm crit} = (1 + \delta_{\rm nonlin})\,\Omega$. In this case it is usually referred to as the non-linear *density contrast* (instead of non-linear overdensity, see e.g. Refs. [30, 31]). For detailed calculations involving the evolution of the density contrast at collapse, $\Delta_{\rm c}(z)$, there is the following fitting formula, from Ref. [13]:

$$\Delta_{\rm c}(z) = \begin{cases} 18\pi^2 + 60x - 32x^2\,, & \text{if} \quad \Omega_\Lambda = 0 \\ 18\pi^2 + 82x - 39x^2\,, & \text{if} \quad \Omega = 1 - \Omega_\Lambda, \end{cases} \tag{2.35}$$

where $x = \Omega(z) - 1$. This expression is accurate to 1% level in the range $\Omega \sim 0.1$–1.

2.5.2 Zel'dovich approximation

The Zel'dovich approximation, [99, 119], is a very successful first–order Lagrangian perturbation theory, which describes perturbations with respect to particle positions rather then to the density field (as described in the Eulerian perturbative method). In this approach, particles move in straight lines after being displaced from their original (comoving) positions by the action of a initial velocity field sourced by the density perturbations. According to this approximation, the comoving position and peculiar velocity of a given particle at the time t are:

$$\mathbf{x}(t) = \mathbf{q} + D(t)\,\mathbf{u}(\mathbf{q}) \quad ; \qquad \dot{\mathbf{x}}(t) = \dot{D}(t)\,\mathbf{u}(\mathbf{q})\,, \tag{2.36}$$

where $\mathbf{x}$ and $\mathbf{q}$ are respectively the final and initial comoving coordinates, $\mathbf{u}(\mathbf{q})$ is the initial velocity displacement field and $D(t) \propto g(\Omega, \Omega_\Lambda)\, t^{2/3}$ is the growing mode factor of the density perturbation. In fluid mechanics terminology, $\mathbf{x}$ and $\mathbf{q}$ are said to be the Eulerian and Lagrangian coordinates, respectively. In these expressions $\mathbf{u}(\mathbf{q})$ is usually assumed to be an irrotational field, which satisfies

$$\delta(q) = -\nabla \cdot \mathbf{u}(q) \quad ; \qquad \nabla \times \mathbf{u} = \mathbf{0}. \tag{2.37}$$

Due to its nature the Zel'dovich approximation is commonly used to set up the initial conditions in numerical N–body simulations. The initial velocity field is computed from Eq. (2.37) by generating a random Gaussian realization of the density power spectrum and then equations (2.36) are used to generate the initial matter and velocity distributions required for the first integration step of the simulations.

The main limitation of the Zel'dovich approximation is that particle trajectories are uniquely set by the initial displacements and as motions intercept, particles keep moving away from the forming structures. At this point, usually referred to as *shell crossing*, the Zel'dovich approximation breaks down. However, being a first-order Lagrangian perturbative method, the Zel'dovich approximation usually achieves the same level of accuracy in describing the perturbations for longer then in the (Eulerian) linear perturbative case.

2.5.3 Press–Schechter theory

Perhaps the most successful analytical method to describe the density perturbations during the early stages of their non-linear evolution is the Press–Schechter (PS) formalism [86]. The central quantity in the theory is the PS mass function (or multiplicity function), which gives the comoving number density, $n(M, z)dM$, of virialized objects forming at the epoch of redshift z, with masses in the infinitesimal range M to $M + dM$,

$$n(M, z)dM = -\sqrt{\frac{2}{\pi}} \frac{\rho_0}{M} \frac{\delta_c}{\sigma^2} \frac{d\sigma(M, t)}{dM} \exp\left(-\frac{\delta_c^2}{2\sigma^2(M, z)}\right) dM\,. \tag{2.38}$$

Here ρ_0 is the comoving matter density, δ_c is the linear overdensity threshold at virialization, $\sigma^2(R(M), z)$ is the variance of the smoothed density contrast filtered on the comoving scale $R(M)$ and M is the mass enclosed in the volume occupied by the smoothing filter, $M = \rho_0 V^3$. With this expression, the total number of virialized objects, per unit of solid angle, with mass above $M_{\rm min}$ is simply

$$\frac{dN}{d\Omega}(> M_{\rm min}) = \int_0^\infty dz \frac{dV}{dz d\Omega} \int_{M_{\rm min}}^\infty dM \frac{dn}{dM} \tag{2.39}$$

where $dV/dzd\Omega$ is the volume element (1.35). In general, the above integral requires the use of Eq. (2.13) to evaluate $\sigma^2(R(M), z)$, with the appropriate smoothing filter and density power spectrum, at each step of the redshift and mass integrations. In practice this can be much simplified by using accurate fitting formulae to approximate $\sigma^2(R(M), z)$ in the

scales of interest and then use those formulae in the integration process. A particular good approximation on scales in the vicinity on $8h^{-1}$Mpc is the following fitting formula from Ref. [109] for a CDM power spectrum and a Top-Hat filter ($R = (3M/4\pi\Omega\rho_{\rm crit})^{1/3}$):

$$\sigma = \sigma_8(z) \left(\frac{R}{8h^{-1}\ {\rm Mpc}} \right)^{-\gamma(R)} , \tag{2.40}$$

where $\sigma_8(z)$ is the normalization of the power spectrum at z and

$$\gamma(R) = (0.3\Gamma + 0.2) \left[2.92 + \log \left(\frac{R}{8h^{-1}\ {\rm Mpc}} \right) \right] . \tag{2.41}$$

Using Eqs. (2.13) and (2.27) we obtain

$$\sigma_8(z) = \frac{\sigma_8(0)}{1+z} \frac{g[\Omega(z), \Omega_\Lambda(z)]}{g[\Omega_0, \Omega_{\Lambda 0}]} , \tag{2.42}$$

where $\sigma_8(0)$ is the power spectrum normalization at the present. The shape parameter Γ is well constrained, in the vicinity of the $8h^{-1}$ Mpc scale, by fitting observations of the galaxy and cluster correlation functions with a CDM power spectrum, $\Gamma = 0.230^{+0.042}_{-0.034}$ at 95% confidence level [77, 108].

Although triaxial perturbations collapse preferentially into flattened structures (known as *pancakes*) it's usually assumed that rare objects like galaxy clusters collapse in a fairly symmetric way [6]. Therefore the density threshold in Eq. (2.38) is usually assumed to be $\delta_c = \delta_{\rm lin}^{\rm coll} = 1.69$, which, as mentioned before, is practically independent on the cosmology for many situations of interest.

2.5.4 Numerical simulations of large–scale structure

Over the past two decades, numerical N–body simulations have become a powerful theoretical tool to investigate the formation of structures in the universe. Complex non-linear physics, acting over a wide range of scales, makes the structure formation process hard or impossible to describe without the use of numerical computation methods. These methods track the growth of structure in time by integrating the equations of motion of the individual particles and following their trajectories under the action of gravity and other physical forces involved. Numerical simulations which only account for the effects of gravity are appropriate to describe the evolution of the dark matter component of the universe. These are usually referred to as N-body simulations. To describe the evolution of perturbations on both baryons (gas) and dark matter, simulations need also to describe the dynamics of the gas and to include the appropriate gas physics in the range of scales probed by the simulations. These are known as hydrodynamical N–body simulations.

Cosmological simulations of structure formation require the appropriate modelling of the physical processes involved (e.g. gravity, gas dynamics, radiative phenomena), a clear definition of the starting (initial) conditions (power spectrum of density perturbations at the simulation

start and background model) and a set of parameters intrinsic to the numerical simulation scheme (e.g. number of particles, box size and softening). Follows a brief description of how these aspects are usually set up in numerical codes of large-scale structure formation.

Initial conditions

All numerical simulations require a clear definition of the initial conditions, from which the simulations start. For structure formation simulations these consist of specifying the background cosmology and the perturbations to this background.

The background model is specified by a set of cosmological parameters, which describe the matter and radiation contents of the universe (e.g. the density parameters of dark matter, baryons and cosmological constant), and the geometry of the universe (usually taken to be flat or open Friedman–Robertson–Walker space-times). The initial perturbations to the background model are set by assuming that when simulations start, at a time t_i, perturbations are still small and well described in linear perturbation theory (see Section 2.2). The Zel'dovich approximation (described in Section 2.2) is then used to assign initial positions and velocities to the simulation particles.

The procedure consists as follows. Particles are originally placed on a cubic grid, with $N_{\rm row}$ cells per side, inside the simulation volume $V = L^3$ (simulation box). Assuming periodic boundary conditions the overdensity field, δ, can be expanded in a Fourier series of the form (2.2), where wavemodes above the *Nyquist frequency*, $k_{\rm Ny} = (2\pi/L)(N_{\rm row}/2)$, are excluded to prevent *aliasing* effects. The largest mode in the box corresponds to a minimum wavenumber $k_{\rm min} = 2\pi/L$. The next step is to generate a Gaussian random realization of the linear theory matter power spectrum, $\mathscr{P}(k, t_i)$, which is normalized from observations of the local abundance of rich clusters, as described at the end of section 2.4.2. The amplitude of σ_8 at $z(t_i)$ is derived from $\sigma_8(z = 0)$ by using the scaling relation (2.42). The initial positions and velocities of the particles are then calculated by using the Zel'dovich approximation, Eq. (2.36), see e.g. Ref. [59].

The matter power spectrum is usually an input of the initial conditions generator codes. This can be giving by reading in a pre-computed table of the power spectrum generated by Boltzmann codes, or by specifying the parameters of transfer function fitting formulas from the literature. For CDM simulations with a cosmological constant, the BBKS transfer function (given by equations (2.25) and (2.26)) is a common choice for setting up the simulations initial conditions. Due to symmetry properties of the Fourier components, $\delta^*_{\mathbf{k}} = \delta_{-\mathbf{k}}$, there's only a finite number ($N_{\rm row}/2$) of possible modes that can be accommodated in the box. To sample the matter power spectrum in a wide range of modes one needs to have both large simulation volumes and number of particles (high resolution simulations). This also implies large computational times and system resources.

Gravity

Gravity plays a central role in the structure formation problem. Even though pure N-body codes are sometimes used to probe scales as big as the Hubble volume in non-flat geometries, gravity is usually modelled by Newton's laws of gravity:

$$\frac{d\mathbf{x}}{dt} = \frac{1}{a}\mathbf{v} \tag{2.43}$$

$$\frac{d\mathbf{v}}{dt} + H\mathbf{v} = -\frac{\nabla\phi}{a} \tag{2.44}$$

$$\nabla^2\phi = 4\pi G a^2[\rho(\mathbf{x}, z) - \bar{\rho}(t)] \; . \tag{2.45}$$

These equations are written in a spatial coordinate system comoving with the cosmological expansion of the universe. Here, $\mathbf{v}$ is the peculiar velocity, $a(t)$ is the cosmological scale factor, ϕ is the gravitational potential, $\nabla = \partial/\partial\mathbf{x}$ is the gradient in comoving coordinates, $H = \dot{a}/a$ is the Hubble constant and ρ and $\bar{\rho}$ are the density and spatial mean density (density of the background model). The quantity $\mathbf{g} = -\nabla\phi/a$ is the peculiar acceleration field. For the numerical computations, periodic boundary conditions are usually adopted, so that a finite expanding volume probed in a simulation is properly embedded in the perturbed background space-time.

In order to obtain the evolution of the particle trajectories in time one needs to integrate equations (2.43) to (2.45). This always has to start with the evaluation of the gravitational potential ϕ. Since gravity is a long-range force, the potential seen by a particle depends, in theory, on the mass and location of all other particles. The art of N-body simulations lies exactly in how numerical codes compute the gravitational potential. In the next subsections we will review some of today's most common algorithms developed to perform this task.

- **The Particle–Particle algorithm:** The usual way to obtain the gravitational potential ϕ is to integrate Eq. (2.45). For a population of point particles, the peculiar acceleration field, $\mathbf{g}(\mathbf{x}_i)$, acting upon a particle at the position $\mathbf{x}_i$ is then given by a summation over all the other mass particles, m_j (see e.g. Ref. [79]):

$$\mathbf{g}\left(\mathbf{x}_i\right) = -\frac{\nabla\phi\left(\mathbf{x}_i\right)}{a} = \frac{G}{a^2}\sum_j m_j \frac{\mathbf{r}_{ij}}{\left|\mathbf{r}_{ij}\right|^3} \tag{2.46}$$

  where G is the gravitational constant and $\mathbf{r}_{ij} = \mathbf{x}_j - \mathbf{x}_i$ is the displacement vector between the particles i and j. The most straightforward way to obtain the gravitational force acting upon each particle is to perform the direct summation in Eq. (2.46). The algorithms which implement this summation are called Particle–Particle or PP algorithms. Usually they also include a smoothing length procedure to soften the gravitational force between particles (gravitational *softening*). This is necessary to prevent two-body effects from dominating, which can lead to the formation of unphysical binaries (see e.g. Ref. [27]).

  The main problem with the PP technique is that the number of calculations needed to follow the evolution of a population of particles increases with the square of the number

of particles $\mathscr{O}(N^2)$. This makes the whole enterprise very expensive in computational time and even with the largest parallel supercomputers the task becomes prohibitive for a number of particles greater than $N > 10^7$.

- **The Particle–Mesh algorithm** Particle–Particle interactions are more important on small scales. On larger scales, such as those probed in large cosmological simulations, the long-range force seen by a particle can be approximated by an average potential generated by a new set of surrounding particles. This requires assigning average masses to points on a Cartesian grid and then evaluate the potential seen by one particle from the interaction of that particle with its surrounding grid neighbours. This is the heart of the so-called Particle–Mesh or PM algorithm, and its operation can be summarised in tree basics steps:

  - **Mass assignments**: first, the mass density field is computed over N_g grid points using a certain assignment scheme. One of the most commonly used schemes is the Cloud–in–Cell (CIC) algorithm, which uses multi-linear interpolation to the eight grid points on the corners of the cubic mesh cell containing the particle.
  - **Potential estimation on the grid**: the Poisson equation is then used on the grid to evaluate the gravitational potential. This is usually accomplished by the use of a fast Poisson solver, which is a Fast Fourier Transform (FFT) algorithm that typically requires $\mathscr{O}(N_g \log N_g)$ operations. The gravity field is then computed on the N_g mesh points by differentiation of ϕ.
  - **Potential estimation on the particles**: the last step is to interpolate the gravity field back to the particles. According to Ref. [50] the interpolation scheme should be the same used in the mass assignment procedure (first step), to ensure that self-forces on the particles vanish.

  The main advantage of the PM algorithms is that they require fewer operations, $\mathscr{O}(N) + \mathscr{O}(N_g \log N_g)$, to evaluate the forces acting on all particles. This means less memory and higher speed per time step than the PP algorithm. However, for separations between particles less then several grid spacings, the forces between particles become poorly approximated and the method starts to give worse results then the PP algorithm.

- **The P^{3}M and Adaptive P^{3}M** P^{3}M stands for the concatenation of four words Particle–Particle–Particle–Mesh. It's an hybrid algorithm, first applied to cosmology in Ref. [28], that makes use of the two previous (PP and PM) methods. At short range distances the Particle–Particle method is employed, while the long range forces are computed using the Particle–Mesh algorithm. The gravitational force, $\mathbf{F}_{ij}$, acting on the particles is then given by a sum of two terms,

$$\mathbf{F}_{ij} = \mathbf{F}_{ij}^{sr} + \mathbf{F}_{ij}^{lr} \tag{2.47}$$

  where $\mathbf{F}_{ij}^{sr}$ and $\mathbf{F}_{ij}^{lr}$ represent the short and long range forces acting on the particles. The short range term, evaluated using the PP method, vanishes after a few inter-particle distances, while $\mathbf{F}_{ij}^{lr}$ is computed using the PM algorithm and is set to zero at short range distances.

The Adaptive P^{3}M algorithm [19] is a mesh refinement of the P^{3}M method, which uses sub-grids in the regions of higher density. The P^{3}M scales as $O(N \log N)$, where N is the number of particles. This method is presently one of the best algorithms to compute the gravitational force for large cosmological N-body simulations.

Gas dynamics

A description of structure formation exclusively based on the behaviour of matter under its self–gravity is obviously insufficient. Gas dynamics, shocks and pressure gradients become more and more important as structures evolve. Hydrodynamical effects are clearly important to determine the behaviour of baryonic matter in galaxies and clusters of galaxies (even if baryons are only a small fraction of the total mass), and play a central role in determining how collapsing structures can reach virial equilibrium.

In comoving coordinates, gas dynamics is described by the following cosmological fluid equations (see e.g. Ref. [8]),

$$\frac{\partial}{\partial t}\left(\frac{\rho_b}{\bar{\rho}_b}\right) + \frac{1}{a}\nabla \cdot \mathbf{v}_b = 0 \tag{2.48}$$

$$\frac{\partial \mathbf{v}_b}{\partial t} + \frac{1}{a}(\mathbf{v}_b \cdot \nabla)\mathbf{v}_b + H\mathbf{v}_b = -\frac{1}{a\rho_b}\nabla p + \mathbf{g}\ , \tag{2.49}$$

where $\mathbf{g} = -\nabla\phi/a$ is the peculiar acceleration field given by Eq. (2.45) and ρ_b, $\bar{\rho}_b$, $\mathbf{v}_b$ and p are, respectively, the baryonic mass density, mean mass density, peculiar velocity and pressure. These equations must be used in conjunction with a third continuity equation for the energy or for the entropy. Outside shocks these can be written as:

$$\frac{\partial u}{\partial t} + \frac{1}{a}\mathbf{v}_b \cdot \nabla u = -\frac{p}{a\rho_b}\nabla \cdot \mathbf{v}_b + \frac{1}{\rho_b}(Q - \Lambda) \tag{2.50}$$

$$\frac{\partial S}{\partial t} + \frac{1}{a}\mathbf{v}_b \cdot \nabla S = \frac{1}{p}(Q - \Lambda)\ , \tag{2.51}$$

where u and S are the gas thermal energy and entropy per unit of mass. For a perfect gas $u = p/[(\gamma-1)\rho_b]$ and $S = (\gamma-1)^{-1}\ln(p\rho_b^{-\gamma})$ where γ is the ratio of the specific heats ($\gamma = 5/3$ for a monotonic perfect gas). The quantities Q and Λ are the heating and cooling rates of the gas. They are important in non-adiabatic calculations and depend on several parameters such as ionization, gas chemistry and radiative energy transfer (see Section 2.5.4).

The strong nonlinearity of these equations makes the test of numerical algorithms of gas dynamics very hard. The accuracy and convergence of these methods are mainly tested by comparing the results from different codes or testing their predictions against simple one–dimensional problems.

Smoothed Particle Hydrodynamics (SPH) was invented by Gingold & Monaghan, Ref. [38], and Lucy, Ref. [68], in 1977 (more recent reviews can be found in Refs. [71, 102]). It is a 'particle-tracking' Lagrangian method for integrating the fluid equations (2.48)–(2.50) or (2.51), which involves the estimation of various fields (such as baryon density, velocity, temperature, pressure

gradient, etc) from a discrete set of particles with a fixed mass The way SPH tackles this problem is by smoothing the particles over a finite volume, which is set by the profile of a spherically–symmetric smoothing kernel, W. For example, according to this method, the value of a scalar quantity $A(\mathbf{x})$ at the position $\mathbf{x}$, is estimated by the formula

$$\langle A(\mathbf{r})\rangle = \sum_{\mathrm{i}} m_{\mathrm{i}} \frac{A_{\mathrm{i}}}{\rho_{\mathrm{i}}} W\left(\left|\mathbf{r}-\mathbf{r}_{\mathrm{i}}\right|, h_{\mathrm{i}}\right) \ , \tag{2.52}$$

where m_{i}, ρ_{i}, h_{i} and A_{i} are, respectively, the mass, mass density, smoothing length and the scalar quantity A of the particle labelled with the index i. The shape of the smoothing kernel, $W(|\mathbf{r}-\mathbf{r}_{\mathrm{i}}|, h_{\mathrm{i}})$, is generally taken to be a spline, such as the normalised spherically–symmetric B_2–spline kernel (see Ref. [72]) below,

$$W(x, h_{\mathrm{i}}) = \frac{1}{4\pi h_{\mathrm{i}}^3} \begin{cases} 4-6x^2+3x^3 \ , & 0 \le x \le 1 \\ (2-x)^3 \ , & 1 < x \le 2 \\ 0 \ , & x > 2 \end{cases} \tag{2.53}$$

where $x = |\mathbf{r}-\mathbf{r}_{\mathrm{i}}| / h_{\mathrm{i}}$. The smoothing length, h_{i}, is usually taken to vary with $\rho_{\mathrm{i}}^{-1/3} \propto \rho_b^{-1/3}$, in order to have a fixed amount of particles (typically 30–100) included in the sum of Eq. (2.52). Particles in low density regions have therefore larger smoothing lengths then particles in high density regions.

Other methods exist to solve the gas dynamical equations. Methods like the Eulerian Grid and the adaptive Grid algorithms are among the 'competitors'. These are grid-based hydrodynamic methods which provide numerical solutions of the Eulerian field equations for fluid dynamics. A discussion of these and some other gas dynamics algorithms is given in Refs. [8, 117].

Additional physics: Cooling and non-gravitational heating

Besides gravity and pressure forces there are several other physical processes which can have considerable impact on the hydrodynamics of the gas. Processes such as radiative cooling, non-gravitational heating and energy feedback from star formation, are among the possible effects that can be included in the simulations to achieve a better description of the structure formation phenomenon. These effects can be modelled by specifying the appropriate heating and cooling rates in equations (2.50), and (2.51).

The lack of the Gunn–Peterson trough (see Ref. [39]) in the spectra of high-redshift quasars indicates that the intergalactic medium (IGM) is already in a very high state of ionization by redshifts as high as $z \simeq 5$ (see also Ref. [42, 67]). This means that a considerable amount of energy is required to reionize the universe from the neutral state it acquires after recombination.

Possible IGM heating mechanisms include sources of astrophysical nature, such as energy injection from stars, winds from supernovae explosions and energy release due to gravitational accretion into Black Holes (e.g. quasars and active galactic nuclei (AGN)), or other more exotic mechanisms such as energy release by late-decaying particles (e.g. decaying neutrinos).

All these processes can induce changes in the thermal state of the gas and therefore influence its dynamics. For example, as shown in Ref. [26], photoionization heating can strongly prevent gas from cooling into the shallow potential wells at high redshifts.

Non-gravitational heating effects are generally difficult to model due to their localized nature and lack of information on the relevant energy release mechanisms. The physical scales on which they occur are also usually below the resolution limit of large-scale structure simulations. In such cases, heating of the IGM can only be implemented at a phenomenological level.

Radiative cooling is believed to play a central role for the condensation and survival of galaxies within larger virialized structures. Unlike heating mechanisms, cooling effects are well understood at least in the case of optically-thin media with primordial gas composition, see Refs. [10, 78, 93]. There are several ways in which gas can dissipate energy. These include processes such as Bremsstrahlung emission from hot electrons, recombinative cooling due to collisional ionization followed by electron recombination, and collisional excitation cooling resulting from the emission of radiation by neutral atoms after excitation due to collisions with free electrons. In all cases the emitted radiation escapes from the gas if the medium is optically thin.

Since all the above process are collisional, i.e. result from two-body encounters, the net cooling rate of the gas scales as $\Lambda = n_e n_p \Lambda_c$, where n_e and n_p are the number densities of the electrons and atoms/ions. The computation of the net cooling function, Λ_c, requires a detailed study of all possible chemical reactions among the different particle species present in the gas. The results are usually tabulated as a function of the temperature and metallicity of the gas. Fig. 2.1 shows the net cooling function obtained from the tables presented in Ref. [105]. The calculation assumes collisional ionization equilibrium and an optically-thin gas with primordial chemical composition. At low temperatures the curves are dominated by collisional excitation cooling from neutral hydrogen and helium. As metallicity builds up collisional excitation from heavier elements starts to dominate. All curves converge at high temperature as the gas becomes fully ionised and Bremsstrahlung emission from hot electrons is the dominant cooling process.

An effect which strongly affects the cooling properties of the gas is photoionization heating due to ultraviolet (UV) radiation, such as that produced by quasars and early generations of massive stars, see Ref. [26]. This can ionize low-density gas at temperatures as low as 10^4 Kelvin and therefore totally suppress collisional excitation cooling, which is the dominant cooling mechanism at these temperatures. As a result, the peaks observed at low temperatures in Fig. 2.1 can be strongly suppressed if a significant UV background is present, see Ref. [102].

An extra factor proportional to $n_e(T - T_{\rm CMB})$ can be added to Λ to take into account Compton cooling of the ionised gas by cosmic microwave background photons, known as the Sunyaev–Zel'dovich (SZ) effect. The SZ effect acts as a cooling mechanism in which thermal energy is depleted from the gas and transfered into the CMB. In practice this process is inefficient at low redshifts ($z \lesssim 8$). This is because below this redshift the characteristic time scale for Compton cooling, $t_{\rm cc}$, is larger then the Hubble time, t_H ($t_{\rm cc}/t_H \simeq 180/(1+z)^{5/2}$). Above $z \simeq 8$ the efficiency of the effect is also small because the SZ distortions become very weak at high redshifts, see e.g. Ref. [10].

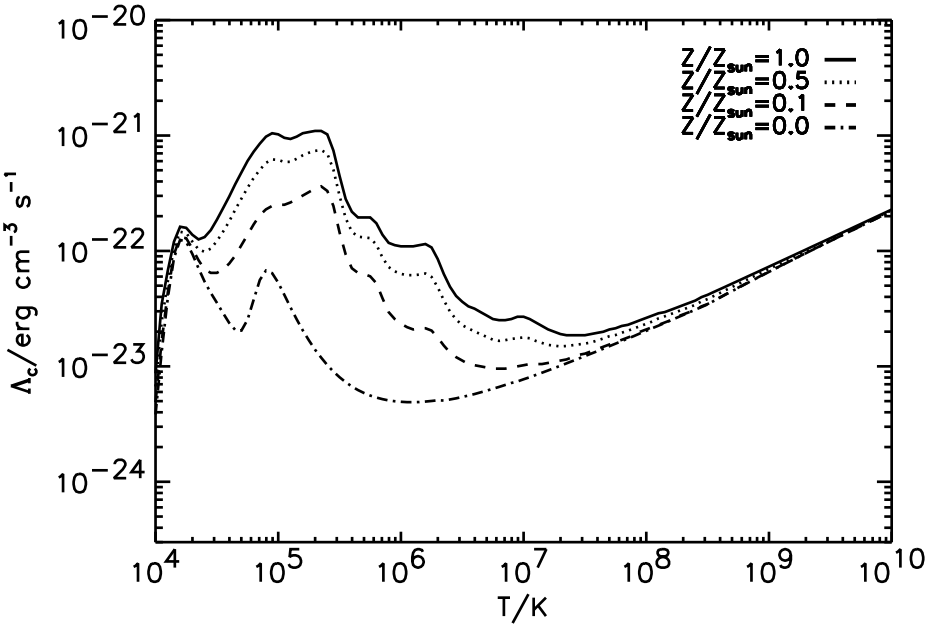

Figure 2.1: Dependence on metallicity of the gas cooling function for an optically thin-medium assuming collisional ionization equilibrium. Lines are obtained from interpolation of the cooling rates tabulated in Ref. [105].

In the absence of significant photoionization heating, the function in Fig. 2.1 provides a simple and accurate description of the cooling mechanisms of the baryonic gas.

Numerical integration and timestepping

The integration of the equations of motion for gas and dark matter is done numerically, assuming a given *timestepping* scheme. A popular timestepping scheme is the PEC (Predict, Evaluate, Correct) algorithm described in Ref. [20]. This uses only positions and velocities (plus densities and thermal energies for the gas) to evaluate the forces on the particles and allows arbitrary changes in the integration time step to account for rapid variations of the forces with time. Though variable during the time integration process, the timestep is spatially constant throughout the simulation box. The timestep is variable (i.e. changes from one integration step to another), but spatially constant throughout the simulation box. It is determined by evaluating different timescales, such as the largest particle acceleration (Δt_a), the largest particle speed (Δt_v), and the Hubble time ($\Delta t_H = 1/H(t)$), at various stages of the force calculation. The $\Delta t_H = 1/H(t)$ scale ensures that adiabatic cooling due to the Hubble expansion is followed accurately. The timescales, Δt_a and Δt_v, depend on the value of the assumed force softening. At early times the effect of Δt_H dominates (see e.g. Refs. [20, 59]).

Simulation output

Simulation outputs (also known as *simulation snapshots*) are files containing a set of particles with masses, positions, velocities, densities, temperatures and smoothing lengths. Other physical properties, such as gas metallicities and gravitational potential at the particles positions, are also possible outputs in public simulation codes. The spatial distribution of the particles gives a representation of the gas and dark matter density fields inside the simulation volume. Figure 2.2 shows the zero redshift output of a ΛCDM simulation made with the public `Hydra` code, Refs. [19, 20]. The green and red points represent the gas and dark matter particles, respectively. The physical size of the box at $z = 0$ is 200 Mpc. Equal number of gas and dark matter particles are used in these plots. The predominance of green points is because gas particles were plotted after the dark matter particles. The lack of visible red points indicates that gas follows the dark matter distribution well. The bottom panels show the aspect of the box when viewed face on from its X-Y and Y-Z planes.

Cosmological simulations usually assume periodical boundary conditions. This implies that structures near one side of the box are in fact close to particles on the opposite side of the box. The boundary periodicity allows us to randomly shift the positions of all particles (simultaneously) in a given direction, provided that particles leaving the simulation volume are forced to re-enter the box from the opposite direction.

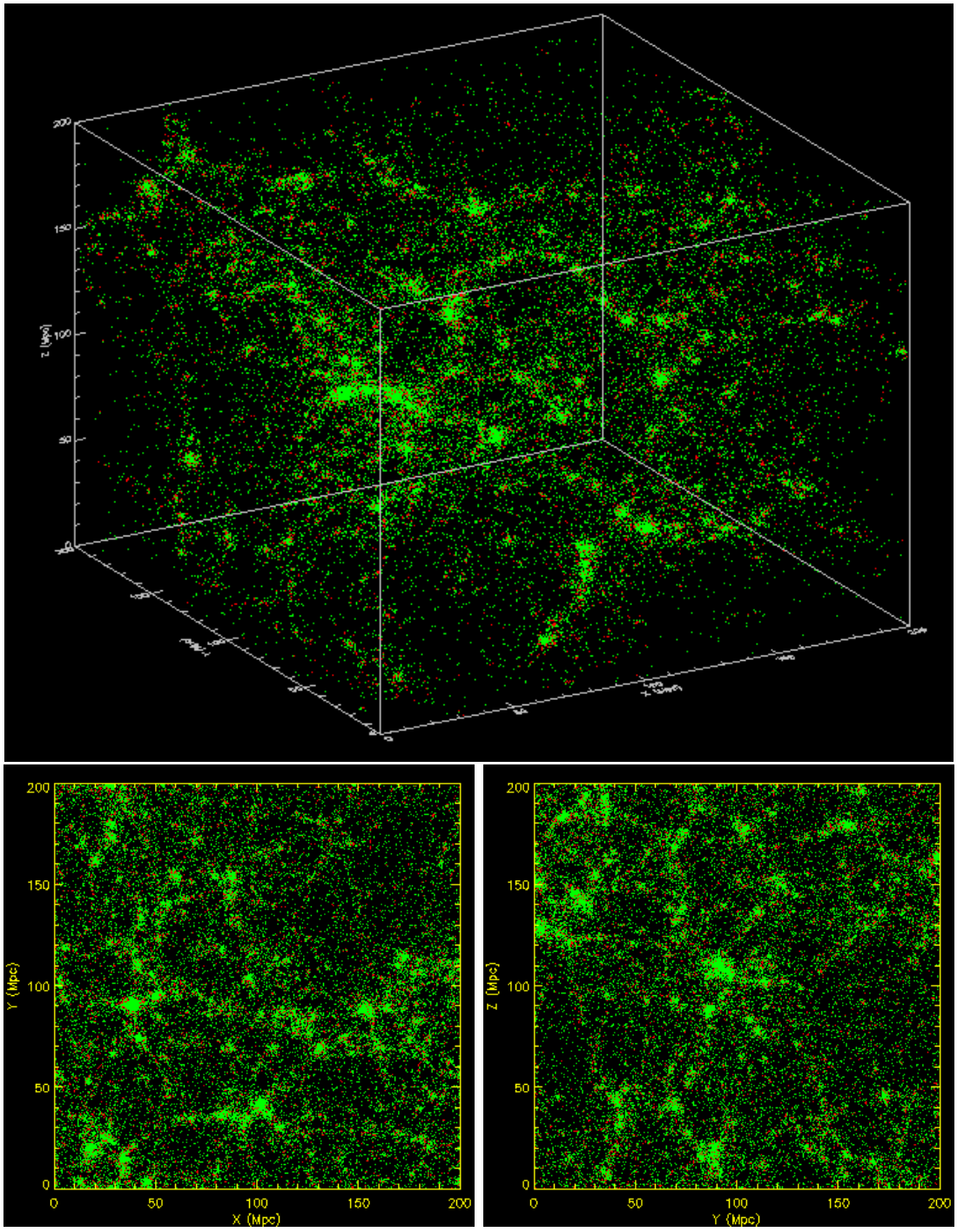

Figure 2.2: The top panel shows the gas (green) and dark matter (red) particles in a simulation box, of volume 200^3 Mpc^3, at redshift $z = 0$. The bottom panels result from viewing the box face on from the X-Y and Y-Z planes, respectively. The gas particles were plotted after the dark matter particles, which explains the predominance of the green points.

Chapter 3

Cosmic Microwave Background Radiation

3.1 The intensity spectrum

The shape of the cosmic microwave background spectrum depends on the physical processes which mediate the interaction between matter and radiation in the early universe. After the epoch of particle–antiparticle annihilation ($z \simeq 10^9$) these processes are essentially Compton scattering, double Compton scattering and *free-free* (or *Bremsstrahlung*) emission. The so called double Compton scattering differs from the usual Compton effect because the photon–electron interaction gives rise to an extra photon. The Bremsstrahlung interaction consists of the emission of photons by accelerated electrons moving in the electrical potential created by positively charged ions. Contrary to what happens with the Compton scattering, neither of these processes preserves the total number of photons. In all cases the energy of the photons is changed. The effectiveness of these processes in shaping the CMB spectrum depends on the characteristic time-scale on which they occur compared to the Hubble time at a given epoch.

It's possible to show that *kinetic* equilibrium between matter and radiation can be achieved via Compton scattering alone, if the radiation spectrum is not too different from a blackbody spectrum after the particle–antiparticle annihilation epoch (see e.g. Refs. [15,78]). This is true at least until a critical redshift $z_{\rm c} = 2.2 \times 10^4 (\Omega_B h^2)^{-1/2}$, below which the electron and photon densities become too low. During this period the kinetic equilibrium ensures a Bose–Einstein spectrum for radiation field,

$$I(\nu) = \frac{2h\nu^3}{c^2} \left[\exp\left(\frac{h\nu}{k_B T} + \mu(\nu) \right) - 1 \right]^{-1} , \tag{3.1}$$

where $\mu(\nu)$ is the chemical potential, T the temperature and h and k_B are the Planck and Boltzmann constants, respectively. The dependence of the chemical potential on frequency can be modelled as $\mu = \mu_0 \exp(-2x_0/x)$ where $x = h\nu/k_B T$, $x_0 = 5 \times 10^{-2} \, (\Omega_0 h^2)^{7/8}$ and μ_0 is the chemical potential at $x \gg x_0$ [118]. Its effect is stronger on the Rayleigh–Jeans spectral region, which is where (3.1) shows larger deviations from a blackbody distribution –

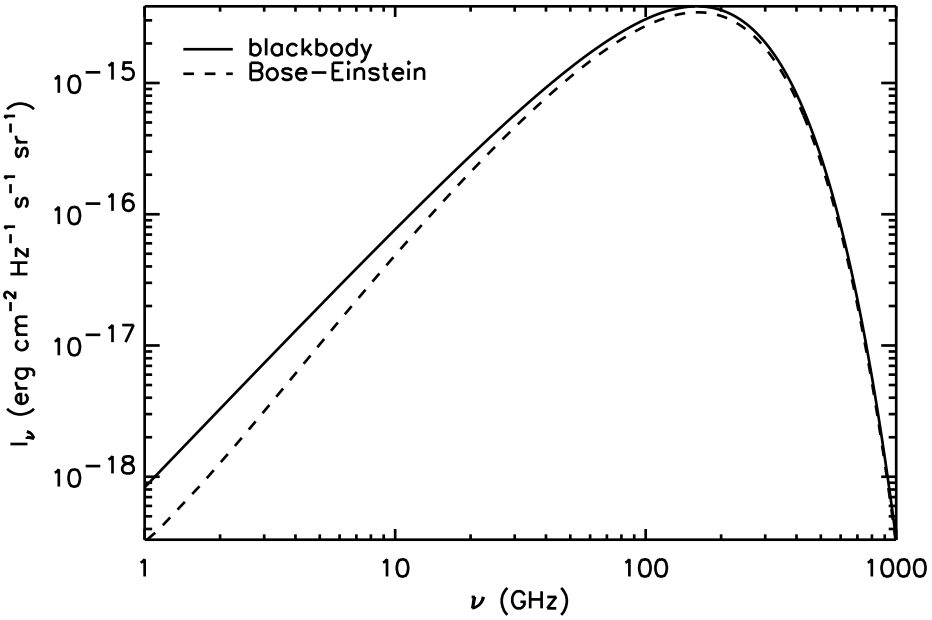

Figure 3.1: CMBR spectral distortion caused by energy release in the early universe. The observed CMBR will deviate from a blackbody spectrum (solid line) if energy is released in the redshift range $z_{\rm th} \simeq 2 \times 10^6 \gtrsim z \gtrsim z_{\rm c} \simeq 3 \times 10^5$. The radiation field will then follow a Bose-Einstein spectrum (dashed line). In both cases the temperature of the radiation field was taken to be $T = 2.725$ K. The chemical potential for the Bose–Einstein spectrum was $\mu_0 = 0.1$ and $\Omega_0 h^2 = 0.17$ (see text).

see Figure 3.1.

For *thermal equilibrium* to be achieved at some epoch, interaction processes that can "create" and "destroy" photons must operate so that a blackbody spectrum can be produced. We know for instance that Bremsstrahlung emission is an efficient process to generate photons at low frequencies (note that the Bremsstrahlung cross section scales with the square of the photons' wavelength). This helps the radiation spectrum to approach the blackbody form. Detailed studies on how radiation can acquire a Planckian shape indicate that double Compton scattering is enough to generate a blackbody spectrum for redshifts $z_{\rm th} \geq 1.5 - 2.5 \times 10^6 (\Omega_B h^2)^{-\alpha} \simeq 2 \times 10^6$, where $\alpha = 0.34 - 0.4$, see Ref. [15]. This is also possible with Bremsstrahlung alone if $\Omega_B h^2 > 0.1$.

Therefore, the CMBR we observe today will have a thermal spectrum, unless energy is added to the radiation field after the redshift $z_{\rm th}$ (energy released before $z_{\rm th}$ would simply be rethermalized into a higher temperature blackbody spectrum). Energy added in the interval, $z_{\rm th} \simeq 2 \times 10^6 \gtrsim z \gtrsim z_{\rm c} \simeq 3 \times 10^5$, would result in a Bose–Einstein CMB spectrum, as kinetic but not thermal equilibrium can occur during this period. At epochs later then $z_{\rm c}$ it's also impossible to establish kinetic equilibrium if more energy is added to the radiation field. Possible mechanisms for this energy release include: particle decay into a much lighter

particle plus a photon; line emission at recombination; Far infrared emission from dust; and inverse Compton scattering by hot plasma, known as the SZ effect. The spectral distortion produced by the later mechanism is the subject of this thesis.

The intensity spectrum of the CMB radiation is now known with high accuracy over a wide range of frequencies. It presents no evident departure from a blackbody spectrum, although somewhat larger deviations are consistent with the data at wavelengths larger then ~ 1 centimetre. The experiment FIRAS (*Far Infrared Absolute Spectrophotometer*) on board of the COBE satellite measured the difference between the CMB spectral intensity and a precise blackbody spectrum. Spectral deviations from a Planck law were found to be very small and only consistent with an upper limit of $|\mu| < 9 \times 10^{-5}$ (95 % confidence level [CL]) for the chemical potential of a Bose-Einstein distribution and an upper limit of $|y| < 1.5 \times 10^{-5}$ (95 % CL) for the Kompaneets y–parameter describing Comptonized spectra via the SZ effect, see Ref. [33]. The CMB blackbody temperature from FIRAS was computed in Ref. [69] to be $T = 2.725 \pm 0.002$ K. This implies a CMB thermal spectrum characterised by a specific intensity maximum of $I_{\max} \sim 3.7 \times 10^{-18}$ J m^{-2} s^{-1} Hz^{-1} rad^{-2} at the frequency $\nu_{\max} \sim 160$ GHz and a photon number and energy densities given by $n_\gamma \sim 4 \times 10^8$ photons m^{-3} and $\rho_\gamma \sim 5 \times 10^{-31}$ kg m^{-3}, respectively.

3.2 The angular power spectrum

The natural way of expanding the CMBR temperature fluctuation field, $\Theta(\hat{n}) = \Delta T/T(\hat{n}) = \Delta T/T(\theta, \phi)$, on the celestial sphere is in terms of spherical harmonics:

$$\Theta(\hat{n}) = \Delta T/T(\theta, \phi) = \sum_{\ell=0}^{\infty} \sum_{m=-\ell}^{\ell} a_{\ell m} Y_{\ell m}(\theta, \phi). \tag{3.2}$$

where $\hat{n}$ denotes a direction in the sky specified by the spherical angles θ, ϕ and $a_{\ell m}$ are the multi-polar moments, given by

$$a_{\ell m} = \int Y^*_{\ell m}(\theta', \phi') \frac{\Delta T}{T}(\theta', \phi') d\Omega', \tag{3.3}$$

where $d\Omega'$ is the solid angle element. In general, the $a_{\ell m}$ are complex quantities. Assuming $\Theta(\hat{n})$ as a random Gaussian field (as predicted by inflation) the temperature fluctuations are fully specified by their angular correlation function:

$$\begin{aligned} C(\hat{n}, \hat{n}') &\equiv \left\langle \frac{\Delta T}{T}(\hat{n}) \frac{\Delta T}{T}(\hat{n}') \right\rangle = \left\langle \frac{\Delta T^*}{T}(\hat{n}) \frac{\Delta T}{T}(\hat{n}') \right\rangle = \\ &= \left\langle \left(\sum_l \sum_m a^*_{lm} Y^*_{lm}(\hat{n}) \right) \left(\sum_{l'} \sum_{m'} a_{l'm'} Y_{l'm'}(\hat{n}') \right) \right\rangle = \\ &= \sum_{l\,l'} \sum_{m\,m'} \langle a^*_{lm} a_{l'm'} \rangle \, Y^*_{lm}(\hat{n}) Y_{l'm'}(\hat{n}') \end{aligned} \tag{3.4}$$

where the angle brackets denote averages over an ensemble of universes with statistically equivalent perturbations and $\hat{n}$ and $\hat{n}'$ are two unit vectors pointing to arbitrary directions in the sky. If we assume rotational symmetry (isotropy) it is conventional to write

$$\langle a^*_{\ell m} a_{\ell' m'} \rangle = C_\ell \delta_{\ell\,\ell'} \delta_{m\,m'} \quad , \quad C_l \equiv \left\langle |a_{\ell m}|^2 \right\rangle, \tag{3.5}$$

(i.e. the $a_{\ell m}$ are not correlated) where C_ℓ is the angular power spectrum of the temperature fluctuation field. Inserting Eq. (3.5) into Eq. (3.4) we find

$$\begin{aligned} C(\hat{n}, \hat{n}') &= \sum_{l\,l'} \sum_{m\,m'} C_l \delta_{l\,l'} \delta_{m\,m'} Y^*_{lm}(\hat{n}) Y_{l'm'}(\hat{n}') = \\ &= \sum_l C_l \sum_m Y^*_{lm}(\hat{n}) Y_{lm}(\hat{n}') = \\ &= \sum_l \frac{(2l+1)}{4\pi} C_l P_l(\cos\vartheta) = C(\cos\vartheta) \end{aligned} \tag{3.6}$$

with $\cos\vartheta = \hat{n}.\hat{n}'$. Using (3.3) and (3.5) one can express the angular power spectrum as,

$$C_l = \left\langle |a_{lm}|^2 \right\rangle = \int d\Omega d\Omega'\, Y_{lm}(\theta,\phi) \left\langle \frac{\Delta T}{T}^*(\theta,\phi) \frac{\Delta T}{T}(\theta',\phi') \right\rangle Y^*_{lm}(\theta',\phi'). \tag{3.7}$$

It is through C_ℓ that theoretical models and the observations can be confronted.

Random fields defined on compact manifolds, such as the sphere S^2, are not ergodic. This is because compact manifolds have finite volumes and the ergodic hypothesis only holds accurately when the spatial averages are done over an infinite volume of space. Therefore, even if we could reduce experimental errors to zero, there's always a limit to the precision we can achieve by converting all the above ensemble averages into spatial averages. This effect is known as *cosmic variance* and it can severely reduce the accuracy with which the angular power spectrum can be measured on large scales. The uncertainty on each multipole is given by $\Delta C_\ell = C_\ell/(\ell+1/2)^{1/2}$, [14]. For each ℓ there are $2\ell+1$ independent $a_{\ell m}$, to be drawn from a distribution of variance C_ℓ. For larger ℓ's this corresponds to a larger number of available samples of the distribution, which implies a lower cosmic variance and better knowledge of the angular power spectrum C_ℓ.

Assuming a primordial power spectrum of the form of Eq. (2.31) and accounting only for scalar (density) perturbations, it is possible to show (see Ref. [11]) that the angular power spectrum is only dependent on the quadrupole normalization amplitude, $\langle Q \rangle$, and the spectral index, n, for small values of ℓ ($\ell \leq 20$)

$$C_\ell = \langle Q \rangle^2 \frac{4\pi}{5} \frac{\Gamma\left(\ell + \frac{n-1}{2}\right) \Gamma\left(\frac{9-n}{2}\right)}{\Gamma\left(\ell + \frac{5-n}{2}\right) \Gamma\left(\frac{3+n}{2}\right)}. \tag{3.8}$$

Equating $n = 1$ (Harrison–Zel'dovich power spectrum) and using the fact that $\Gamma(x+1) = x\Gamma(x)$ one easily obtains

$$\left[\frac{\ell(\ell+1)C_\ell}{2\pi}\right]^{1/2} = \sqrt{\frac{12}{5}} \langle Q \rangle = \text{const.} \tag{3.9}$$

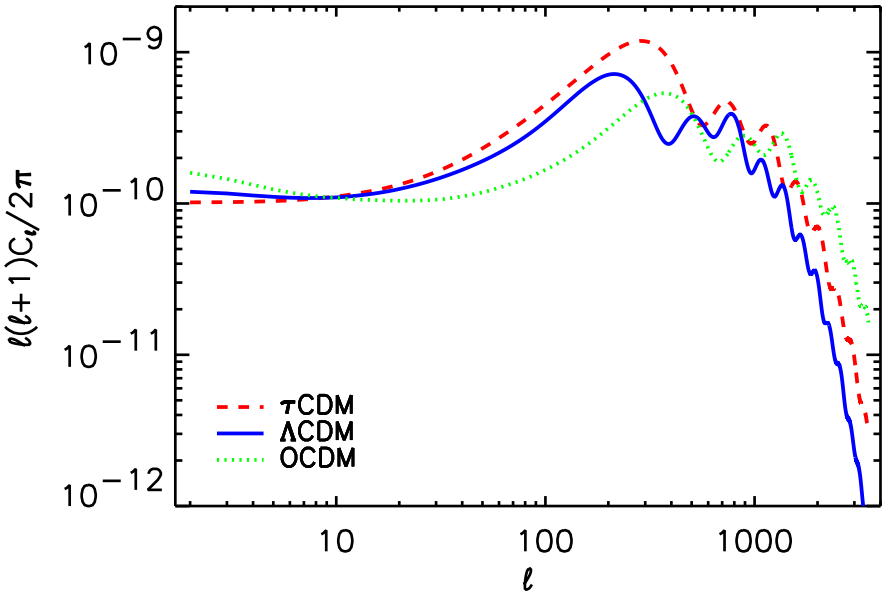

Figure 3.2: CMBR angular power spectra for three CDM models investigated in this thesis: a ΛCDM model with $\Omega_0 = 0.35$, $\Omega_\Lambda = 0.65$ (blue solid line); a critical density model τCDM with $\Omega_0 = 1$ (red dashed line); and an open model OCDM with $\Omega_0 = 0.35$, $\Omega_\Lambda = 0$ (green dotted line). In each case the shape parameter of the matter power spectrum was chosen to be $\Gamma = 0.21$, which provides a good fit to the large scale structure observations. For the critical density model, this implies a first Doppler peak located at much higher ℓ then that found in the (flat) ΛCDM case (see e.g. Ref. [113]), being the later in much better agreement with present CMB observations. All curves were generated with the CMBFAST code [1, 98]).

This result explains the Sachs–Wolfe [95] plateau in Figure 3.2. The quantity $\langle Q \rangle$ is the best fit to the angular power spectrum normalization, given the observed data, and should not be confused with the measured value of the quadrupole amplitude, $Q_{\rm rms}$. Assuming a scale-invariant primordial spectrum and using the COBE data set, the best fit of the power spectrum normalization is $\langle Q \rangle = 1.8 \pm 1.6 \mu$K, [7].

General features of the CMBR angular power spectra in Figure 3.2 are: (1) a Sachs-Wolfe plateau, for $\ell \lesssim 30$, resulting from perturbations larger then the size of the Hubble horizon at the present; (2) a series of peaks, named acoustic, with a dominant peak at $\ell_p \approx 220$ followed by secondary peaks and valleys; (3) and "**cut off**" from $\ell \gtrsim 1000$ due to the damping of perturbations on small scales (Silk damping and finite LSS thickness effects, which cause a mixture of photons coming from different points inside the LSS). The peaks observed in the intermediate multipole region, (angular scales inferior to 1^o) reflect the acoustic oscillations of the baryon-photon fluid at the recombination epoch. (see e.g. Ref. [51]).

Primárias	Gravidade	
	Doppler	
	Flutuações de densidade	
	Diffusion Damping	
	Defeitos Topológicos	
Secundárias	Gravidade	Early ISW
		Late ISW
		Rees-Sciama
		Lensing
	Reionização Local	SZ cinético
		SZ térmico
	Reionização Global	Supressão
		Novo doppler
		Vishniac
"Terciárias" (foregrounds)	Extragaláctios	Fontes Rádio pontuais
		Fontes IR pontuais
	Galácticos	Poeira
		Free-free
		Synchroton
	Locais	Sistema Solar
		Atmosfera
		Ruído, etc.

Table 3.1: Processos que geram anisotropias na CMBR. Adaptado de [107].

3.3 Fontes geradores de anisotropias CMB: "A primer"

Nesta secção faz-se um resumo dos processos que podem gerar anisotropias na radiação cósmica de fundo (para *reviews* ver Tegmark 1996 [107], Hu *et al.* 1997 [53], Barreiro 1999 [5]). Estes processos são normalmente catalogados de acordo com a sua origem. Designam-se por anisotropias primárias as flutuações de temperatura porvocadas pelos processos que ocorreram até ou durante o período de desacoplamento matéria-radiação. Anisotropias secundárias são as anisotropias geradas posteriormente, por fenómenos que alteram o espectro da radiação de fundo à medida que esta se propaga desde a última superfície de scattering (LSS) até nós. Para além destes efeitos existe todo um conjunto de outros efeitos, tais como emisso galatica e fontes pontuais extragalacticas que se adicionam e contaminam o espectro de anisotropia do CMB. Estas fontes de contaminação so normalmente denominadas de anisotropias "terciárias" do CMB. Na tabela 3.1 apresenta-se um resumo dos processos que podem originar ou contaminar o espectro de anisotropias da radiação de fundo.

3.3.1 Anisotropias Primárias

Gravidade, Doppler e flutuações de densidade

Os fotões CMB que hoje observamos interagiram pela ultima vez com a matéria para um redshift $z \simeq 10^3$, quando o universo tinha cerca de 300 mil anos de idade e quando se encontravam a uma distância de $\sim 6000h^{-1}$ Mpc. Consigo transportam diferentes "impressões digitais" da região aonde sofreram o último scattering. Essas impressões podem ser modeladas pelo potencial local (ϕ); a velocidade radial peculiar da matéria (v_r); e a flutuação de densidade do fluído (δ). Estes três campos influênciam o comportamento da radiação da seguinte forma:

1. Fotões que sofreram o último scattering num poço de potencial ($\phi < 0$) experimentam um redshift gravitacional à medida que sobem esse poço.

2. Fotões dispersos pela matéria cuja velocidade peculiar está a afastar-se de nós ($v_r > 0$), sofrem redshift.

3. Fotões que saem duma região de sobre-densidade ($\delta > 0$) possuem temperaturas mais elevadas, porque regiões mais densas são intrinsecamente mais quentes.

Estes três efeitos correspondem às três primeiras entradas da tabela 3.1 e podem ser equacionados do seguinte modo:

$$\frac{\Delta T}{T}(\hat{r}) = \phi(\vec{r}) - \hat{r}.\vec{v}(\vec{r}) + \frac{1}{3}\delta(\vec{r}) \tag{3.10}$$

onde $\vec{r}$ é a distância própria à superfície de último scattering, $\hat{r}$ é o versor na direccção $\vec{r}$ e os campos ϕ, $\vec{v}$ e δ devem ser calculados no instante de recombinação ($z \sim 10^3$; $r \sim 6000h^{-1}$Mpc). A forma do espectro de potência angular, Fig. 3.2, pode ser intrepretado à luz desta equação:

- **Efeito Sachs-Wolfe:** Para escalas angulares superiores à escala que subentende o horizonte na altura da recombinação, $\vartheta \gg 1.7^o\,\Omega_0^{1/2}$, as flutuações dos campos ϕ, $\vec{v}$ e δ estão "congeladas". Como, nos molelos adiabáticos, as condições iniciais fazem coincidir os locais de sobre-densidade com os poços de potencial, o terceiro termo em (3.10) é aproximadamente dado por $\delta \approx -2\phi$ e cancela parcialmente com o primeiro termo do segundo membro, resultando:

  $$\frac{\Delta T}{T}(\hat{r}) = \frac{1}{3}\phi(\vec{r}) - \hat{r}.\vec{v}(\vec{r}). \tag{3.11}$$

  Este efeito é denominado efeito Sachs-Wolfe e é responsável pela parte plana do espectro de potência para os baixos valores de l ($l \ll 100$. Ver gráfico 3.2).

- **Oscilações acústicas:** Para escalas angulares inferiores à escala que do horizonte do som na última superfície de scattering, $\vartheta \ll 1.7^o\,\Omega_0^{1/2}$ (ver Eq. (1.37)), as flutuações em ϕ, $\vec{v}$ e δ tiveram tempo para entrar em oscilações "acústicas" antes de se iniciar a recombinação. Isto dá origem aos picos "doppler" que se observam na Fig. 3.2. A posição

destes picos é essencialmente determinada pela geometria do universo (Kamionkowski *et al.* 1994 [58], Frampton *et al.* 1998 [34]), uma vez que uma mesma escala física subentende diferentes escalas angulares para universos com diferentes curvaturas. De acordo com (1.37) o ângulo subentendido por uma dada escala diminui com Ω_0. Deste modo os picos doppler do gráfico 3.2 deslocam-se no sentido das pequenas escalas angulares (l's elevados) à medida que Ω_0 diminui.

Diffusion Damping

Para pequenas escalas, $\vartheta < 0.1^o\,\Omega_0^{1/2}$ ($l > 10^3$), as flutuações de temperatura começam a esbater-se. Isto acontece porque o processo de desacoplamento da radiação com a matéria não é instantâneo e a última superfície de scattering não é infinitamente fina. Com efeito, como o período de decoupling decorre durante um intervalo de redshifts $\Delta z \simeq 100$ ([57, 62]), a temperatura CMB que se observa numa dada direcção do céu é na realidade uma "média ponderada", correspondendo a uma mistura de fotões vindos das partes mais próximas e mais afastadas da LSS. Este efeito é designado de efeito de "damping" e apaga/destroi quaisquer flutuações em escalas inferiores à espessura da LSS.

Para além do 'diffusion damping' existem outros mecanismos de difusão que destroiem e apagam a assinatura das anisotropias na região das pequenas escalas. Um destes mecanismos é o chamado **Silk damping** (Silk 1968 [100]) e consiste numa diminuição das flutuações da radiação e da matéria bariónica na LSS, por via da difusão de fotões que arrastam consigo bariões das regiões de sobredensidade. Como a radiação não interage com matéria escura não bariónica, este efeito não afecta as flutuações de densidade dos constituintes deste tipo de matéria. No entanto existe um outro mecanismo de difusão (*free–streeming*) das regiões de sobredensidade para as regiões menos densas, que pode diminuir as flutuações de densidade de partículas não interactivas (como é o caso dos constituintes da matéria escura). De acordo com Bond & Szalay 1983 [**?**], este mecanismo depende essencialmente da velocidade e da massa das partículas em causa. Partículas "frias", cuja velocidade é baixa (por exemplo matéria escura fria - CDM), praticamente não são afectadas. Partículas susceptíveis de sofrerem free–streeming (como por exemplo matéria escura quente - HDM) podem apresentar fortes diminuições nas flutuações de densidade a partir de uma certa escala física. A escala física a partir da qual este efeito se torna mais significativo, depende da massa das partículas. Por exemplo para neutrinos com massa $m_\nu \simeq 10$ eV, as flutuações de densidade correspondentes podem ser fortemente suprmidas para escalas inferiores ou da ordem do tamanho actual dos super enxames de galáxias [?] (alguns Mpc h^{-1}).

Defeitos Topológicos

Apesar de actualmente existirem modelos híbridos de defeitos topológicos e inflação (Jeannerot 1996 [**?**], Linde *et al* 1997 [**?**], Avelino *et al* 1998 [**?**]), tradicionalmente os modelos topológicos são considerados como uma teoria alternativa ao paradigma inflacionário para gerar perturbações de densidade no universo primordial. Cordas cósmicas (*strings*), texturas e monopólos constam entre os exemplos de defeitos topológicos que, de acordo com a teoria,

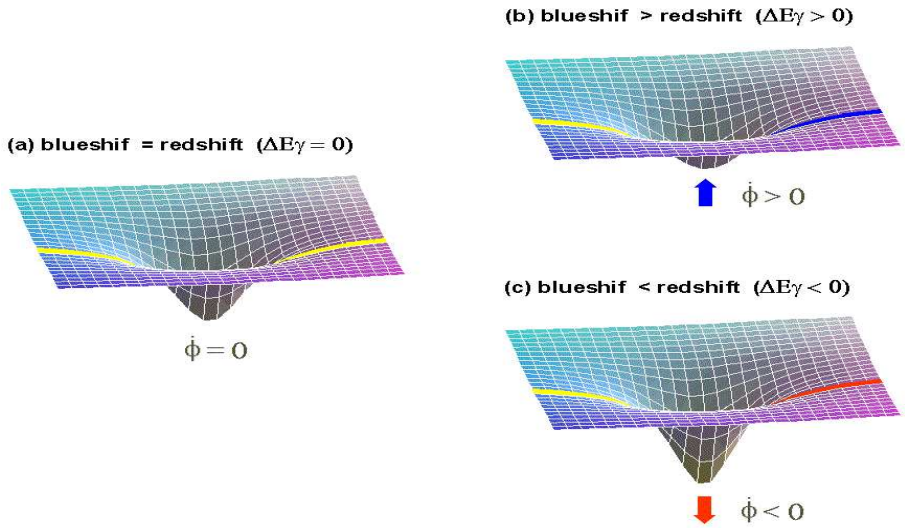

Figure 3.3: Efeito da variação de ϕ na energia dos fotões CMBR

podem ter sido formados por mecanismos de transição de fase associados a quebras de simetria do universo primordial. Contrariamente ao que acontece nos modelos inflacionários standard, as anisotropias CMB geradas por defeitos topológicos apresentam um caracter não gausseano[1]. Esta importante característica pode ser utilizada como meio de descriminar entre estes dois tipos de cenário. Até ao momento as observações da radiação de fundo não dão indicações de fugas significativas à gausseanidade.

3.3.2 Anisotropias Secundárias

Classificam-se de anisotropias secundárias todas as flutuações de temperatura originadas por processos que actuam sobre os fotões CMB após o último scattering. Enquanto a radiação se propaga livre pelo espaço apenas efeitos gravíticos e de rescattering (dispersão) podem gerar novas anisotropias na radiação de fundo. O estudo destes efeitos é normalmente utilizado como uma fonte de informação preciosa sobre a evolução do universo após o decoupling do CMB.

Efeitos Gravíticos

Em teoria, quaisquer perturbações na métrica após o último scattering induzem anisotropias secundárias na radiação de fundo. A acção da gravidade sobre os fotões CMB pode ocorrer de várias formas, sendo algumas delas manifestações de um mesmo efeito: O efeito **Sachs Wolfe Integrado** (ISW). Este efeito dá conta das flutuações de temperatura originadas pela variação do potencial gravítico ao longo das geodésicas dos fotões. Admitindo apenas perturbações

[1]No seio dos modelos inflacionários é igualmente possível originar anisotropias de natureza não gausseana (Salopek 1992 [**?**], Peebles 1999 [**?**, **?**])

escalares na métrica, a sua magnitude é dada por

$$\frac{\Delta T}{T} = \int \dot{\phi}\left[(\hat{r}(\eta), \eta\right]\, d\eta \tag{3.12}$$

onde η é o tempo conforme, $\dot{\phi} = \partial\phi/\partial\eta$ e o integral é feito ao longo da linha de voo do fotões. Se um fotão atravessa um poço de potencial sempre com $\dot{\phi} = 0$, o blueshift que adquire na queda é compensado, com o redshift que sofre quando "sobe" o poço de potencial (situação (a) da figura 3.3). Se o potencial ficar mais ou menos profundo enquanto o fotão se encontra no poço, o blueshift da descida e o redshift da subida já não se cancelam totalmente. Se $\dot{\phi} > 0$ tem-se um blueshift residual (situação (b) da figura 3.3). Se $\dot{\phi} < 0$ tem-se um redshift residual (situação (c) da figura 3.3). Em regime linear, a partir da altura em que o universo fica dominado pela matéria, o potencial gravítico peculiar ϕ permanece constante e portanto não existe qualquer efeito Sachs-Wolfe integrado.

Para além do efeito ISW, a gravidade pode actuar sobre a radiação de fundo como uma lente gravitacional. Neste caso a energia dos fotões permanece constante (em primeira ordem de aproximação), mas as suas trajectorias variam. Em resumo, os principais efeitos gravíticos geradores de anisotropias secundárias são (os três primeiros items da lista tratam-se diferentes manifestações do efeito ISW):

- **Efeito Sachs-Wolfe integrado inicial** (Early ISW)

  Para modelos típicos, a época de igualdade matéria radiação ocorre um pouco antes da recombinação. Sendo assim, logo após o último scattering, a densidade de radiação contribui ainda de forma não negligível para a densidade total do universo. À medida que o universo se expande e se torna dominado pela matéria isto provoca um decaimento no potencial ϕ, logo após o último scattering, a que se dá o nome de efeito ISW inicial (early). Tendo em conta que a densidade dos fotões está fixa pela temperatura actual do CMB, este efeito torna-se tanto mais importante quanto menor for a densidade total do universo, Ω.

- **Efeito Sachs-Wolfe integrado tardio** (Late ISW)

  Se $\Lambda > 0$ o universo eventualmente acabará por ser dominado pelo vácuo. Se $k \neq 0$ ($\Omega + \Omega_\Lambda \neq 1$) o universo poderá passar por uma fase em que é dominado pela curvatura (ver secção 1.2.1). Em ambas as situações o universo experimenta mudanças bruscas na taxa de expansão o que acarreta variações em ϕ para baixos valores de z ($z < \Omega^{-1}$).

- **Efeito Rees-Sciama**

  Em regime linear de perturbações, após o domínio da matéria, $\dot{\phi} = 0$. No entanto à medida que se formam estruturas não lineares (enxames e galáxias) o regime linear deixa de ser válido e $\dot{\phi}$ deixa de ser nulo. Este é um efeito igualmente "tardio" uma vez que a formação de estruturas não lineares, por colapso gravitacional, inicia-se somente para baixos redshifts. Apesar de ser ainda um assunto em aberto, tudo indica que a intensidade relativa do efeito Rees-Sciama (Rees & Sciama 1968 [**?**], Sanz *et al* 1996, [**?**]) é pequena face à amplitude das anisotropias primárias. Nos modelos CDM standart, por exemplo, o efeito é em geral negligível, à excepção de escalas angulares muito pequenas.

- **Lensing Gravitacional**

  É um efeito complementar ao efeito ISW, também relacionado com a variação de ϕ ao longo das geodésicas dos fotões. No efeito ISW os fotões perdem ou ganham energia por troca de pequenos impulsos de momento com o gradiente do campo gravítico paralelo à linha de voo, $\nabla\phi_{\perp}$. No entanto a componente perpendicular a essa mesma linha, $\nabla\phi_{||}$, provoca igualmente alterações no momento dos fotões, que em primeira ordem não altera a energia da radiação mas provoca deflecções na sua trajectória. Se θ for a distância angular entre dois fotões sem deflecções e $\theta + \Delta\theta$ o ângulo real com deflecções, é possível mostrar que $\Delta\theta/\theta \ll 1$ (Seljak 1996 [**?**]). Para modelos típicos $\Delta\theta/\theta \simeq 0.1 - 0.2$. Isto significa que este é essencialmente um efeito de lensing fraco. Se imaginarmos as flutuações CMB (na ausência deste efeito) pintadas sobre a superfície de uma esfera, a acção do lensing constituiria um esticar e deformar da esfera, de forma aleatória, tal como acontece com a imagem distorcida dos espelhos dos parques de diversão. O efeito resultante traduz-se por um deformar da imagem da LSS. No entanto como $\Delta\theta/\theta << 1$, estas distorções constituem sempre mapas injectivos (one-to-one) e por isso em nenhuma região a imagem se sobrepõe sobre si própria. Na figura 3.4 (gráfico da esquerda) pode observar-se uma estimativa da acção do lensing gravítico sobre o espectro de potência angular. As linhas a tracejado e a cheio representam curvas com e sem lensing do CMB.O resultado final deste efeito é pequeno (tipicamente introduz variações inferiores a poucos pontos percentuais nas regiões das pequenas escalas angulares) e consiste essencialmente em redistribuir potência dos picos para os vales. Algumas das futuras experiências CMB poderão vir a detectar este efeito.

- **Ondas gravitacionais**

  Ondas gravitacionais podem gerar anisotropias secundárias através do efeito ISW. A sua acção sobre o espectro da radiação, a observar-se, afecta as escalas angulares superiores à escala do horizonte à época da recombinação (Crittenden *et al.* 1994, [**?**]).

Reonização e rescattering

Se o universo se reoniza após o último scattering, electrões livres podem voltar a dispersar os fotões da radiação cósmica de fundo (resacttering). A existência de rescattering faz apagar as anisotropias primárias e cria novas anisotropias. Isto pode acontecer localmente, por exemplo no interior de enxames de galáxias, ou de uma forma global por todo o universo.

- **Reionização Global**

  As anisotropias primárias podem ser fortemente suprimidas se o universo se reonizou de uma forma global para um redshift suficientemente elevado ($z_r \sim 100$). Na região das pequenas escalas angulares essa supressão pode ser total. Existindo reionização global, os fotões provenientes de uma dada região do céu não tem necessariamente que provir dessa mesma direcção, desde a última superficie de scattering até nós. Na figura 3.5 vemos que um fotão que sofra rescattering, por exemplo, para $z_r = 10$ pode ter tido

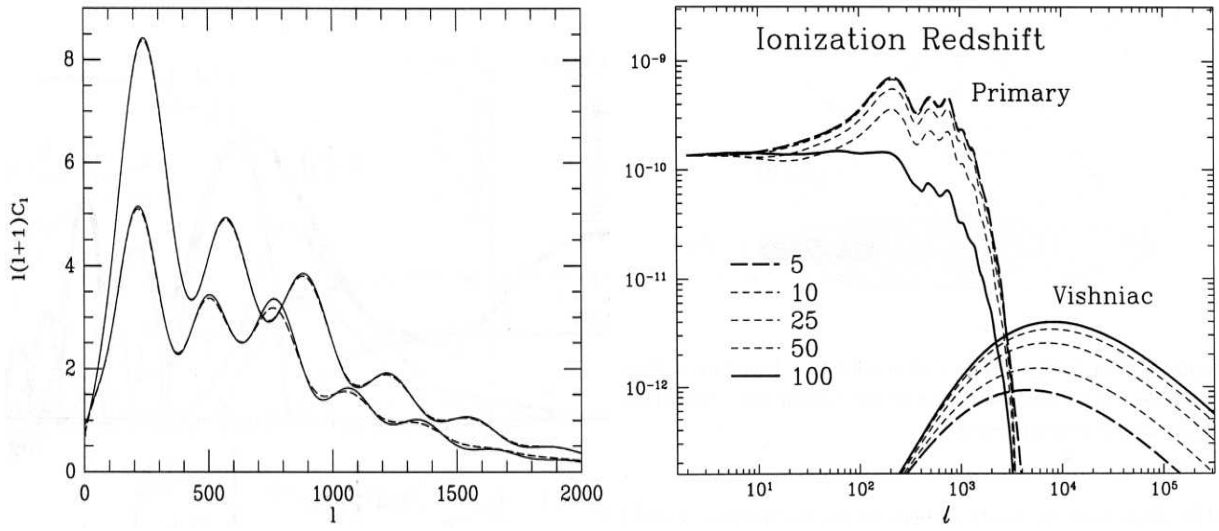

Figure 3.4: Efeitos do lensing gravitacional (à esquerda), reionização global e efeito Vishniac (à direita) sobre o espectro CMBR. Imagens reimpressas de [?] e [52], respectivamente.

origem em qualquer ponto da região a escuro na LSS. Sendo assim num universo aonde ocorra reonização global, a temperatura medida numa dada direcção do céu corresponde a uma média ponderada de temperaturas de uma fração da LSS. Na figura 3.4 (gráfico da direita) pode observar-se os efeitos da reonização global no espectro de potência angular.As diferentes curvas correpondem a diferentes redshifts z_r a partir do quais o universo subitamente se reionizou e assim permaneceu até à actualidade. As principais conclusões a retirar são: (i) Na região das grandes escalas angulares (pequenos l) o espectro praticamente não se altera. (ii) Na região das pequenas escalas (grandes l) o espectro é suprimido por um factor $e^{-2\tau}$, onde $\tau = \sigma_T \int n_e d\eta$ é a profundidade óptica do universo (Tegmark & Silk 1995 [**?**]):

$$\tau \approx \Omega_0^{-1/2} \left(\frac{h\Omega_B}{0.06}\right) \left(\frac{z_r}{92}\right)^{3/2} \tag{3.13}$$

(n_e é a densidade de electrões e σ_T é a secção eficaz de Thomson).

- **Efeito Vishniac**

  É um efeito associado a uma reonização global do universo, que cria novas flutuações de temperatura na região das pequenas escalas angulares (Ostriker & Vishniac 1986 [**?**], Vishniac 1987 [**?**]). A sua origem está relacionada com o acoplamento das flutuações de velocidade e de densidade dos electrões livres. É na realidade um efeito cinemático da mesma natureza que o efeito SZ cinético (ver abaixo) relacionado com a evolução linear das perturbações de densidade. Conforme se pode observar no gráfico da direita da figura 3.4 a intensidade deste efeito é pequena.

- **Reionização Local. Efeito Sunyaev Zel'dovich (SZ).**

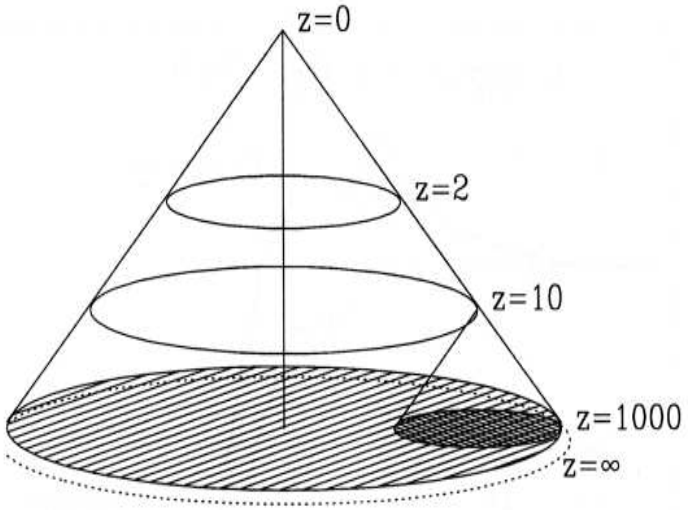

Figure 3.5: Cone de luz do passado num universo plano com $\Omega = 1$. Um fotão que sofra rescattering para $z = 10$ pode ter tido origem em qualquer ponto dentro da região a escuro na LSS. Neste diagrama o eixo vertical é medido em tempo conforme η e as dimensões espaciais em coordenadas comoveis. Imagem reimpressa de [107].

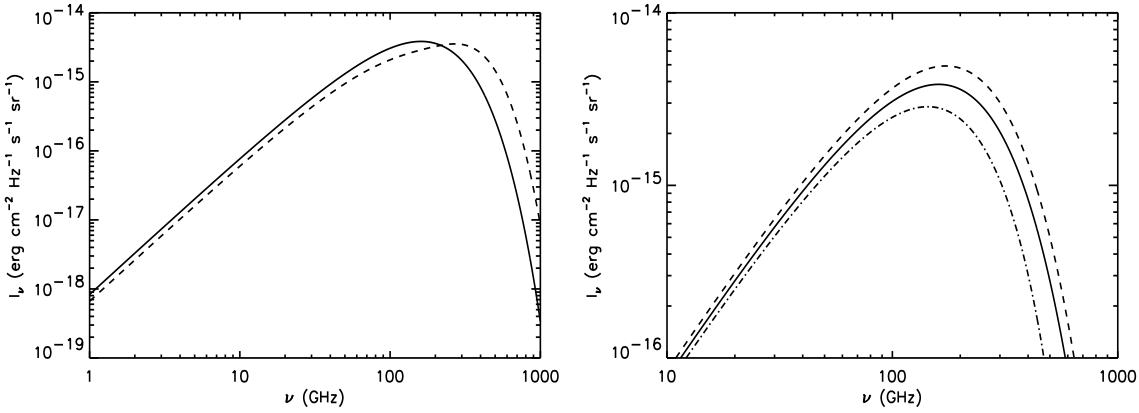

Figure 3.6: **À esquerda**: Distorção espectral provocada pelo efeito SZ térmico, com $y = 0.1$ (valor muito exagerado). O campo de radiação ganha energia ao ser disperso, através do efeito compton inverso, por gas a elevada temperatura no interior de enxames de galáxias. Como o número total fotões permanece constante, fotões na região de Rayleigh-Jeans ganham energia e deslocam-se para a região espectral de Wien. **À direita**: Distorção espectral provocada pelo efeito SZ cinético, com $\tau = 0.9$ e $v_r = \mp 0.1$c. Estas quantidades estão igualmente exageradas para se poder observar melhor a acção deste efeito sobre o espectro térmico CMBR.Em ambos os gráficos as linhas a tracejado e a cheio representam, respectivamente, o espectro CMB com e sem distorções SZ, [?].

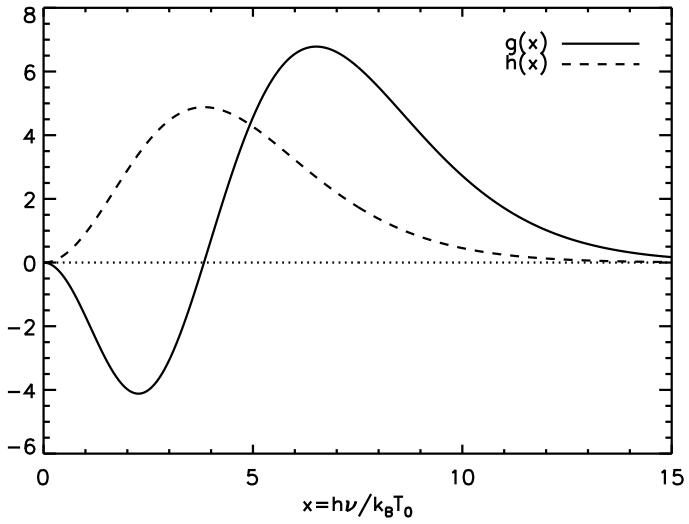

Figure 3.7: Funções de distorção espectral $g(x)$ (linha a cheio) e $h(x)$ (linha a tracejado) dos efeitos SZ térmico e cinético. A função de distorção do efeito térmico anula-se para $x = 3.83$, o que, para $T_{cmb} = 2.728$, corresponde à frequência $\nu = 217$ GHz. Deste modo a distorção SZ total no canal 217 GHz é apenas devida ao efeito cinético. Esta é uma propriedade importante do efeito SZ, que poderá permitir separar as anisotropias geradas pelo efeito cinético do efeito térmico, [?].

Ao contrário do que se passa com a reionização global, é um dado adquirido que existem fenómenos de reionização local no universo. O colapso gravitacional de gas para os poços de potêncial faz elevar a temperatura das partículas ao ponto de estas se reionizarem. Nos enxames de galáxias, por exemplo, a temperatura do gas pode atingir as várias dezenas de milhões de graus Kelvin, temperatura que é manifestamente suficiente para manter o hidrogénio e o hélio ionozados. A acção da reonização local sobre o espectro da radiação de fundo manifesta-se de uma forma característica, através do efeito Sunyaev Zel'dovich (Sunyaev & Zel'dovich 1970,1972 [**?**, **?**]). Este efeito, que consite na variação de energia da radiação de fundo quando esta sofre dispersão de compton pelos electrões livres existentes no interior das massas de gas, actua localmente ao nível das pequenas escalas angulares e pode ser separado em duas componentes:

Efeito SZ - Térmico: É o efeito SZ dominante. É devido ao movimento térmico dos electrões, cuja destribuição de velocidades é aproximadamente isotrópica em torno do centro de massa. Como os electrões estão a uma temperatura mais elevada do que os fotões CMB, a radiação ganha energia (por efeito de Compton inverso), sem que haja variação do número de fotões. Conforme se pode observar no gráfico da esquerda da figura 3.6 isto dá origem a uma sobre-população do espectro térmico da radiação na região de Wien (altas frequências) e um decréscimo na região espectral de Rayleigh-Jeans. A distorção espectral do efeito SZ térmico é dada por:

$$\Delta I_{th} = I_0\, g(x) \int \frac{k_B \sigma_T}{m_e c^2} T_e\, n_e\; dl \tag{3.14}$$

onde $I_0 = 2(k_B T_{cmb})^3/(hc)^2$ é uma constante, $g(x)$ é uma função da frequência adimensional $x = h\nu/k_B T_{cmb}$ (ver figura 3.7) e o integral (feito ao longo da linha de visão) é o chamado parametro de comptonização y. Conforme se pode ver a partir de (3.14), o efeito SZ térmico é tanto mais intenso quanto maior for a densidade e a temperatura dos electrões na direcção da linha de observação. A sua dependência espectral característica (ver figura 3.7) permite-nos separa-lo das restantes anisotropias CMB. Experiências, que observam em múltiplos canais de frequência, como é o caso do satélite Planck, permitem já observar um grande número (mais de um milhar) de fontes SZ térmico (essencialmente enxames de galáxias). Estas observações são de grande importância, porque permitem, em conjunção com observações em raios X e no óptico, impor constrangimentos adicionais em parametros cosmológicos importantes como a normalização do espectro de potência da matéria e, h e Ω_0. Por outro lado permite igualmente estudar as características da distribuição de matéria no interior dos enxames de galáxias.

Efeito SZ - Cinético: É devido à velocidade do centro de massa do gas relativamente ao referêncial do observador. Se a massa de gas se está a aproximar/afastar do observador, o scattering dos fotões CMB provoca um efeito de doppler, que se traduz num blueshift/redshift dos fotões observados na direcção da massa de gas. A variação de intensidade espectral correspondente é dada por:

$$\Delta I_k = -I_0\, h(x)\, \frac{v_r}{c}\tau \tag{3.15}$$

e pode ser observada no diagrama da direita da figura 3.6. Nesta expressão $h(x)$ é a função de distorção espectral do efeito cinético (ver figura 3.7), τ é a profundidade óptica e v_r é a velocidade do centro de massa do gas (positiva em caso de afastamento, negativa em caso de aproximação) na diracção de observação. O efeito SZ cinético é tipicamente mais fraco que o efeito térmico (para valores típicos de y, v_r e τ a razão de intensidade entre os efeitos é geralmente inferior a 0.1). Este facto, associado a uma dependência espectral idêntica à dependência das anisotropias primárias, faz com que o efeito SZ cinético seja de difícil observação.

- **Reionização não Homogénia**

  Fenómenos de reionização não homogénia, provocados por estrelas e quasars formados a elevados redshifts, podem gerar (via efeito doppler) anisótropias secundárias na radiação de fundo.

3.3.3 Anisotropias Terciárias

Não se tratam de anisotropias CMBR no sentido convencional. São antes foregrounds e ruídos, que se sobrepoem, na mesma região espectral, às anisotropias da radiação cósmica de fundo - ver figura 3.9. Para se poder ter acesso à informação contida nas anisotropias primárias e secundárias do CMB, torna-se imprescindível estimar e remover, da melhor forma possível, todos os tipos de contaminação espectral, que possam estar presentes no sinal CMB que se observa. Qualquer tentativa credível para determinação de parâmetros cosmológicos ou

informação acerca do universo permordial, que use a radiação de fundo, exige trabalho aturado e um estudo profundo de todas estas contaminações. É convencional catalogar os vários foregrounds quanto à proximidade da sua origem. Estes podem ter origem,

- **Extra-galáctica**: Essencialmente podem-se destinguir dois tipos de contaminações com origem extra-galática. A baixas frequências, $\nu < 300$ GHz, as contaminações são dominadas por populações de fontes radio emissoras (como Nucleos Galácticos Activos compactos, blazers, radio loud QSOs). A frequências elevadas, $\nu > 300$ GHz, dominam fontes emissoras no infra-vermelho longínquo (exemplo, galáxias espirais inactivas). Pelo facto de se encontrarem a grandes distancias, estas fontes surgem nos mapas como fontes pontuais (*point sources*). O seu impacto sobre o fundo de mico-ondas tem maior expressão nas experiências de elevada resolução anglar, como é o caso da missão Planck.

- **Galáctica**: As princípais fontes de contaminação do CMB têm origem na nossa galáxia. São elas poeira, bremsstrahlung (free-free) e emissão de sincrotrão. No primeiro caso, os grãos de poeira interstelar são aquecidos por radiação visível e re-emitem energia no infra-vermelho longínquo. Isto afecta essencialmente frequências acima de $\nu > 90$ GHz (grãos de poeira com rotação podem igualmente contaminar frequências entre os ~ 10 GHz e os ~ 100 GHz, ver [5] e referências aí incluidas). A emissão bremsstrahlung tem origem quando electrões livres, a elevada temperatura ($T > 10^4$), interagem com o potencial dos iões existentes nas massas de gas interestelar, emitindo radiação. A faixa de frequências afectada é $\nu \sim 25 - 75$ GHz. Finalmente, a emissão de sincrotrão ocorre sempre que electrões relativistas são acelerados em campos magnéticos e domina as restantes contaminações galácticas na região das baixas frequências, $\nu < 20$ GHZ.

- **Contaminações locais**: O Sol, a Lua a Terra e outros corpos planetários, que emitam ou reflectem na região das micro-ondas, devem de ser tidos em conta por qualquer dispositivo experimental que pretenda medir flutuações de temperatura da ordem dos 10^{-5} K. A esta escala de temperaturas a própria emisão térmica do aparato experimental introduz ruído "electrónico" nas medições. Experiências baseadas em terra ou em balões, sofrem igualmente das consequências da emissão atmosférica. Estes são alguns dos muitos problemas que podem afectar as observações CMB e são naturalmente tratados caso-a-caso, uma vez que estão directamente dependentes das características do aparato experimental.

Na figura 3.8 faz-se uma síntese da sensibilidade angular e de frequência de algumas experiências CMB. As zonas a tracejado representam as regiões do plano $\nu - l$ onde os foregrounds dominam o o fundo de radiação de micro-ondas.

As anisotropias secundárias devidas a fenómenos de reionização são normalmente incluidas nesta lista de foregrounds. O facto de terem origem extra–galáctica faz com que elas próprias contenham geralmente informação de caracter cosmológico e por isso mesmo sejam tratadas em separado. O efeito Sunyaev Zel'dovich, por exemplo, (responsável pelas últimas duas camadas de foregrounds da figura 3.9) apresenta um espectro de potência angular muito semelhante a ruído gausseano (i.e. C_l constante com l), que importa "isolar" para se poder estudar

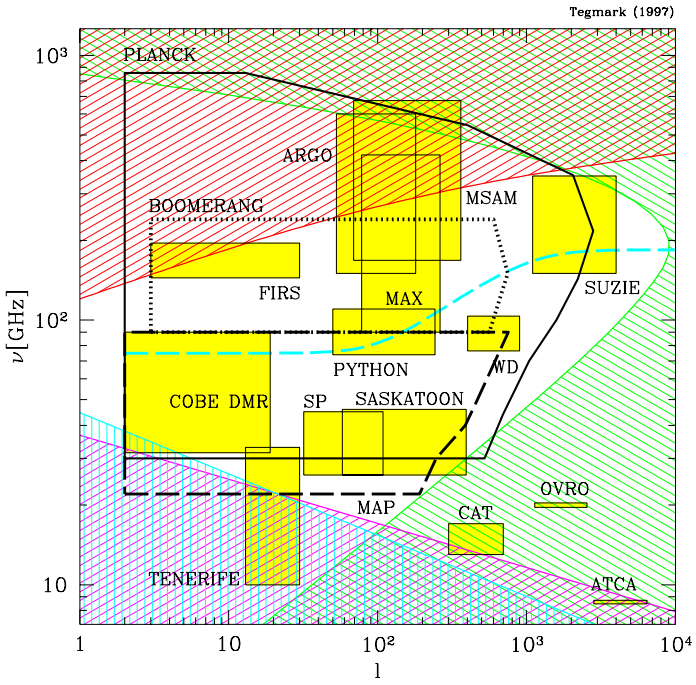

Figure 3.8: As formas poligonais representam as regiões de frequências e multipolos analizadas por diferentes experiências CMB. As zonas a tracejado representam as regiões do plano $\nu - l$ onde se espera que os foregrounds excedam as anisotropias CMBR nas 20% regiões mais limpas do céu. O esquema de cores adoptado para os foregrounds é o seguinte: Poeira (vermelho), point-sources (verde), sincrotrão (magenta) e emissão free-free (azul claro). A linha a tracejado azul clara indica o lugar do plano onde a contribuição total dos foregrounds é minima para cada multipolo (Tegmark & Efstathiou 1996, [?])

separadamente a informação contida nas anisotropias primárias do CMB e nas anisotropias introduzidas pelo próprio efeito SZ.

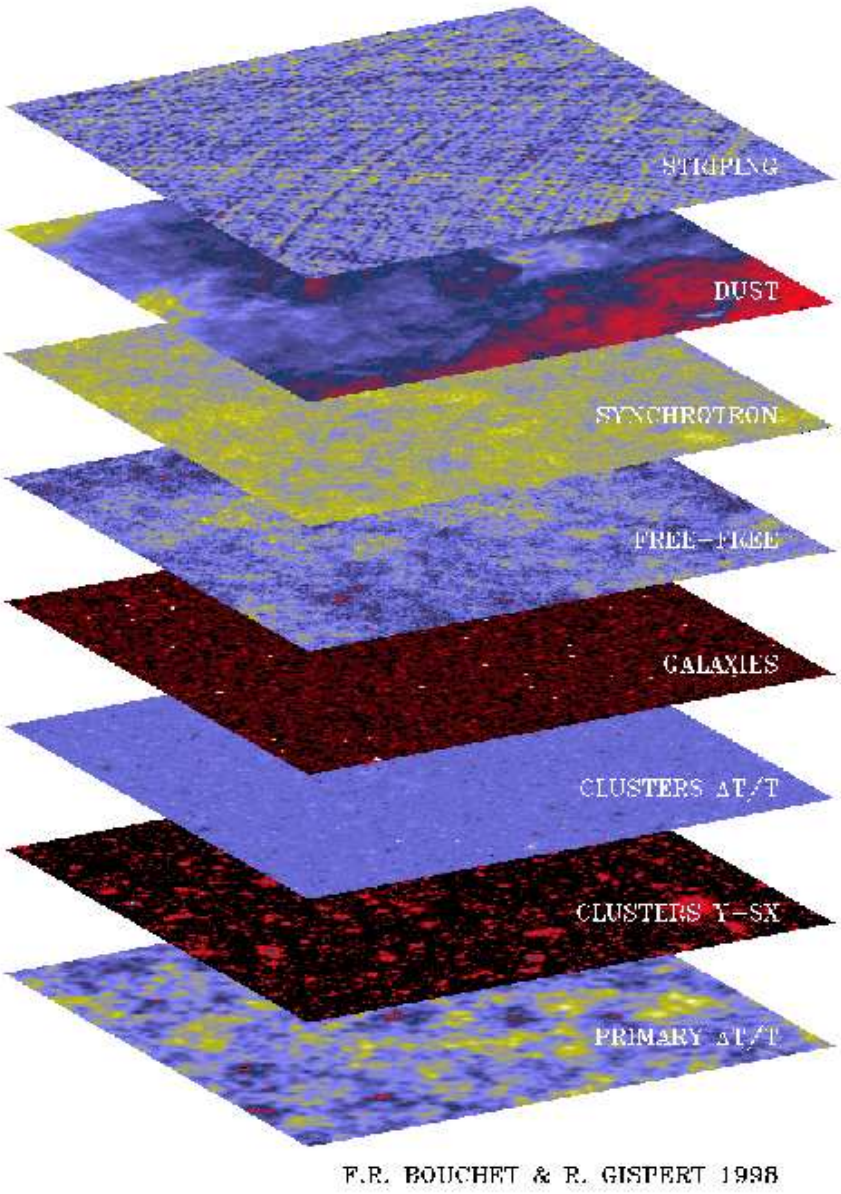

Figure 3.9: Visão esquemática dos vários componentes do fundo de micro-ondas ("sandwich cósmica"). O sinal CMB que se mede no céu contém, para além das anisótropias CMB primárias, todo um conjunto de foregrounds e ruídos que importa remover. Cada uma das camadas corresponde a um foreground que se adiciona ao sinal cosmológico CMB (na base). Os mapas têm uma extensão angular de 10^0 e estão representados na vertical consoante a proximidade da sua origem. No topo estão representados os efeitos de ruido (striping) intrínsecos à experiência. À medida que "descemos na sandwich" encontramos os foregrounds com origem na nossa galáxia, poeira (DUST), emissão de sincrotrão (SYNCHROTRON), bremsstrahlung (FREE-FREE) e com origem extra–galáctica, emissão em infravermelho e rádio de galáxias (GALAXIES) e contaminação devida a enxames (efeitos Sunyaev Zeldovich cinético, $\Delta T/T$, e térmico, Y-SX).

Bibliography

[1] CMBFAST web site: `physics.nyu.edu/matiasz/CMBFAST/cmbfast.html`.

[2] J. M. Bardeen. *Phys. Rev.*, D22:1882, 1980.

[3] J. M. Bardeen, J. R. Bond, N. Kaiser, and A. S. Szalay. 304:15, 1986.

[4] J. M. Bardeen, P. J. Steinhardt, and M. S. Turner. *Phys. Rev.*, D28:679, 1983.

[5] R. Belén Barreiro. The cosmic microwave background: State of the art. astro-ph/9907094, 1999.

[6] F. Benardeau. 427, 51 1994.

[7] C. L. Bennett, A. J. Banday, K. M. Gorski, G. Hinshaw, P. Jackson, P. Keegstra, A. Kogut, G. F. Smoot, D. T. Wilkinson, and E. L. Wright. Four-year cobe dmr cosmic microwave background observations: Maps and basic results. 464, L1 1996.

[8] E. Bertschinger. Simultations of structure formation in the universe. *Ann. Rev. Astron. Astrophys.*, 36:599–654, 1998.

[9] G. D. Birkhoff. *Relativity and Modern Physics*. Harvard University Press, Cambridge, Mass., 1923.

[10] A. Blanchard. The physics of baryons in cosmology. In David Valls-Gabaud et al., editors, *ASP Conf. Ser. 126: From Quantum Fluctuations to Cosmological Structures*, volume 1 of *329-347*. Astronomical Society of the Pacific, 1997.

[11] J. R. Bond and G. Efstathiou. The statistics of cosmic background radiation fluctuations. *MNRAS*, 226:655, 1987.

[12] J. R. Bondi and A. S. Szalay. 276:443, 1983.

[13] G. L. Bryan and M. L. Norman. *Ap. J*, 495:80, 1998.

[14] E. F. Bunn. Calculation of cosmic background radiation anisotropies and implications. In *NATO ASIC Proc. 502: The Cosmic Microwave Background*, pages 135+, 1997. astro-ph/960788.

[15] C. Burigana, L. Danese, and G. De Zotti. Formation and evolution of early distortions of the microwave background spectrum: a numerical study. *Astron. Astrophys.*, 246:49, 1991.

[16] S. M. Carroll, W. H. Press, and E. L. Turner. The cosmological constant. *Annu. Rev. Astron. Astrophys.*, 30:499–542, 1992.

[17] S. Cole and C. Lacey. *MNRAS*, 281:716, 1996.

[18] P. Coles and F. Lucchin. *Cosmology – The Origin and Evolution of Cosmic Structure.* John Wiley & Sons, 1995.

[19] H. M. P. Couchman. Mesh-refined p3m - a fast adaptive n-body algorithm. 368:L23–L26, 1991.

[20] H. M. P. Couchman, P. A. Thomas, and F. R Pearce. Hydra: an adaptive-mesh implementation of p 3m-sph. 452:797, 1995.

[21] P. de Bernardis, P. A. R. Ade, J. J. Bock, J. R. Bond, J. Borrill, A. Boscaleri, K. Coble, C. R. Contaldi, B. P. Crill, G. De Troia, P. Farese, K. Ganga, M. Giacometti, E. Hivon, V. V. Hristov, A. Iacoangeli, A. H. Jaffe, W. C. Jones, A. E. Lange, L. Martinis, S. Masi, P. Mason, P. D. Mauskopf, A. Melchiorri, T. Montroy, C. B. Netterfield, E. Pascale, F. Piacentini, D. Pogosyan, G. Polenta, F. Pongetti, S. Prunet, G. Romeo, J. E. Ruhl, and F. Scaramuzzi. Multiple Peaks in the Angular Power Spectrum of the Cosmic Microwave Background: Significance and Consequences for Cosmology. 564:559–566, January 2002.

[22] R. D'Inverno. *Introducing Einstein Relativity.* Clarendon Press, Oxford, 1992.

[23] Ray D'Inverno. *Introducing Einstein Relativity.* Clarendon Press, Oxford, 1992.

[24] S. Dodelson, G. Gyuk, and M. S. Turner. Is a massive tau neutrino just what cold dark matter needs? *Phys. Rev. Lett.*, 72:3754–3757, 1994. astro-ph/9402028.

[25] R. Durrer, M. Kunz, and A. Melchiorri. Cosmic structure formation with topological defects. astro-ph/0110348, 2001.

[26] G. Efstathiou. Suppressing the formation of dwarf galaxies via photoionization. *MNRAS*, 256:43–47, 1992.

[27] G. Efstathiou, M. Davis, C. S. Frenk, and S. D. M. White. Numerical techniques for large cosmological n-body simulations. *Ap. J. Suppl.*, 57:241–260, 1985.

[28] G. Efstathiou and J. W. Eastwood. On the clustering of particles in an expanding universe. *MNRAS*, 194:503–525, 1981.

[29] D. G. Eisenstein and W. Hu. 511:5, 1999.

[30] V. R. Eke, S. Cole, and C. S. Frenk. Cluster evolution as a diagnostic for omega. *MNRAS*, 282:263–280, 1996.

[31] V. R. Eke, J. F. Navarro, and C. S. Frenk. The evolution of x-ray clusters in a low-density universe. 503:569, 1998.

[32] A. E. Evrard. Biased cold dark matter theory - trouble from rich clusters? 341:L71–L74, 1989.

[33] D. J. Fixsen, E. S. Cheng, J. M. Gales, Mather J. C., R. A. Shafer, and E. L. Wright. The cosmic microwave background spectrum from the full cobe firas data set. 473:576, 1996.

[34] P. Frampton, Y Jack Ng, and Ryan Rohm. Cosmic background radiation temperature anisotropy: Position of the first doppler peak. astro-ph/9806118, 1998.

[35] W. L. Freedman. The measure of cosmological parameters. astro-ph/0202006.

[36] W. L. Freedman. Determination of the hubble constant. In N. Turok, editor, *Critical Dialogs in Cosmology*, Singapore, 1997. World Scientific. astro-ph/9612024.

[37] W. L. Freedman, B. F. Madore, B. K. Gibson, L. Ferrarese, D. D. Kelson, S. Sakai, J. R. Mould, R. C. Kennicutt, H. C. Ford, J. A. Graham, J. P. Huchra, S. M. G. Hughes, G. D. Illingworth, L. M. Macri, and P. B. Stetson. Final Results from the Hubble Space Telescope Key Project to Measure the Hubble Constant. 553:47–72, May 2001.

[38] R. A. Gingold and J. J. Monaghan. Smoothed particle hydrodynamics - theory and application to non-spherical stars. *MNRAS*, 181:375–389, 1977.

[39] J. E. Gunn and B. A. Peterson. On the density of neutral hydrogen in intergalactic space. 142:1633–1636, 1965.

[40] A. H. Guth. *Phys. Rev.*, D23:347, 1981.

[41] A. H. Guth and S.-Y. Pi. *Phys. Rev. Lett.*, 49:1110, 1982.

[42] Z. Haiman and L. Knox. Reionization of the intergalactic medium and its effect on the cmb. In A. de Oliveira-Costa & M. Tegmark, editor, *Microwave Foregrounds*, volume 181 of *ASP Conference Series*. ASP Conference Series, 1999.

[43] R. Harrison. *Phys. Rev.*, D1:2726, 1970.

[44] S. M. Harun-or-Rashid and M. Roos. Statistical evaluation of the observational information on ω_m and ω_Λ. *Astron. and Astrophys.*, 373:369–376, July 2001.

[45] S. W. Hawking. *Phys. Lett.*, B115:295, 1982.

[46] P. Helbig. Constraints in the λ_0 and ω_0 plane from gravitational lensing. In *IAU Symposium*, page 295, 2000. astro-ph/0011031.

[47] M. A. Hendry and R. J. Tayler. *Contemp. Phys.*, 37:263, 1996.

[48] J. P. Henry and K. A. Arnaud. A measurement of the mass fluctuation spectrum from the cluster x-ray temperature function. 372:410–418, 1991.

[49] M. B. Hindmarsh and T. W. B. Kibble. *Rep. Prog. Phys.*, 58:477, 1995.

[50] R. W. Hockney and J. W. Eastwood. *Computer Simulation Using Particles*. Adam Hilger, Bristol, 1988.

[51] W. Hu. *Wandering in the Background: A Cosmic Microwave Background Explorer*. PhD thesis, University of California at Berkeley, 1995. astro-ph/9508126.

[52] Wayne Hu. *Wandering in the Background: A Cosmic Microwave Background Explorer*. PhD thesis, University of California at Berkeley, 1995. astro-ph/9508126.

[53] Wayne Hu, Naoshi Sugiyama, and Joseph Silk. The physics of microwave background anisotropies. *Nature*, 386:37–43, 1997. astro-ph/9604166.

[54] G. H. Jacoby, D. Branch, R. Clardullo, R. L. Davies, W. E. Harris, M. J. Pierce, C. J. Pritchet, J. L. Tonry, and D. L. Welch. A critical review of selected techniques for measuring extragalactic distances. *Pub. Astron. Soc. Pac.*, 104:599–662, August 1992.

[55] J. H. Jeans. The stability of spiral nebula. *Phill. Trans. R. Soc.*, 199A:1, 1902.

[56] S. Jha, P. M. Garnavich, R. P. Kirshner, P. Challis, A. M. Soderberg, L. M. Macri, J. P. Huchra, P. Barmby, E. J. Barton, P. Berlind, W. R. Brown, N. Caldwell, M. L. Calkins, S. J. Kannappan, D. M. Koranyi, M. A. Pahre, K. J. Rines, K. Z. Stanek, R. P. Stefanik, A. H. Szentgyorgyi, P. Väisänen, Z. Wang, J. M. Zajac, A. G. Riess, A. V. Filippenko, W. Li, M. Modjaz, R. R. Treffers, C. W. Hergenrother, E. K. Grebel, P. Seitzer, G. H. Jacoby, P. J. Benson, A. Rizvi, L. A. Marschall, J. D. Goldader, M. Beasley, W. D. Vacca, B. Leibundgut, J. Spyromilio, B. P. Schmidt, and P. R. Wood. The Type IA Supernova 1998BU in M96 and the Hubble Constant. *Ap. J. Supp.*, 125:73–97, November 1999.

[57] B. Jones and R. Wyse. *A&A*, 149(14), 1985.

[58] M. Kamionkowski, D. Spergel, and N. Sugiyama. *ApJ*, 426(57), 1994.

[59] S. Kay. *Modelling Properties of Galaxies and Clusters*. PhD thesis, University of Durham, 2000.

[60] T. W. B. Kibble. *J. Phys.*, A9:1387, 1976.

[61] E. Kolb and M. Turner. *The Early Universe*, volume 69 of *Frontiers in Physics*. Addison-Wesley Publishing Company, 1990.

[62] Edward Kolb and Michael Turner. *The Early Universe*, volume 69 of *Frontiers in Physics*. Addison-Wesley Publishing Company, 1990.

[63] A. R. Liddle. The early universe. In David Valls-Gabaud et al., editors, *ASP Conf. Ser. 126: From Quantum Fluctuations to Cosmological Structures*, volume 1 of *31-62*. Astronomical Society of the Pacific, 1997.

[64] A. R Liddle and D. H. Lyth. The cold dark matter density perturbation. *Phys Reports*, 231:1, 1993.

[65] A. R. Liddle and D. H. Lyth. *Cosmological Inflation and Large Scale Structure*. Cambridge University Press, 2000.

[66] E. M. Lifshitz. On the gravitational instability of the expanding universe. *Sov. Phys. JETP*, 10:116, 1946.

[67] A. Loeb and R. Barkana. The reionization of the universe by the first stars and quasars. *Ann. Rev. Astron. Astrophys.*, 39:19–66, 2001.

[68] L. C. Lucy. A numerical approach to the testing of the fission hypothesis. *Astron. J.*, 82:1013–1024, 1977.

[69] J. C. Mather, D. J. Fixsen, R. A. Shafer, C. Mosier, and D. T. Wilkinson. Calibrator Design for the COBE Far-Infrared Absolute Spectrophotometer (FIRAS). 512:511–520, February 1999.

[70] W. Mattig. *Astron. Nach.*, 284:109, 1958.

[71] J. J. Monaghan. Smoothed particle hydrodynamics. *Ann. Rev. Astron. Astrophys.*, 30:543–574, 1992.

[72] J. J. Monaghan and J. C. Lattanzio. Further studies of a fragmentation problem. *Astron. and Astrophys.*, 158:207–211, 1986.

[73] V. F. Mukhanov, H. A. Feldman, and R. H. Brandenberger. The theory of cosmological perturbations. *Phys. Rep.*, 215:203–333, 1992.

[74] C. B. Netterfield, P .A. R. Ade, J. J. J.J. Bock, J. R. Bond, J. Borrill, A. Boscaleri, K. Coble, C. R. Contaldi, B. P. Crill, P. de Bernardis, P. Farese, K. Ganga, M. Giacometti, E. Hivon, V. V. Hristov, A. Iacoangeli, A.H. Jaffe, W.C. Jones, A. E. Lange, L. Martinis, S. Masi, P. Mason, P.D. Mauskopf, A. Melchiorri, T. Montroy, E. Pascale, F. Piacentini, D. Pogosyan, F. Pongetti, S. Prunet, G. Romeo, J. E. Ruhl, and F. Scaramuzzi. A measurement by BOOMERANG of multiple peaks in the angular power spectrum of the cosmic microwave background. astro-ph/0104460.

[75] T. Padmanabham. *Structure formation in the Universe*. Cambridge University Press, Cambridge, UK, 1993.

[76] J. A. Peacock. *Cosmological Physics*. Cambridge University Press, Cambridge, UK, 1999.

[77] J. A. Peacock and S. J. Dodds. Reconstructing the linear power spectrum of cosmological fluctuations. *MNARS*, 267:1020, 1994.

[78] P. J. E. Peebles. *Physical Cosmology*. Princeton University Press, Princeton, 1971.

[79] P. J. E. Peebles. *The Large-Scale Structure of the Universe*. Princeton University Press, Princeton, 1980.

[80] P. J. E. Peebles. *Principles of Physical Cosmology*. Princeton University Press, Princeton, 1993.

[81] Ue-Li Pen. Normalizing the temperature function of clusters of galaxies. *Ap. J. S.*, 498:60, 1998.

[82] Ue-Li Pen. Brief note: Analytical fit to the luminosity distance for flat cosmologies with a cosmological constant. *Ap. J. S.*, 120:49, 1999.

[83] S. Perlmutter, G. Aldering, M. della Valle, S. Deustua, R. S. Ellis, S. Fabbro, A. Fruchter, G. Goldhaber, D. E. Groom, I. M. Hook, A. G. Kim, M. Y. Kim, R. A. Knop, C. Lidman, R. G. McMahon, P. Nugent, R. Pain, N. Panagia, C. R. Pennypacker, P. Ruiz-Lapuente, B. Schaefer, and N. Walton. Discovery of a supernova explosion at half the age of the universe. *Nature*, 391:51, January 1998.

[84] S. Perlmutter, G. Aldering, G. Goldhaber, R. A. Knop, P. Nugent, P. G. Castro, S. Deustua, S. Fabbro, A. Goobar, D. E. Groom, I. M. Hook, A. G. Kim, M. Y. Kim, J. C. Lee, N. J. Nunes, R. Pain, C. R. Pennypacker, R. Quimby, C. Lidman, R. S. Ellis, M. Irwin, R. G. McMahon, P. Ruiz-Lapuente, N. Walton, B. Schaefer, B. J. Boyle, A. V. Filippenko, T. Matheson, A. S. Fruchter, N. Panagia, H. J. M. Newberg, W. J. Couch, and The Supernova Cosmology Project. Measurements of Omega and Lambda from 42 High-Redshift Supernovae. 517:565–586, June 1999.

[85] E. Pierpaoli, D. Scott, and M. White. Power-spectrum normalization from the local abundance of rich clusters of galaxies. *MNRAS*, 325:77–88, 1999.

[86] W. H. Press and P. Schechter. Formation of galaxies and clusters of galaxies by selfsimilar gravitational condensation. 187:425–438, 1974.

[87] J. R. Primack. Cosmological Parameters. In *Sources and Detection of Dark Matter and Dark Energy in the Universe*, pages 3–25, 2001. astro-ph/0007187.

[88] C. Pryke, N. W. Halverson, E. M. Leitch, J. Kovac, J. E. Carlstrom, W. L. Holzapfel, and M. Dragovan. Cosmological Parameter Extraction from the First Season of Observations with the Degree Angular Scale Interferometer. *Ap J.*, 568:46–51, March 2002.

[89] A. G. Riess, A. V. Filippenko, P. Challis, A. Clocchiatti, A. Diercks, P. M. Garnavich, R. L. Gilliland, C. J. Hogan, S. Jha, R. P. Kirshner, B. Leibundgut, M. M. Phillips, D. Reiss, B. P. Schmidt, R. A. Schommer, R. C. Smith, J. Spyromilio, C. Stubbs, N. B. Suntzeff, and J. Tonry. Observational Evidence from Supernovae for an Accelerating

Universe and a Cosmological Constant. *Astronomical Journal*, 116:1009–1038, September 1998.

[90] A. G. Riess, W. H. Press, and R. P. Kirshner. A Precise Distance Indicator: Type IA Supernova Multicolor Light-Curve Shapes. 473:88, December 1996.

[91] M. Roos and S. M. Harun-or Rashid. How flat is the universe? astro-ph/0003040.

[92] M. Rowan-Robinson. *The Cosmological Distance Ladder*. Freeman, New York, 1985.

[93] G. B. Rybicki and A. P Lightman. *Radiative Processes in Astrophysics*. John Wiley and Sons, New York, 1979.

[94] R. Sachs and A. Wolfe. *ApJ*, 147(1):73–90, 1967.

[95] R. K. Sachs and A. M. Wolfe. Perturbations of cosmological model and angular variations of the microwave background. 147:73–90, 1967.

[96] A. R. Sandage, R. G. Korn, and M. S. Longair. *The Deep Universe*. Saas-Fee Advanced Course 23. Springer-Verlag, 1993.

[97] B. Schutz. *A first course in General Relativity*. Cambridge University Press, Cambridge, 1990.

[98] U. Seljak and M. Zaldarriaga. A line-of-sight integration approach to cosmic microwave background anisotropies. 469:437–444, 1996.

[99] S. F. Shandarin and Ya. B. Zel'dovich. *Rev. Mod. Phys.*, 61:185, 1989.

[100] J. Silk. *ApJ*, 151:459, 1968.

[101] A. A. Starobinsky. *Phys. Lett. B*, 117:175, 1982.

[102] M. Steinmetz. Simulating galaxy formation. In A. Provenzale S. Bonometto, J. Primack, editor, *International School of Physics Enrico Fermi - Course CXXXII: Dark Matter in the Universe*. IOP, 1995. Vardena.

[103] R. Stompor, M. Abroe, P. Ade, A. Balbi, D. Barbosa, J. Bock, J. Borrill, A. Boscaleri, P. de Bernardis, P. G. Ferreira, S. Hanany, V. Hristov, A. H. Jaffe, A. T. Lee, E. Pascale, B. Rabii, P. L. Richards, G. F. Smoot, C. D. Winant, and J. H. P. Wu. Cosmological Implications of the MAXIMA-1 High-Resolution Cosmic Microwave Background Anisotropy Measurement. 561:L7–L10, November 2001.

[104] N. Sugiyama. *Ap. J. Supp.*, 100:281, 1995.

[105] R. S. Sutherland and M. A. Dopita. Cooling functions for low-density astrophysical plasmas. *Ap. J. S.*, 88:253–327, 1993.

[106] M. Tegmark. *Probes of the Early Universe*. PhD thesis, University of California at Berkeley, April 1994.

[107] Max Tegmark. Doppler peaks and all that: Cmb anisotropies and what can they tell us. astro-ph/9511148, 1996.

[108] P. T. P. Viana and A. R. Liddle. The cluster abundance in flat and open cosmologies. *MNRAS*, 281:323, 1996.

[109] P. T. P. Viana and A. R. Liddle. Galaxy clusters at $0.3 < z < 0.4$ and the value of ω_0. *MNRAS*, 303:535, 1999.

[110] A. Vilenkin and E. P. S. Shellard. *Cosmic Strings and Other Topological Defects*. Cambridge University Press, Cambridge, 1994.

[111] S. Weinberg. *Gravitation and Cosmology*. John Wiley & Sons, 1972.

[112] M. White, J. E. Carlstrom, M. Dragovan, and W. L. Holzapfel. Interferometric observation of cosmic microwave background anisotropies. 514:12–24, 1999.

[113] M. White, G. Gelmini, and J. Silk. Structure formation with decaying neutrinos. *Phys. Rev. D*, 51:2669–2676, March 1995.

[114] Martin White and Wayne Hu. The sachs-wolfe effect. astro-ph/9609105, 1996.

[115] Martin White, Douglas Scott, and Joseph Silk. Anisotropies in the cosmic microwave background. *Ann. Rev. Astron. & Astrophys.*, 32:319–370, 1994.

[116] S. D. M. White, G. Efstathiou, and C. S. Frenk. The amplitude of mass fluctuations in the universe. *MNRAS*, 262:1023–1028, 1993.

[117] G. Yepes. Cosmological numerical simulations. In David Valls-Gabaud et al., editors, *ASP Conf. Ser. 126: From Quantum Fluctuations to Cosmological Structures*, pages 279–311. Astronomical Society of the Pacific, 1997.

[118] Y. B. Zeldovich. *My universe. Selected reviews*. Chur: Harwood Academic Publishers, 1992, edited by Zeldovich, Boris Ya.; Sazhin, M.V., 1992.

[119] Ya. B. Zel'dovich. Gravitational instability: an approximate theory for large density perturbations. *Astron. Astrophys.*, 5:84, 1970.

Appendix A

Cálculo das anisotropias do CMB a grandes escalas angulares

Neste capítulo apresenta-se a derivação do cálculo da amplitude das anisotropias na temperatura da radiação de fundo a grandes escalas, seguindo o artigo histórico por Sachs e Wolfe de 1967.

A.1 Integração da equação das geodésicas para fotões

Um passo importante para o cálculo das flutuações de temperatura na radiação de fundo é a integração da equação das geodésicas para os fotões CMBR ao longo do seu percurso, desde a última superfície de Scattering até nós.

Nos modelos de Friedmann Robertson Walker (FRW) sujeitos a pequenas pertubações, esta tarefa simplifica-se substancialmente se considerarmos apenas perturbações sobre modelos planos

$$ds^2 = g_{ab}dx^a dx^b = a^2(\eta)\left[\eta_{ab} + h_{ab}\right] dx^a dx^b. \tag{A.1}$$

A parte não perturbada da métrica é $a^2(\eta)\eta_{ab}$, onde η_{ab} é o tensor métrico de Minkowski e $a(\eta)$ é o factor de escala das métricas FRW escrito em termos do tempo conforme η ($d\eta = dt/a$). A perturbação h_{ab} é considerada pequena relativamente a η_{ab} no sentido que as suas componentes em módulo verificam $|h_{ab}| << |\eta_{ab}|$. Nos cálculos que se seguem vamos utilizar a assinatura $(+,-,-,-)$ para η_{ab}.

De acordo com Sachs & Wolfe no seu artigo original de 1967, [94], a integração da equação das geodésicas para estes modelos perturbados simplifica-se bastante se notar-mos que as métricas ds^2 e $d\bar{s}^2$, relacionadas por uma transformação conforme

$$ds^2 = a^2\left(\eta\right) d\bar{s}^2, \tag{A.2}$$

apresentam geodésicas do género luz coincidentes [94]. Este facto, permite-nos começar por colocar o problema da integração da equação das geodésicas dos fotões em

$$d\bar{s}^2 = \bar{g}_{ab}dx^a dx^b = \left[\eta_{ab} + h_{ab}\right] dx^a dx^b \tag{A.3}$$

e só depois transpor os resultados para ds^2. A simplificação resulta de $d\bar{s}^2$ não depender explicitamente do factor de escala $a(\eta)$. Naturalmente, os parâmetros afins que parametrizam uma mesma geodésica em ds^2 e $d\bar{s}^2$ são diferentes. Se ξ, ω forem os parâmetros afins de uma dada geodésica do género luz em ds^2 e $d\bar{s}^2$, $x^a(\xi) = x^a(\omega)$, e $k^a = dx^a/d\xi$, $\bar{k}^a = dx^a/d\omega$ os seus respectivos vectores tangentes, é possível demonstrar que se verificam as seguintes relações entre ξ e ω:

$$\bar{k}^a = a^2 k^a \Leftrightarrow \bar{k}_a = k_a \Leftrightarrow d\xi = a^2 d\omega. \tag{A.4}$$

No que toca às partículas materiais pode-se igualmente concluir que o quadrivector velocidade própria dessas partículas se transforma de ds^2 para $d\bar{s}^2$ do seguinte modo

$$u_a = a\bar{u}_a \Leftrightarrow u^a = a^{-1}\bar{u}^a \tag{A.5}$$

Estas expressões são úteis porque permitem transpor os resultados obtidos em $d\bar{s}^2$ para ds^2.

O cálculo das geodésicas em $d\bar{s}^2$ pode efectuar-se recorrendo ao método variacional descrito, por exemplo, em [23] (pp 99-101) e que consiste em resolver as equações de Euler-Lagrange:

$$\frac{\partial \bar{\mathscr{L}}}{\partial x^a} - \frac{d}{d\omega}\left(\frac{\partial \bar{\mathscr{L}}}{\partial \dot{x}^a}\right) = 0 \tag{A.6}$$

para o lagrangeano

$$\bar{\mathscr{L}}\left(x^a, \dot{x}^a, \omega\right) = \bar{g}_{ab}\dot{x}^a\dot{x}^b. \tag{A.7}$$

Os pontos significam derivação em ordem ao parametro afim, ω ($d\dot{x}^a = dx^a/d\omega$). A partir de (A.7) tem-se:

$$\frac{\partial \bar{\mathscr{L}}}{\partial x^a} = h_{bc,a}\dot{x}^b\dot{x}^c \tag{A.8}$$

$$\frac{\partial \bar{\mathscr{L}}}{\partial \dot{x}^a} = 2\left(\eta_{ac} + h_{ac}\right)\dot{x}^c. \tag{A.9}$$

Substituindo estas expressões na equação de Euler-Lagrange, (A.6), obtemos

$$h_{ab,c}\dot{x}^a\dot{x}^b - 2\frac{d}{d\omega}\left[\left(\eta_{cd} + h_{cd}\right)\dot{x}^d\right] = 0. \tag{A.10}$$

A quantidade dentro de parênteses rectos, $(\eta_{cd} + h_{cd})\dot{x}^d = \dot{x}_c$, pode escrever-se em termos do 4-momento fotões, $\bar{k}_c$, que tal como $\dot{x}_c$, é um vector tangente às geodésicas. Para isso basta escolher uma parametrização, ζ, para a qual

$$\bar{k}^0 = \frac{dx^0}{d\zeta} \quad ; \quad \bar{k}^\mu = \bar{k}^0\frac{dx^\mu}{d\eta}, \tag{A.11}$$

onde $\bar{k}^\mu$ é o momento espacial dos fotões. Para um observador comóvel com a expansão, $\bar{k}^0$ dá justamente energia da radiação ($\bar{k}^0 = \bar{E}$), com $\bar{k}_\mu\bar{k}^\mu = \bar{E}^2$. A relação entre os parâmetros afins ω e ζ é assim $\omega = \bar{E}\zeta$ e portanto,

$$\bar{k}^a = \frac{dx^a}{d\zeta} = \frac{dx^a}{d\omega}\frac{d\omega}{d\zeta} = \bar{E}\dot{x}^a. \tag{A.12}$$

Usando esta relação na equação (A.10) podemos então escrever

$$\frac{d}{d\omega}\left[\bar{k}_c\right] = \frac{\bar{E}}{2} h_{ab,c}\dot{x}^a\dot{x}^b. \tag{A.13}$$

Se tivermos em conta que as perturbações são pequenas, podemos admitir que $\bar{E} = \bar{E}_{(0)} + \bar{E}_{(1)}$ e $\dot{x}^a = \dot{x}^a_{(0)} + \dot{x}^a_{(1)}$, com $\bar{E}_{(1)} << \bar{E}_{(0)}$ e $\left|\dot{x}^a_{(1)}\right| << \left|\dot{x}^a_{(0)}\right|$. Isto significa que a energia medida por um observador comóvel, $\bar{E}$, e o momento por unidade de energia, $\dot{x}^\mu$, são essencialmente dominados pelos valores que estas grandezas assumem no universo não perturbado, $\bar{E}_{(0)}$ e $\dot{x}^\mu_{(0)}$. Deste modo a integração de (A.13) para um ponto genérico sobre as geodésicas, ω, em primeira ordem de aproximação conduz a

$$\bar{k}_a(\omega) = \bar{k}_{(0)a} + \frac{\bar{E}_{(0)}}{2}\int_0^\omega h_{bc,a}\dot{x}^b_{(0)}\dot{x}^c_{(0)}d\omega' \tag{A.14}$$

onde $\bar{E}_{(0)}$; $\bar{k}_{(0)a} = \bar{E}_{(0)}\dot{x}^a_{(0)}$ e $x^a_{(0)}$ são respectivamente a energia; o 4-momento e o percurso percorrido pela radiação no universo não perturbado de $d\bar{s}^2$. O termo $\bar{k}_{(0)a}$ surge como constante de integração ao impormos a condição $\bar{k}_a = \bar{k}_{(0)a}$ nos casos limite $\omega = 0$ (último scattering) e/ou $h_{ab} \to 0$ (inexistência de pertubações).

Para podermos avançar no cálculo de (A.14) é agora conveniente determinar a trajectória que os fotões descrevem no universo de fundo (não perturbado), $x^a_{(0)}(\omega)$. A equação das geodésicas para a parte não perturbada de $d\bar{s}^2$, reduz-se a [1]

$$\frac{d^2x^a_{(0)}}{d\omega^2} = 0. \tag{A.15}$$

Integrando esta equação componente a componente temos

$$\begin{cases} \frac{d^2x^\mu_{(0)}}{d^2\omega} = 0 \\ \frac{d^2\eta_{(0)}}{d^2\omega} = 0 \end{cases} \quad \Rightarrow \quad \begin{cases} x^\mu_{(0)} = A^\mu\omega + B^\mu \\ \eta_{(0)} = C\omega + D \end{cases} \tag{A.16}$$

onde $\mu = 1, 2, 3$ e A^μ, B^μ, C, D são constantes de integração a determinar mediante a escolha dos eventos de emissão (último scattering) e recepção (observação) dos fotões. Se escolhermos uma parametrização cujos os acontecimentos de emissão, E, e de recepção, R, ocorram em (ver figura A.1)

$$E \to x^a_{(0)}(\omega = 0) \equiv (\eta_E, c^\mu) \quad ; \quad R \to x^a_{(0)}(\omega = \eta_R - \eta_E) \equiv (\eta_R, \vec{0}) \tag{A.17}$$

vem que:

$$A^\mu = -\frac{c^\mu}{(\eta_R - \eta_E)} \quad ; \quad B^\mu = c^\mu \quad ; \quad C = 1 \quad ; \quad D = \eta_E. \tag{A.18}$$

[1] A obtenção desta expressão é imediata quer se utilise o método variacional ou a equação das geodésicas, $u^a_{;b}u^b = (\partial_b\dot{x}^a + \Gamma^a_{bc}\dot{x}^c)\,\dot{x}^b = 0$. No primeiro caso obtém-se uma equação análoga a (A.13), com η_{ab} no lugar de h_{ab}, e portanto (A.15) resulta de η_{ab} ser constante. No segundo caso (A.15) resulta igualmente de η_{ab} ser constante o que implica que todas as conexões $\Gamma^a_{bc} = 0$.

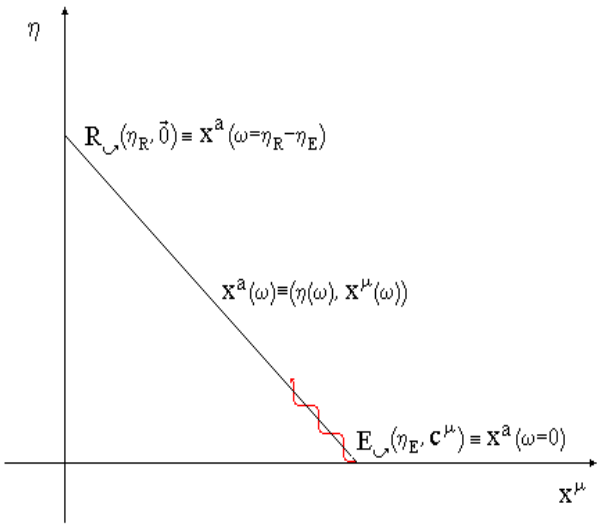

Figure A.1: Diagrama espaço-tempo com a parametrização escolhida para geodésicas da radiação de fundo no universo não perturbado de $d\bar{s}^2$. Os pontos $E \to (\eta_E, c^\mu) = x^a(\omega = 0)$ e $R \to (\eta_R, \vec{0}) = x^a(\omega = \eta_R - \eta_E)$ representam os eventos de último scattering (emissão) e observação (recepção) dos fotões CMB. A coordenada temporal, η, é o tempo conforme $(d\eta = dt/a)$ e o vector espacial x^μ está escrito em coordenadas comóveis.

Sendo assim, o caminho percorrido pelos fotões na parte não perturbada de $d\bar{s}^2$ é

$$x^a_{(0)}(\omega) \equiv \left(\omega + \eta_E, -\frac{c^\mu}{(\eta_R - \eta_E)}\omega + c^\mu\right) \tag{A.19}$$

e portanto,

$$\dot{x}^a_{(0)}(\omega) = \frac{dx^a_{(0)}}{d\omega}(\omega) \equiv (1, -\vec{e}), \tag{A.20}$$

onde o vector $\vec{e} \equiv c^\mu/(\eta_R - \eta_E)$ representa a direcção espacial de ordem zero percorrida pelos fotões, tal como é vista por um observador que se move com o fluido. Tendo em conta que $\dot{x}^a_{(0)}(\omega)$ é um vector nulo, tem-se que:

$$\vec{e}^2 = 1 \tag{A.21}$$

Voltando à equação (A.14) e utilizando (A.20) obtém-se

$$\bar{k}_a(\omega) \equiv \bar{E}_{(0)}\left(1 + \frac{1}{2}\int_0^\omega h_{bc,0}\dot{x}^b_{(0)}\dot{x}^c_{(0)}d\omega', e_\mu + \frac{1}{2}\int_0^\omega h_{bc,\mu}\dot{x}^b_{(0)}\dot{x}^c_{(0)}d\omega'\right). \tag{A.22}$$

Esta expressão é válida em primeira ordem de aproximação. Os integrais que nela figuram dão a correcção de primeira ordem ao momento não perturbado $\bar{k}_{(0)a} \equiv \bar{E}_{(0)}(1, e_\mu)$, onde $\bar{E}_{(0)}$ é a energia da radiação medida por um observador comóvel no universo não perturbado de $d\bar{s}^2$.

Consideremos agora um observador material que se move ao longo de uma linha do universo de $d\bar{s}^2$, com velocidade $\bar{u}^a$, e que se cruza num determinado instante, ω, com os fotões CMB.

A energia da radiação de fundo medida por esse obsevador em $d\bar{s}^2$ é

$$\bar{E}_{obs}(\omega) = -\bar{k}_a \bar{u}^a(\omega). \tag{A.23}$$

Admitindo que a velocidade espacial do obsevador é pequena relativamente à velocidade da luz, $|\vec{v}| << 1$, e tendo em conta a condição $\bar{u}_a \bar{u}^a = 1$, é possível verificar (ver apêndice B.2) que, em primeira ordem de aproximação,

$$\bar{u}^a \equiv \left(1 - \frac{1}{2}h_{00}, \vec{v}\right). \tag{A.24}$$

Substituindo (A.24) e (A.22) em (A.23) e desprezando todos os termos de ordem superior a um vem,

$$\bar{E}_{obs}(\omega) = -\bar{k}_a \bar{u}^a(\omega) = -\bar{E}\left(1 - \frac{1}{2}h_{00} + \vec{e}.\vec{v} + \frac{1}{2}\int_0^{\omega} h_{bc,0}\dot{x}^b_{(0)}\dot{x}^c_{(0)}d\omega'\right) \tag{A.25}$$

(os termos onde aparecem produtos de $\vec{v} \equiv v^\mu$ com elementos de h_{ab} desprezam-se por serem de segunda ordem).

Este resultado pode agora ser transposto de $d\bar{s}^2$ para ds^2. Deste modo, a energia medida pelo observador em ds^2 é

$$E_{obs}(\omega) = -k_a u^a = -\frac{1}{a}\bar{k}_a \bar{u}^a = \frac{1}{a(\omega)}\bar{E}_{obs}(\omega) \tag{A.26}$$

onde na segunda igualdade se utilizaram as expressões (A.4) e (A.5) que relacionam o momento dos fotões, $k_a = \bar{k}_a$, e a velocidade do observador, $\bar{u}^a = a u^a$, entre ds^2 e $d\bar{s}^2$.

A.2 O Efeito de Sachs-Wolfe

Para calcularmos o redshift sofrido pela radiação desde o seu último scattering em E até ser observada em R (ver figura A.1), basta efectuar a razão entre a energia medida por dois observadores materiais que se encontram instantaneamente com a radiação em E e R,

$$z + 1 = \frac{\lambda_R}{\lambda_E} = \frac{E_{obs}(\omega_E)}{E_{obs}(\omega_R)} = \frac{a_R}{a_E}\frac{\bar{E}_{obs}(\omega_E)}{\bar{E}_{obs}(\omega_R)} = \frac{a_R}{a_E}\frac{\bar{k}_a \bar{u}^a(0)}{\bar{k}_a \bar{u}^a(\eta_R - \eta_E)}. \tag{A.27}$$

Na segunda igualdade utilizou-se a relação entre a energia e o comprimento de onda de um fotão [2] e nas terceira e quarta iguadades utilizaram-se, respectivamente, (A.26) e (A.23). Os índices "E" e "R" significam que as grandezas devem ser calculadas, respectivamente, nos instantes de emissão, $\omega_E = 0$, e recepção $\omega_R = \eta_R - \eta_E$.

Substituindo (A.25) em (A.27) resulta,

$$\begin{aligned} z + 1 \;\; = \;\; & \frac{a_R}{a_E}\left(1 - \frac{1}{2}h_{00}\Big|_E + \vec{e}.\vec{v}|_E\right). \\ & \left[1 - \frac{1}{2}h_{00}\Big|_R + \vec{e}.\vec{v}|_R + \frac{1}{2}\int_0^{\eta_R - \eta_E} h_{bc,0}\,\dot{x}^b_{(0)}\dot{x}^c_{(0)}d\omega\right]^{-1} \end{aligned} \tag{A.28}$$

[2] Num sistema de unidades aonde c é a velocidade da luz no vazio e h é a constante de Planck, a relação entre a energia, E_γ, e o comperimento de onda dos fotões, λ, é $E_\gamma = hc/\lambda$.

(o símbolo "$X|_A$" significa que a grandeza "X" deve ser calculada no ponto "A"). Os três últimos termos que figuram no interior do parênteses recto são pequenos face à unidade. Sendo assim podemos utilizar a aproximação $(1+x)^{-1} = 1-x$, para calcular $z+1$. Após efectuarmos todos os produtos e despresando uma vez mais os termos de ordem superior a um, obtém-se

$$z+1 = \frac{a_R}{a_E}\left(1 + \left[\frac{1}{2}h_{00}\right]_E^R - [\vec{e}.\vec{v}]_E^R - \frac{1}{2}\int_0^{\eta_R-\eta_E} h_{bc,0}\dot{x}^b_{(0)}\dot{x}^c_{(0)}d\omega'\right) \tag{A.29}$$

(o símbolo "$[X]_B^A$" significa $X(A) - X(B)$). A expressão que relaciona o redshift com a temperatura da radiação de fundo entre os eventos E e R é

$$T_R = T_E\left[z+1\right]^{-1}. \tag{A.30}$$

Substituindo (A.29) nesta expressão e utilizando uma vez mais a aproximação $(1+x)^{-1} = 1-x$, concluimos que

$$\begin{aligned} T_R &= \frac{a_E}{a_R}T_E\left[1 + \left[\frac{1}{2}h_{00}\right]_E^R - [\vec{e}.\vec{v}]_E^R - \frac{1}{2}\int_0^{\eta_R-\eta_E} h_{bc,0}\dot{x}^b_{(0)}\dot{x}^c_{(0)}d\omega'\right]^{-1} \\ &= \frac{a_E}{a_R}T_E\left[1+\frac{\delta T_R}{T_R}\right] \end{aligned} \tag{A.31}$$

com

$$\frac{\delta T_R}{T_R} = -\left[\frac{1}{2}h_{00}\right]_E^R + [\vec{e}.\vec{v}]_E^R + \frac{1}{2}\int_0^{\eta_R-\eta_E} h_{bc,0}\dot{x}^b_{(0)}\dot{x}^c_{(0)}d\omega'. \tag{A.32}$$

Para interpretarmos cada um dos termos que figuram nesta expressão é conveniente especificar a forma do tensor métrico das perturbações, h_{ab}. A escrita esplícita das componentes de h_{ab} está intimamente relacionada com a escolha de uma **gauge** para a descrição das flutuações. A escolha da gauge corresponde à escolha das hipersuperfícies aonde essas flutuações são definidas ([52] §2.11; §4.2). Se pretendermos trabalhar num referencial aonde a nossa intuição newtoniana faça sentido devemos escolher a chamada **gauge newtoniana** [114], para a qual se tem

$$h_{00} = 2\Psi \quad ; \quad h_{11} = h_{22} = h_{33} = -2\Phi \quad ; \quad \underset{a\neq b}{h_{ab}} = 0, \tag{A.33}$$

no caso de considerar-mos apenas flutuações de natureza escalar (i.e. de densidade). Nesta gauge as grandezas $\Psi = \Psi(\eta,\vec{x})$ e $\Phi = \Phi(\eta,\vec{x})$ podem ser interpretadas, respectivamente, como um potencial newtoniano e um potencial de perturbação da curvatura espacial ([52] §2.11). Apartir das equações de Einstein é possível concluir que $\Phi = -\Psi$ sempre que a pressão for desprezável ($p = 0$).

Voltando a (A.32) na gauge newtoniana,

$$\frac{\delta T_R}{T_R} = -[\Psi]_E^R + [\vec{e}.\vec{v}]_E^R + \frac{1}{2}\int_0^{\eta_R-\eta_E} h_{bc,0}\dot{x}^b_{(0)}\dot{x}^c_{(0)}d\omega', \tag{A.34}$$

é agora relativamente simples dar uma interpretação física para cada um dos factores que aparecem nesta expressão.

As perturbações de densidade na última superfície de scattering (LSS) dão origem a potênciais graviticos. Os fotões CMB ao abandonarem a última superfície de scattering sofrem assim um redshift gravitacional que se reflecte numa variação da sua energia. A contribuição desse redshift para as flutuações de temperatura traduzem-se justamente no termo $[\Psi]_E^R = \Psi(R) - \Psi(E)$ que figura na expressão (A.34). Quanto ao termo $[\vec{e}.\vec{v}]_E^R = \vec{e}.(\vec{v}(R) - \vec{v}(E))$, trata-se de um efeito Doppler provocado pelos movimentos peculiares do observador (Receptor) e da matéria (Emissor) aonde se dá o último scattering da radiação. Finalmente o último termo de (A.34) tem a ver com a possibilidade de existirem dependências temporais nos elementos da métrica h_{ab}, ao longo do percurso dos fotões após a sua última interecção com a matéria.

À parte do termo de Doppler [3] , o primeiro e terceiro termos de (A.34) são ambos designados por **efeito de Sachs-Wolfe**. No entanto por uma questão de distinção é muito frequente designar o último termo por **efeito de Sachs-Wolfe integrado**, uma vez que dá conta das flutuações de temperatura provocadas pela evolução das perturbações h_{ab} após o último scattering.

Se considerarmos que h_{ab} é dada por (A.33) e que a pressão é despresável, ($\Phi = -\Psi$) a função integranda do terceiro termo de (A.34) é

$$h_{bc,0}\,\dot{x}^b_{(0)}\dot{x}^c_{(0)} = 2\frac{d\Psi}{d\eta} - 2\frac{d\Phi}{d\eta}\vec{e}^2 = 2\frac{d}{d\eta}(\Psi - \Phi) = 4\frac{d\Psi}{d\eta}, \tag{A.35}$$

onde na segunda igualdade se utilizou (A.21) (i.e., $\vec{e}^2 = 1$). Deste modo

$$\frac{\delta T_R}{T_R} = -(\Psi(R) - \Psi(E)) + \vec{e}.\,(\vec{v}(R) - \vec{v}(E)) + 2\int_0^{\eta_R - \eta_E} \frac{d\Psi}{d\eta} d\omega. \tag{A.36}$$

A expressão (A.36) não enumera todos os processos que originam flutuações na temperatura da radiação de fundo. A integração da equação das geodésicas contabiliza apenas "efeitos cinemáticos" sofridos pela radiação ao propagar-se livremente através de um universo perturbado, desde o último scattering.

No entanto a última superfície de scattering apresenta flutuações de temperatura intrínsecas, $\delta T_E/T_E$, originadas por todo um conjunto de processos físicos, relacionados com a existência de perturbações intrínsecas de densidade na LSS. Na época em que se dá o descoplamento da radiação com a matéria, η_d, as flutuações de densidade nos vários componetes do fluído cosmológico são ainda pequenas e podem ser tratadas no quadro da teoria linear de perturbações. Nesse sentido, $\delta T_E/T_E$ é igualmente pequeno face à unidade e, em primeira ordem de aproximação, tem-se que [4]

$$\frac{\delta T_E}{T_E} = \frac{1}{4}\frac{\delta\rho_\gamma}{\rho_\gamma}, \tag{A.37}$$

onde $\delta\rho_\gamma/\rho_\gamma$ é a fluatuação de densidade de radiação na LSS.

[3] que se traduz essencialmente numa anisotropia de dipólo na temperatura da radiação de fundo e que por isso é normalmente tratada em separado.

[4] Para establecer esta expressão basta expandir em serie de Taylor a densidade de radiação ρ_γ em torno de $< T_E >$, até à primeira ordem, e em seguida utilizar a lei de radiação de Stefan-Boltzmann $\rho_\gamma = const.T^4$.

As expressões (A.30) e (A.31) relacionam a temperatura observada, T_R, com a temperatura medida sobre um único ponto da última superfície de scattering, T_E. Se $< T_E >$ for a temperatura média na LSS e $\delta T_E/T_E(\eta_d, \vec{x})$ a flutuação de temperatura intrínseca no ponto de emissão $(\eta_d, \vec{x})$ podemos escrever

$$T_E = T_E(\eta_d, \vec{x}) =< T_E > \left(1 + \frac{\delta T_E}{T_E}\right). \tag{A.38}$$

Substituindo (A.38) em (A.30) temos, igualmente em primeira ordem de aproximação,

$$T_R = \frac{a_E}{a_R}\left[1 + \frac{\delta T_R}{T_R} + \frac{\delta T_E}{T_E}\right] = \frac{a_E}{a_R}\left[1 + \frac{\delta T}{T}\right], \tag{A.39}$$

sendo

$$\frac{\delta T}{T} = \frac{\delta T_R}{T_R} + \frac{\delta T_E}{T_E} \tag{A.40}$$

a flutuação de temperatura total observada em R com $\delta T_R/T_R$ dado pelas expressões (A.32), (A.34) e (A.36).

A formação das flutuações $\delta T_E/T_E$ a partir das heterogeneidades que surgem na última superficie de scattering é em geral um processo complexo e está directamente relacionado com a natureza e dimensão (escala física) das perturbações. No entanto para perturbações de dimensão superior ao *horizonte* à época da recombinação, este processo é relativamente simples de analizar. Enquanto as perturbações estão fora do horizonte, as flutuações de densidade nos vários componentes do fluido cosmológico reflectem as *condições iniciais* do processo que originou a formação de perturbações no universo primordial. Para perturbações de natureza adiabática, as densidades parciais de radiação e de materia são perturbadas simultaneamente, por forma a que

$$\frac{\delta \rho_m}{\rho_m} - \frac{3}{4}\frac{\delta \rho_\gamma}{\rho_\gamma} = 0. \tag{A.41}$$

Para perturbações de isocurvatura a distribuição de matéria é perturbada sem que a densidade de radiação sofra alterações significativas [62] (expressão (9.51), pag. 339). Neste caso, enquanto as perturbações permanecem fora do horizonte,

$$\frac{\delta \rho_\gamma}{\rho_\gamma} \approx 0 \tag{A.42}$$

e portanto a temperatura no interior de uma região perturbada, cuja dimensão seja superior ao horizonte, mantem-se praticamente inalterada, i.e. $T_E =< T_E >$, $\delta T_E/T_E = 0$. (Por esta razão as perturbações de isocurvatura são igualmente designadas de perturbações isotérmicas).

Sendo assim, utilizando (A.41) e (A.42) em (A.37), concluimos que para perturbações em escalas de dimensão superior ao horizonte tem-se,

$$\frac{\delta T_E}{T_E} = \begin{cases} \frac{1}{3}\frac{\delta \rho_m}{\rho_m} & (Adiab.) \\ 0 & (Isocur.) \end{cases}, \tag{A.43}$$

consoante as condições iniciais sejam adiabáticas ou de isocurvatura.

A partir desta expressão vemos que, para perturbações adiabáticas, as regiões de sobre-densidade/sub-densidade são intrinsecamente mais quentes/ frias do que a temperatura média na LSS. De acordo com [115], $\delta\rho_m/\rho_m = -2\Psi + \mathscr{O}\left[(k/H)^2\right]$ onde k é o momento associado à escala da perturbação. Quanto maior é a escala menor é k e portanto para perturbações de dimenção superior ao horizonte $k << H$, os locais de sobre-densidade coincidem com os poços de potencial, resultando

$$\frac{\delta T_E}{T_E} \approx -\frac{2}{3}\Psi(E). \tag{A.44}$$

Substituindo (A.44) e (A.36) em (A.40) verificamos que, no caso das perturbações serem adiabaticas, os termos $\delta T_R/T_R$ e $\delta T_E/T_E$ canselam parcialmente, dendo origem à seguinte expressão para flutuação de temperatura total observada em R

$$\frac{\delta T}{T} = \frac{1}{3}\Psi(E) + \vec{e}.\left(\vec{v}(R) - \vec{v}(E)\right) + 2\int_0^{\eta_R - \eta_E} \frac{d\Psi}{d\eta} d\omega, \tag{A.45}$$

onde sem perda de generalidade, se colocou $\Psi(R) = 0$. Esta expressão é válida apenas quando a observação é feita para escalas angulares que subentendam regiões mais extensas que o horizonte na época da recombinação ($\vartheta >> 1^o$). Se as perturbações são de isocurvatura $\delta T/T$ coincide com $\delta T_R/T_R$ dado por (A.36).

Ignorando os termos de Doppler e o integral de $\dot{\Psi}$ ao longo do percurso da radiação, a expressão (A.45) é a forma mais comum de escrever o efeito Sachs-Wolfe para flutuações adiabaticas (eg [114], [107], [115]). O cancelamento parcial das flutuações de temperatura intrínseca com as flutuações provocadas pelo redshift dos fotões ao deslocarem-se através do potencial Ψ, $\delta T/T = 1/3\Psi$, acaba por transformar as regiões de sobre-densidade ($\Psi < 0$) em regiões frias e as de sub-densidade em regiões quentes, quando observadas em R.

A.2.1 Cálculo de C_l para grandes ϑ. Patamar de Sachs-Wolfe

Em Teoria linear de perturbações, é possível obter uma expressão analítica para C_l, na região das grandes escalas angulares ϑ (i.e. $l \lessapprox 20$). Para estas escalas verifica-se o efeito Sachs-Wolfe [94], e as flutuações de temperatura são dadas por:

$$\frac{\Delta T}{T}(\vec{x}) = -\frac{1}{3}\delta\phi(\vec{x}, t_d) \tag{A.46}$$

onde $\delta\phi$ é a perturbação no potencial devido à existencia de uma flutuação de densidade $\delta\rho = \rho_0\delta$ ($\rho = \rho_0(1+\delta)$; ρ_0 a densidade mdia do universo e $\delta \equiv$ função excesso). A perturbao $\delta\phi$ verifica a equação de Poisson (escrita num sistema de coordenadas cómovel com a expansão):

$$\frac{1}{a^2}\nabla_x^2\delta\phi = 4\pi G\rho_0\delta. \tag{A.47}$$

Aplicando Transformadas de Fourrier a $\delta\phi$ e a δ

$$\delta\phi\left(\vec{x}\right) = \frac{1}{\left(2\pi\right)^3}\int d^3k\delta\phi_k e^{-i\vec{k}.\vec{x}} \quad ; \quad \delta\left(\vec{x}\right) = \frac{1}{\left(2\pi\right)^3}\int d^3k\delta_k e^{-i\vec{k}.\vec{x}} \tag{A.48}$$

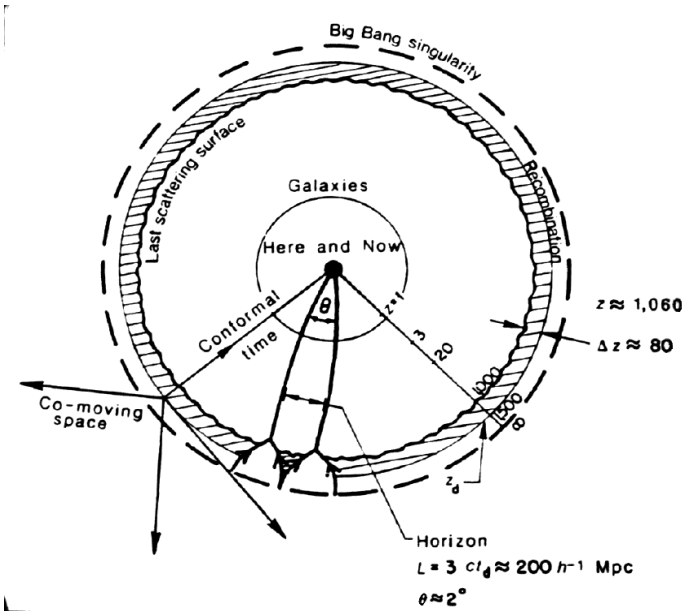

Figure A.2: Última superfície de scattering.

e substituindo em (A.47) e (A.46) temos:

$$k^2\delta\phi_k = 4\pi G\rho_0 a^2\delta_k \Leftrightarrow \delta\phi_k = 4\pi G\rho_0 a^2\frac{\delta_k}{k^2} \tag{A.49}$$

$$\frac{\Delta T}{T}(\vec{x}) = \frac{1}{3}\frac{1}{(2\pi)^3}\int d^3k\delta\phi_k e^{-i\vec{k}.\vec{x}} \Leftrightarrow \frac{\Delta T}{T}(\vec{x}) = \frac{4\pi G\rho_0 a^2}{3(2\pi)^3}\int d^3k\frac{\delta k}{k^2}e^{-i\vec{k}.\vec{x}} \tag{A.50}$$

Introduzindo esta expressão em (3.7) resulta

$$C_l = \frac{1}{9}\frac{1}{(2\pi)^6}\left(4\pi G\rho_0(t_d)\,a_{t_d}^2\right)^2\int d\Omega_1 d\Omega_2 Y_{lm}(\Omega_1).Y_{lm}^*(\Omega_2)\int d^3kd^3k' e^{i\vec{k}.\vec{x}_1 - i\vec{k}'.\vec{x}_2}\left\langle\delta_k^*\delta_{k'}\right\rangle. \tag{A.51}$$

Se admitirmos que as flutuações são gausseanas:

$$\left\langle\delta_k^*\delta_{k'}\right\rangle = P(k)\,\delta(k-k')(2\pi)^3 \tag{A.52}$$

e usarmos a fórmula

$$e^{i\vec{k}.\vec{x}} = 4\pi\sum_{lm}(i)^l j_l(kx)\,Y_{lm}^*(\hat{x})\,Y_{lm}(\hat{k}) \tag{A.53}$$

vem:

$$\begin{aligned} C_l &= \frac{1}{9}\frac{1}{(2\pi)^3}\left(4\pi G\rho_0(t_d)\,a_{t_d}^2\right)^2\int d^3kk^{-4}P(k)\sum_{l'm'}\sum_{l''m''}(4\pi)^2(i)^{l'}(-i)^{l''}j_{l'}(kx_1)\,j_{l''}(kx_2) \\ &\int d\Omega_1 d\Omega_2\left[Y_{lm}(\Omega_1)\,Y_{l'm'}^*(\Omega_1)\right]\left[Y_{lm}^*(\Omega_2)\,Y_{l''m''}(\Omega_2)\right]\left[Y_{l'm'}(\hat{k})Y_{l''m''}^*(\hat{k})\right] \end{aligned}$$

Utilizando as relações de ortogonalidade dos harmónicos esféricos e o facto de

$$|\vec{x}_1| = |\vec{x}_2| = x \quad \Rightarrow \quad \left(j_l\left(kx_1\right) j_l\left(kx_2\right) = j_l^2\left(kx\right)\right) \tag{A.54}$$

podemos integrar sobre $d\Omega_k \equiv d\hat{k}$, de onde resulta

$$C_l = \frac{\left(4\pi\right)^2}{9\left(2\pi\right)^3}\left[4\pi G\rho_0\left(t_d\right) a_{t_d}^2\right]^2 \int_0^{+\infty} dk \frac{k^2}{k^4}\left[j_l\left(kx\right)\right]^2 \int d\Omega_k Y_{lm}(\hat{k}) Y_{lm}^*(\hat{k}) \tag{A.55}$$

ou seja:

$$C_l = \frac{\left(4\pi\right)^2}{9\left(2\pi\right)^3}\left[4\pi G\rho_0\left(t_d\right) a_{t_d}^2\right]^2 \int_0^{+\infty} dk\, k^{-2} P\left(k\right)\left[j_l\left(kx\right)\right]^2 \tag{A.56}$$

Para calcular este integral é necessário definir $P\left(k\right)$. Normalmente considera-se que o espectro de potência é dado por:

$$P\left(k\right) = Ak^n \tag{A.57}$$

Substituindo (A.57) em (A.56), usando a relação matemática

$$j_l\left(x\right) = \sqrt{\frac{\pi}{2x}} J_{l+\frac{1}{2}}\left(x\right) \tag{A.58}$$

(onde $J_\nu\left(x\right) = \left(\frac{1}{2}x\right)^\nu \sum_k \frac{\left(-\frac{1}{4}x^2\right)^k}{k!\Gamma(\nu+k+1)}$ é a função J de Bessel) e fazendo uma mudança de variável de integração

$$y = kx \Leftrightarrow k = \frac{y}{x} \quad ; \quad \frac{dk}{dy} = x^{-1} \tag{A.59}$$

obtém-se:

$$C_l = \left\langle |a_{lm}|^2 \right\rangle = \frac{1}{9}\left[4\pi G\rho_0\left(t_d\right) a^2\left(t_d\right)\right]^2 A x^{1-n} \int_0^{+\infty} dy\, y^{n-3}\left[J_{l+\frac{1}{2}}\left(y\right)\right]^2 \tag{A.60}$$

O integral anterior pode ser calculado através da seguinte relação, válida para $n < 3$:

$$\int_0^{+\infty} dy\, y^{n-3}\left[J_{l+\frac{1}{2}}\left(y\right)\right]^2 = \frac{\Gamma\left(3-n\right)\Gamma\left[\frac{2l+n-1}{2}\right]}{2^{3-n}\Gamma^2\left(\frac{4-n}{2}\right)\Gamma\left[\frac{2l+5-n}{2}\right]} \tag{A.61}$$

e portanto:

$$C_l = \left\langle |a_{lm}|^2 \right\rangle = \frac{1}{9}\left[4\pi G\rho_0\left(t_d\right) a^2\left(t_d\right)\right]^2 A x^{1-n} \frac{\Gamma\left(3-n\right)\Gamma\left[\frac{2l+n-1}{2}\right]}{2^{3-n}\Gamma^2\left(\frac{4-n}{2}\right)\Gamma\left[\frac{2l+5-n}{2}\right]}. \tag{A.62}$$

Para $(l = 2)$ temos que

$$C_2 = \left\langle |a_{lm}|^2 \right\rangle = \frac{1}{9}\left[4\pi G\rho_0\left(t_d\right) a\left(t_d{}^2\right)\right]^2 A x^{1-n} \frac{\Gamma\left(3-n\right)\Gamma\left[\frac{3+n}{2}\right]}{2^{3-n}\Gamma^2\left(\frac{4-n}{2}\right)\Gamma\left[\frac{9-n}{2}\right]}. \tag{A.63}$$

Desta forma podemos escrever a parte "constante" de (A.62) em termos de C_2

$$\frac{1}{9}\left[4\pi G\rho_0\left(t_d\right)a^2\left(t_d\right)\right]^2 Ax^{1-n}\frac{\Gamma\left(3-n\right)}{2^{3-n}\Gamma^2\left(\frac{4-n}{2}\right)} = C_2\frac{\Gamma\left(\frac{9-n}{2}\right)}{\Gamma\left(\frac{3+n}{2}\right)} \tag{A.64}$$

Substituindo-se em (A.62) fica então que:

$$C_l = C_2\frac{\Gamma\left(\frac{2l+n-1}{2}\right)\Gamma\left(\frac{9-n}{2}\right)}{\Gamma\left(\frac{2l+5-n}{2}\right)\Gamma\left(\frac{3+n}{2}\right)} \tag{A.65}$$

ou se quisermos:

$$C_l = \frac{4\pi}{5}Q^2\frac{\Gamma\left(l+\frac{n-1}{2}\right)\Gamma\left(9-n\right)}{\Gamma\left(l+\frac{5-n}{2}\right)\Gamma\left(\frac{3+n}{2}\right)} \tag{A.66}$$

com a definição:

$$Q^2 \equiv \left\langle \frac{\Delta T}{T}\left(\hat{n}\right)\frac{\Delta T}{T}\left(\hat{n}'\right)\right\rangle_{\substack{\hat{n}=\hat{n}'\\ l=2}} = \left[\sum_l \frac{2l+1}{4\pi}C_l P_l\left(\cos\theta\right)\right]_{\substack{\theta=0\\ l=2}} = \frac{5}{4\pi}C_2. \tag{A.67}$$

Se admitirmos que o índice espectral é $n = 1$ (espectro de potência de Harrison-Zel'dovich) e utilizando o facto de $\Gamma(x+1) = x\Gamma(x)$ obtem-se

$$C_l = \frac{24\pi}{5}\frac{Q^2}{l(l+1)} \tag{A.68}$$

e portanto

$$\left[\frac{l(l+1)C_l}{2\pi}\right]^{1/2} = \sqrt{\frac{12}{5}}Q = const. \tag{A.69}$$

Este resultado explica porque motivo o espectro de potência angular apresenta uma parte plana para $l \leq 20$ (*patamar de Sachs-Wolfe*). Este facto está igualmente na origem da escolha das unidades frequentemente utilizadas no eixo dos y para representar graficamente o espectro de potencia angular CMBR (ver figura 3.2).

Appendix B

Geodésicas e velocidades próprias

B.1 Geodésicas nulas e velocidades próprias em ds^2 e $d\bar{s}^2$

Duas métricas ds^2 e $d\bar{s}^2$ (como (A.1), (A.3) na secção A.2) relacionadas por uma transformação conforme

$$ds^2 = g_{ab}dx^a dx^b = a^2(\eta)\bar{g}_{ab}dx^a dx^b = a^2(\eta)d\bar{s}^2 \tag{B.1}$$

apresentam geodésicas do género luz coincidentes [94]. Com efeito, como para fotões $ds^2 = 0$, de (B.1) concluimos que existe uma correspondencia "one-to-one" entre as trajectorias descritas pelos fotões em ds^2 e $d\bar{s}^2$. No entanto para uma mesma geodésica s parâmetros afins em ds^2 e $d\bar{s}^2$ são naturalmente distintos. Considermos uma dada geodésica do género luz, $x^a(\xi) = x^a(\omega)$, em que ξ e ω são os parâmetros afins em ds^2 e $d\bar{s}^2$ e $k^a = dx^a/d\xi$, $\bar{k}^a = dx^a/d\omega$ os seus respectivos vectores tangentes. Nestas condições é possível concluir que

$$\bar{k}^a = a^2 k^a \Leftrightarrow \bar{k}_a = k_a \Leftrightarrow d\xi = a^2 d\omega. \tag{B.2}$$

No que toca às partículas materiais pode-se igualmente concluir que velocidade própria dessas partículas se transforma de ds^2 para $d\bar{s}^2$ do seguinte modo

$$u_a = a\bar{u}_a \Leftrightarrow u^a = a^{-1}\bar{u}^a \tag{B.3}$$

B.2 Velocidades próprias de partículas materias em universos perturbados (1^a ordem de aprox.)

Consideremos um observador material que se move ao longo de uma dada linha do universo com um campo de velocidades

$$u^a = \frac{dx^a}{d\tau}, \tag{B.4}$$

onde τ é o tempo próprio. De $|u^2| = u_a u^a = g_{ab} u^a u^b$ vem que $ds^2 = |u^2|\, d\tau^2$. Tendo em conta que ds^2 é um invariante, no referêncial próprio do observador $ds^2 = d\tau^2$. Logo

$$\left|u^2\right| = u_a u^a = g_{ab} u^a u^b = 1. \tag{B.5}$$

Consideremos agora que

$$g_{ab} = \eta_{ab} + h_{ab},$$

onde o tensor de Minkowski tem a assinatura $(+,-,-,-)$ e h_{ab} é diagonal

$$h_{ab} = \begin{bmatrix} h_{00} & 0 & 0 & 0 \\ 0 & h_{11} & 0 & 0 \\ 0 & 0 & h_{22} & 0 \\ 0 & 0 & 0 & h_{33} \end{bmatrix} \tag{B.6}$$

com $h_{11} = h_{22} = h_{33}$. Da condição (B.5), vem

$$\begin{aligned} u_a u^a = \left|g_{ab} u^a u^b\right| &= \left|(\eta_{ab} + h_{ab})\, u^a u^b\right| \\ &= \left|(1+h_{00})(u^0)^2 + (-1+h_{11})(u_x^2 + u_y^2 + u_z^2)\right| \\ &= \left|(1+h_{00})(u^0)^2 - (1-h_{11})v^2\right| = 1 \end{aligned}$$

($v^2 = \vec{v}^2 = u_x^2 + u_y^2 + u_z^2$) e portanto

$$(1+h_{00})(u^0)^2 = 1 + (1-h_{11})v^2. \tag{B.7}$$

Se considerarmos que a velocidade espacial do observador é pequena,

$$|\vec{v}| << 1 \Rightarrow v^2 << 1, \tag{B.8}$$

de (B.7) concluimos que em primeira ordem de aproximação

$$u^0 = (1+h_{00})^{-\frac{1}{2}} = 1 - \frac{1}{2} h_{00} \tag{B.9}$$

e portanto, também em primeira ordem, o 4-vector velocidade do obsevador material pode-se escrever como

$$u^a = \left(1 - \frac{1}{2} h_{00}, \vec{v}\right). \tag{B.10}$$

Appendix C

Temperature fluctuations in a small patch of sky

On a small patch of sky, small enough to be considered flat, the usual spherical harmonics expansion of the temperature fluctuation field, Eq. (3.2), can be approximated by a Fourier series (see e.g. Ref. [112]). Assuming the patch is square of side L we can write [76]:

$$\frac{\delta T}{T}(\mathbf{x}) = \sum_{lm} a_{\ell m} Y_{\ell m} \simeq \frac{L^2}{(2\pi)^2} \int d^2k \, T_k(\mathbf{k}) \exp(i\mathbf{k}.\mathbf{x}) \tag{C.1}$$

$$T_k(\mathbf{k}) = \frac{1}{L^2} \int d^2x \, \frac{\delta T}{T}(\mathbf{x}) \exp(-i\mathbf{k}.\mathbf{x}) \, . \tag{C.2}$$

Here $\mathbf{x}$ and $\mathbf{k}$ are 2-dim vectors giving the angular position on the sky and the wavenumber in the Fourier space, respectively. This is known as the *flat-sky approximation*. Note that in the definitions above, both $\delta T/T$ and T_k are dimensionless quantities. Equation (C.1) implies a relation between the wavenumber k and the multipole ℓ which will be presented below.

As in the case of the density power spectrum, the temperature angular power spectrum is usually defined in a dimensionless form,

$$\mathscr{T}^2(k) \equiv \frac{L^2}{(2\pi)^2} 2\pi k^2 \left|T_k\right|^2 \, , \tag{C.3}$$

where $\mathscr{T}^2$ is the fractional variance of the temperature fluctuations from modes in unit range of $\ln k$. As before, the 2-point correlation function of the temperature fluctuations is the Fourier transform of the power spectrum. In the flat-sky approximation the angular correlation function of the temperature fluctuation field can be written as [76]

$$C(\vartheta) = \left\langle \frac{\delta T}{T}(\hat{n}_1) \frac{\delta T}{T}(\hat{n}_2) \right\rangle = \int \frac{dk}{k} \, \mathscr{T}^2(k) J_0(k\vartheta) \tag{C.4}$$

where

$$\mathscr{T}^2 \left(k = \ell + \frac{1}{2} \right) = \frac{\left(\ell + \frac{1}{2}\right)^2}{2\pi} C_\ell \, . \tag{C.5}$$

Here, $C_\ell = \langle |a_{\ell m}| \rangle$ is the angular power spectrum of the temperature fluctuation field and the J_0 is the Bessel function of order 0, arising from the integration of the angular part of the Fourier transforms when using Eq. (C.1) into the definition of $C(\vartheta)$. Since the angle formed by any two unit vectors n, n' within the patch is assumed to be small (large ℓ), the last equation tells us that $k \simeq \ell$ and $\mathscr{T}^2(k = \ell) \simeq \ell(\ell + 1)C_\ell/2\pi$. Equating this into Eq. (C.3) we obtain

$$\frac{\ell\,(\ell+1)}{2\pi} C_\ell \simeq \frac{L^2}{(2\pi)^2} 2\pi\ell^2 \left|T_{k=\ell}\right|^2 \ . \tag{C.6}$$

We will use this approximation to compute the angular power spectrum of SZ effect from simulated temperature fluctuation maps of size one square degree.